



RESSES  
2  
2006



This is to certify that the  
dissertation entitled

**MICROWAVE PROCESSING OF EPOXY RESINS AND  
SYNTHESIS OF CARBON NANOTUBES BY MICROWAVE  
PLASMA CHEMICAL VAPOR DEPOSITION**

presented by

**LIMING ZONG**

has been accepted towards fulfillment  
of the requirements for the

Ph.D. degree in Chemical Engineering

*Mark C Hawley*  
Major Professor's Signature

*May 10, 2005*  
Date

**PLACE IN RETURN BOX** to remove this checkout from your record.  
**TO AVOID FINES** return on or before date due.  
**MAY BE RECALLED** with earlier due date if requested.

<b>DATE DUE</b>	<b>DATE DUE</b>	<b>DATE DUE</b>

**MICROWAVE PROCESSING OF EPOXY RESINS AND SYNTHESIS OF CARBON  
NANOTUBES BY MICROWAVE PLASMA CHEMICAL VAPOR DEPOSITION**

**By**

**Liming Zong**

**A DISSERTATION**

**Submitted to  
Michigan State University  
in partial fulfillment of the requirements  
for the degree of**

**DOCTOR OF PHILOSOPHY**

**Department of Chemical Engineering and Materials Science**

**2005**

## ABSTRACT

### MICROWAVE PROCESSING OF EPOXY RESINS AND SYNTHESIS OF CARBON NANOTUBES BY MICROWAVE PLASMA CHEMICAL VAPOR DEPOSITION

By

Liming Zong

Microwave processing of advanced materials has been studied as an attractive alternative to conventional thermal processing. In this dissertation, work was performed in four sections. The first section is a review on research status of microwave processing of polymer materials.

The second section is investigation of the microwave curing kinetics of epoxy resins. The curing of diglycidyl ether of bisphenol A (DGEBA) and 3, 3'-diaminodiphenyl sulfone (DDS) system under microwave radiation at 145 °C was governed by an autocatalyzed reaction mechanism. A kinetic model was used to describe the curing progress.

The third section is a study on dielectric properties of four reacting epoxy resins over a temperature range at 2.45 GHz. The epoxy resin was DGEBA. The four curing agents were DDS, Jeffamine D-230, *m*-phenylenediamine, and diethyltoluenediamine. The mixtures of DGEBA and the four curing agents were stoichiometric. The four reacting systems were heated under microwave irradiation to certain cure temperatures. Measurements of temperature and dielectric properties were made during free convective cooling of the samples. The cooled samples were analyzed with a Differential Scanning Calorimeter to determine the extents of cure. The Davidson-Cole model can be used to describe the dielectric data. A simplified Davidson-Cole expression was proposed to

calculate the parameters in the Davidson-Cole model and describe the dielectric properties of the DGEBA/DDS system and part of the dielectric data of the other three systems. A single relaxation model was used with the Arrhenius expression for temperature dependence to model the results. The evolution of all parameters in the models during cure was related to the decreasing number of the epoxy and amine groups in the reactants and the increasing viscosity of the reacting systems.

The last section is synthesis of carbon nanotubes (CNTs) on silicon substrate by microwave plasma chemical vapor deposition of a gas mixture of methane and hydrogen. The catalyst was nickel, which was not directly deposited on the substrate but migrated from catalyst supplier during microwave plasma pretreatment. The Si wafer was coated with amorphous carbon before synthesis. Additional heating sources and DC bias on graphite substrate were not employed. Scanning Electron Microscopy and Transmission Electron Microscopy were used to characterize the morphologies and microstructures of the synthesized CNTs. The lengths and diameters of the CNTs changed with gas composition and growth temperature. Vertically-aligned CNTs with a length range of 350-500  $\mu\text{m}$  were synthesized. The diameter of CNTs is around 30-60 nm. The plasma gases included 20 sccm methane and 80 sccm hydrogen. The growth temperature was 800-810°C and the growth time was 20 minutes. The CNTs exhibit bamboo-like structure and appear to grow via a root-growth mechanism.

Copyright by

LIMING ZONG

2005

## **ACKNOWLEDGEMENTS**

The author would like to thank his academic advisor, Dr. Martin C. Hawley, for his invaluable guidance during this research. Appreciation is also given to the other Ph.D. committee members, Dr. Krishnamurthy Jayaraman, Dr. Michael E. Mackay, Dr. Leo C. Kempel, and Dr. Gregory L. Baker, for their time and insightful suggestions.

The author is grateful to Dr. Shuangjie Zhou and Rensheng Sun for their countless help during the research. Acknowledgement is extended to Michael Rich for help in DSC operation and Gregory Charvat for building the dielectric measurement and heating switch system. Furthermore, Dr. Jes Asmussen, Stanley S. Zuo, Nikki A. Sgriccia, and Susan Farhat helped the author in experiments on carbon nanotubes. Ewa Danielewicz and Dr. Xudong Fan helped the author in SEM and TEM imaging at the Center for Advanced Microscopy at Michigan State University. Yijun Zhang and Dr. David Grummon made the nickel coated silicon substrates for the CNT synthesis.

Last but not the least, special thanks are expressed to the author's family members for their endless love and support that words cannot describe.

This work was supported by the National Science Foundation under contract number DMI-0200346.

## TABLE OF CONTENTS

LIST OF FIGURES.....	x
LIST OF TABLES.....	xv
CHAPTER 1 INTRODUCTION .....	1
CHAPTER 2 BACKGROUND ON MICROWAVE PROCESSING.....	4
2.1 ELECTROMAGNETIC FIELDS IN A MICROWAVE ENCLOSURE .....	4
2.1.1 Maxwell's Equations .....	4
2.1.2 Resonant Modes in a Cylindrical Single Mode Cavity.....	6
2.1.3 Electromagnetic Fields in a Cylindrical Single Mode Cavity .....	9
2.2 MICROWAVE/MATERIALS INTERACTIONS .....	10
2.2.1 Mechanisms of Microwave/Materials Interactions.....	10
2.2.2 Dielectric Properties.....	13
2.3 LITERATURE SURVEY .....	16
2.3.1 Polymer Dielectric Properties .....	17
2.3.2 Microwave-Assisted Polymer Processing.....	19
2.3.2.1 Thermosets.....	19
2.3.2.2 Reaction Rate and Kinetics.....	19
2.3.2.3 Properties .....	21
2.3.2.4 Monitor and Heat Transfer Model .....	22
2.3.2.5 Thermoplastics.....	24
2.3.2.6 Composites Bonding.....	24
2.3.3 Microwave-Assisted Polymer Synthesis.....	25
2.3.4 Microwave Plasma Modified Polymer Surface .....	28
2.3.5 Microwave Plasma Polymerization .....	34
2.3.6 Polymer Degradation .....	35

2.3.7	Nanomaterials .....	36
2.3.8	Applications .....	36
<b>CHAPTER 3 MICROWAVE CURING MECHANISM OF EPOXY RESINS .....</b>		<b>38</b>
3.1	INTRODUCTION .....	38
3.2	MECHANISMS OF EPOXY RESIN CURING REACTIONS .....	39
3.3	EPOXY RESIN CURING KINETICS .....	42
3.3.1	Thermal Curing.....	42
3.3.1.1	Mechanistic Models .....	42
3.3.1.2	Phenomenological Models.....	45
3.3.1.3	Microwave Curing Kinetic Model .....	46
3.3.2	Kinetic Model Used in This Study.....	46
3.4	EXPERIMENTAL.....	47
3.4.1	Experimental Equipment .....	47
3.4.1.1	Experimental Circuit.....	47
3.4.1.2	Temperature Sensing Systems .....	48
3.4.1.3	Microwave Applicators.....	49
3.4.1.4	Cavity Characterization and Process Control .....	51
3.4.2	Experimental Materials and Procedure.....	53
3.5	RESULTS AND DISCUSSION .....	55
3.5.1	Temperature and Power Deposition Profiles .....	55
3.5.2	Kinetics .....	58
3.6	CONCLUSIONS.....	60
<b>CHAPTER 4 DIELECTRIC ANALYSIS OF CURING EPOXY RESINS .....</b>		<b>62</b>
4.1	INTRODUCTION .....	62
4.2	BACKGROUND ON DIELECTRIC ANALYSIS .....	64
4.2.1	Fundamental Theories for Dielectric Relaxation.....	64
4.2.1.1	Complex Dielectric Constant.....	64
4.2.1.2	Typical Graphs.....	69
4.2.1.3	Dielectric Relaxation Time .....	70

4.2.1.4	Typical Dielectric Relaxation Processes.....	71
4.2.2	Literature Review.....	72
4.3	EXPERIMENTAL.....	74
4.3.1	Experimental Systems.....	74
4.3.2	Experimental Materials.....	75
4.3.3	Sample Preparation .....	76
4.3.4	Measurements .....	77
4.4	RESULTS AND DISCUSSION .....	78
4.4.1	DGEBA/DDS System.....	79
4.4.2	DGEBA/Jeffamine D-230 System.....	95
4.4.3	DGEBA/mPDA System.....	105
4.4.4	DGEBA/Epikure W System .....	114
4.4.5	Parameters in the Models for the Four Systems .....	121
4.5	CONCLUSIONS.....	127
CHAPTER 5 SYNTHESIS OF CARBON NANOTUBES BY MPCVD .....		130
5.1	INTRODUCTION .....	130
5.2	LITERATURE REVIEW .....	134
5.3	EXPERIMENTAL.....	138
5.3.1	Experimental System .....	138
5.3.2	Experimental Materials.....	140
5.3.3	Experimental Procedure.....	140
5.4	RESULTS AND DISCUSSION .....	142
5.4.1	CNT Growth Conditions.....	142
5.4.2	CNT Growth Results.....	145
5.4.3	Morphology of CNTs by SEM .....	146
5.4.4	TEM Results .....	149
5.4.5	CNT Growth Mechanism.....	151
5.5	CONCLUSIONS.....	154
CHAPTER 6 CONCLUSIONS.....		155

CHAPTER 7 FUTURE WORK..... 159

REFERENCES ..... 160

## LIST OF FIGURES

Figure 2.1 TE modes in an empty cavity with a diameter of 17.78 cm .....	8
Figure 2.2 TM modes in an empty cavity with a diameter of 17.78 cm .....	8
Figure 3.1 Three-step epoxy curing mechanism .....	40
Figure 3.2 Uncatalyzed and autocatalyzed epoxy curing reaction mechanisms .....	41
Figure 3.3 Circuit of the microwave curing system .....	48
Figure 3.4 A cylindrical single-mode resonant cavity .....	50
Figure 3.5 Mode spectrum of the loaded cavity for microwave curing .....	52
Figure 3.6 Electrical field of TM 020 mode .....	52
Figure 3.7 Electrical field of TM 021 mode .....	53
Figure 3.8 Temperature profiles during microwave cure at 145 °C .....	55
Figure 3.9 Power profiles during microwave cure at 145°C .....	56
Figure 3.10 Extent of cure vs. curing time .....	59
Figure 4.1 Schematic diagram of the Debye model .....	65
Figure 4.2 Schematic diagram of the Davidson-Cole model .....	67
Figure 4.3 Schematic diagram of Cole-Cole plot of the Debye model .....	69
Figure 4.4 Schematic diagram of Cole-Cole plot of the Davidson-Cole model .....	69
Figure 4.5 Schematic illustration of the microwave processing and diagnostic system ...	75
Figure 4.6 Dielectric properties vs. temperature for DGEBA, DDS, and uncured DGEBA/DDS mixture .....	79
Figure 4.7 Temperature dependence of dielectric properties for the DGEBA/DDS epoxy resins at different extents of cure (%) .....	81

Figure 4.8 DGEBA resin curing mechanism .....	82
Figure 4.9 $\epsilon''$ vs. $\epsilon'$ for the DGEBA/DDS epoxy resins at different extents of cure (%)..	87
Figure 4.10 $\ln(\epsilon' - \epsilon_\infty)$ vs. $1000/T$ for the curing DGEBA/DDS system.....	88
Figure 4.11 $\ln(\epsilon'')$ vs. $1000/T$ of the curing DGEBA/DDS system .....	88
Figure 4.12 Comparison between the experimental and calculated dielectric properties of the curing DGEBA/DDS system.....	89
Figure 4.13 Cole-Cole plots for the curing DGEBA/DDS system .....	90
Figure 4.14 $n$ and $(\epsilon_0 - \epsilon_\infty)$ vs. extent of cure for the curing DGEBA/DDS system .....	92
Figure 4.15 $E_a$ vs. extent of cure for the curing DGEBA/DDS system .....	93
Figure 4.16 $\tau$ vs. $1000/T$ for the curing DGEBA/DDS system .....	94
Figure 4.17 Dielectric properties vs. temperature for DGEBA, Jeffamine D-230, and uncured DGEBA/Jeffamine D-230 mixture.....	95
Figure 4.18 Temperature dependence of dielectric properties for the curing DGEBA/Jeffamine system .....	97
Figure 4.19 $\epsilon''$ vs. $\epsilon'$ for the curing DGEBA/Jeffamine system .....	98
Figure 4.20 $\ln(\epsilon' - \epsilon_\infty)$ vs. $1000/T$ for the curing DGEBA/Jeffamine system .....	99
Figure 4.21 $\ln(\epsilon'')$ vs. $1000/T$ for the curing DGEBA/Jeffamine system .....	99
Figure 4.22 Cole-Cole plots for the curing DGEBA/Jeffamine system .....	101
Figure 4.23 $n$ and $(\epsilon_0 - \epsilon_\infty)$ vs. extent of cure for the curing DGEBA/Jeffamine system .	102
Figure 4.24 $E_a$ vs. extent of cure for the curing DGEBA/Jeffamine system .....	103
Figure 4.25 $\tau$ vs. $1000/T$ for the curing DGEBA/Jeffamine system.....	104

Figure 4.26 Dielectric properties vs. temperature for DGEBA, mPDA, and uncured DGEBA/mPDA mixture.....	105
Figure 4.27 Temperature dependence of dielectric properties for the curing DGEBA/mPDA system.....	107
Figure 4.28 $\epsilon''$ vs. $\epsilon'$ for the curing DGEBA/mPDA system.....	108
Figure 4.29 $\ln(\epsilon' - \epsilon_\infty)$ vs. $1000/T$ for the curing DGEBA/mPDA system.....	109
Figure 4.30 $\ln(\epsilon'')$ vs. $1000/T$ for the curing DGEBA/mPDA system.....	109
Figure 4.31 Cole-Cole plots for the curing DGEBA/mPDA system.....	110
Figure 4.32 $n$ and $(\epsilon_0 - \epsilon_\infty)$ vs. extent of cure for the curing DGEBA/mPDA system.....	112
Figure 4.33 $E_a$ vs. extent of cure for the curing DGEBA/mPDA system.....	112
Figure 4.34 $\tau$ vs. $1000/T$ for the curing DGEBA/mPDA system.....	113
Figure 4.35 Dielectric properties vs. temperature for DGEBA, W, and uncured DGEBA/W mixture.....	114
Figure 4.36 Temperature dependence of dielectric properties for the curing DGEBA/W system.....	115
Figure 4.37 Comparison between the experimental and calculated data of the curing DGEBA/W system.....	118
Figure 4.38 $n$ and $(\epsilon_0 - \epsilon_\infty)$ vs. extent of cure for the curing DGEBA/W system.....	119
Figure 4.39 $E_a$ vs. extent of cure for the curing DGEBA/W system.....	120
Figure 4.40 $\tau$ vs. $1000/T$ for the curing DGEBA/W system.....	120
Figure 4.41 $(\epsilon_0 - \epsilon_\infty)$ vs. extent of cure for the four curing systems.....	123
Figure 4.42 $n$ vs. extent of cure for the four curing systems.....	124

Figure 4.43 $E_a$ vs. extent of cure for the four curing systems.....	125
Figure 4.44 $\tau$ vs. extent of cure for the four curing systems at 80°C.....	126
Figure 4.45 Calculated $\epsilon'$ and $\epsilon''$ vs. extent of cure for the four curing systems .....	126
Figure 5.1 Schematic illustrations of four carbon forms .....	130
Figure 5.2 Schematic illustrations of relation between graphite and CNTs .....	131
Figure 5.3 Schematic illustrations of CNTs: (a) SWNT, (b) MWNT. ....	132
Figure 5.4 Schematic illustrations of three SWNTs of different chiralities: (a) armchair, (b) zigzag, (c) chiral. ....	132
Figure 5.5 TEM picture of a bamboo-like carbon tube .....	134
Figure 5.6 Schematic diagram of the MPCVD apparatus at MSU .....	138
Figure 5.7 Photo of the microwave plasma reactor .....	139
Figure 5.8 Photo of the control panel of the microwave plasma reactor .....	139
Figure 5.9 Photo of Si wafer on a graphite substrate.....	141
Figure 5.10 Temperature profile during CNT growth in experiment No. 1-4: solid points represent Si wafer; hollow points represent Ni catalysts. ....	144
Figure 5.11 Optical images of the Si wafers: (a) before CNT growth, after CNT growth in (b) experiment 1, (c) experiment 2, (d) experiment 3, (e) experiment 4, (f) experiment 5. ....	145
Figure 5.12 Optical images of the graphite substrate with Si wafer and Ni catalyst in experiment 3: (a) before CNT growth, (b) after CNT growth.....	146
Figure 5.13 SEM images (45° tilted) at different magnifications of CNTs in sample 1.	147
Figure 5.14 SEM images (45° tilted) at different magnifications of CNTs in sample 2.	147

Figure 5.15 SEM images (45° tilted) at different magnifications of CNTs in (a) sample 3, (b) curled CNT part and (c) aligned CNT part. ....	148
Figure 5.16 TEM images of CNTs in sample 1: (a) body, (b) tip, (c) root.....	150
Figure 5.17 TEM images of CNTs in sample 2: (a) body, (b) tip, (c) root.....	150
Figure 5.18 TEM images of CNTs in sample 3: (a) body, (b) root, (c) root with a catalyst particle. ....	151
Figure 5.19 Schematic illustrations of root-growth mechanism of a bamboo-like CNT	153

## LIST OF TABLES

Table 1.1 Comparison between microwave and thermal heating methods .....	2
Table 3.1 Properties of the reactants at 25°C .....	53
Table 3.2 Time and average power required in the two modes .....	57
Table 3.3 Resonant frequencies of the two microwave modes.....	58
Table 3.4 DSC results of cured epoxy resins.....	59
Table 3.5 Values of the kinetic parameters.....	60
Table 4.1 Properties of the epoxy resin and curing agents .....	76
Table 4.2 DSC results of the curing DGEBA/DDS system.....	81
Table 4.3 Values of the parameters for the curing DGEBA/DDS system.....	91
Table 4.4 DSC results of the curing DGEBA/Jeffamine system.....	96
Table 4.5 Values of the parameters for the curing DGEBA/Jeffamine system .....	102
Table 4.6 DSC results of the curing DGEBA/mPDA system.....	106
Table 4.7 Values of the parameters for the curing DGEBA/mPDA system.....	111
Table 4.8 DSC results of the curing DGEBA/W system .....	116
Table 4.9 Values of the parameters for the curing DGEBA/W system .....	117
Table 5.1 Literature summary on synthesis of CNTs by MPCVD.....	136
Table 5.2 Experimental conditions of the CNT growth.....	142
Table 5.3 CNT growth pressure (Torr).....	143
Table 5.4 CNT growth and catalyst temperatures (°C).....	143
Table 5.5 Summary of morphology, length, and diameter of CNTs .....	146

## CHAPTER 1 INTRODUCTION

Microwaves are one form of electromagnetic radiation. It is a wave motion associated with electric and magnetic forces. Microwave refers to electromagnetic waves in a frequency range from 300MHz to 300GHz or a characteristic wavelength range from 1m to 1mm. Heating is one of the major non-communication applications of microwaves. The fundamental electromagnetic property of nonmagnetic materials for microwave heating and diagnosis is complex dielectric constant ( $\epsilon^* = \epsilon' - j\epsilon''$ ). The real part of the complex dielectric constant is dielectric constant, which is related to the microwave energy stored in the materials. The imaginary part is dielectric loss factor, which is related to microwave energy dissipated as heat in materials. The dielectric loss factor of materials is generally due to contributions from the motion of dipoles and charges, conductivity, etc. Polymers have polar groups to interact with electromagnetic fields and exhibit dielectric relaxation. These polar groups can absorb microwave energy directly and the localized heating on the reactive polar sites can initiate or promote polymerizations that require heat.

Microwave processing of materials has been studied as an attractive alternative to conventional thermal processing. Thermal heating is a surface-driven, non-selective process. The heating efficiency is controlled by the heat transfer coefficient at the material surface and the thermal conductivity of the material. During thermal heating, heat flows from the surface to the interior of the material. This tends to cause remarkable temperature gradients in thick materials. Residual thermal stresses resulting from large temperature gradients will reduce the physical and mechanical properties of the materials.

In addition, the production cycle is long because of the difficulty in heating poor thermal conductors like polymers.

Microwave heating offers a number of advantages over thermal heating in a wide range of heating applications. A comparison between microwave and thermal heating is summarized in Table 1.1. Microwave heating is selective, instantaneous, and volumetric with heat loss at the boundaries while thermal heating is nonselective and depends on temperature gradient. Microwave heating can be easily controlled by fast changes in the applied electric field whereas thermal heating is characterized with long lag times and difficulty for composite cure control. The heat source of microwave heating can be readily removed to prevent thermal excursion. Microwave processing has potential for rapid processing of thick-section and complex-shaped composites.

Table 1.1 Comparison between microwave and thermal heating methods

Thermal heating	Microwave Heating
Heat conduction/convection	Energy coupling/transport
Surface heating	Molecular level coupling
Slow	Fast
Surface	Volumetric
Non-selective	Selective
Less property dependent	Material property dependent
Surface temperature control	Intelligent control
Established technology	Emerging technology

This research is directed towards investigation of microwave processing of polymer and composites. Four specific topics are studied and discussed in the following chapters. The first research topic in Chapter 2 is survey of the research status of microwave processing of polymers and composites. The second research topic in Chapter

3 is study on kinetics of epoxy/amine curing at 2.45 GHz microwave. The third topic in Chapter 4 is modeling the dielectric properties of curing epoxy/amine systems at 2.45 GHz. The fourth topic in Chapter 5 is synthesis of carbon nanotubes using microwave plasma chemical vapor deposition method. The research findings and achievements are summarized in Chapter 6, and suggestions for future work are proposed in Chapter 7.

## CHAPTER 2 BACKGROUND ON MICROWAVE PROCESSING

### 2.1 Electromagnetic Fields in a Microwave Enclosure

Electromagnetic field strength and distribution patterns are essential factors that influence microwave heating efficiency and uniformity. They are determined by microwave operating conditions, applicator dimensions, and material properties. To understand microwave heating characteristics, the fundamentals in microwave processing are reviewed.

#### 2.1.1 Maxwell's Equations

The basic laws governing electromagnetic wave propagation are Maxwell's Equations [1], which describe the relations and variations of the electric and magnetic fields, charges, and currents associated with electromagnetic waves. Maxwell's Equations can be written in either differential or integral form. The differential form, shown as follows, is most widely used to solve electromagnetic boundary-value problems.

$$\nabla \times \mathbf{E} = -\frac{\partial \mathbf{B}}{\partial t} \text{ (Faraday's law)} \quad (2.1)$$

$$\nabla \times \mathbf{H} = \mathbf{J} + \frac{\partial \mathbf{D}}{\partial t} \text{ (Ampere's law)} \quad (2.2)$$

$$\nabla \cdot \mathbf{D} = \rho \text{ (Gauss law)} \quad (2.3)$$

$$\nabla \cdot \mathbf{B} = 0 \text{ (Gauss law - magnetic)} \quad (2.4)$$

where  $\mathbf{E}$  is the electric field intensity,  $\mathbf{H}$  is the magnetic field intensity,  $\mathbf{D}$  is the electric displacement density or electric flux density,  $\mathbf{B}$  is the magnetic flux density,  $\mathbf{J}$  is the electric current density, and  $\rho$  is the charge density.  $\mathbf{D}$  is defined as:

$$\mathbf{D} = \epsilon_0 \mathbf{E} + \mathbf{P} \quad (2.5)$$

where  $\epsilon_0$  is the dielectric constant of free space,  $\mathbf{P}$  is the volume density of polarization, the measure of the density of electric dipoles.  $\mathbf{B}$  can be expressed as:

$$\mathbf{B} = \mu_0 (\mathbf{H} + \mathbf{M}) \quad (2.6)$$

where  $\mu_0$  is the permeability of free space,  $\mathbf{H}$  is the magnetic field intensity, and  $\mathbf{M}$  is the volume density of magnetization, the measure of the density of magnetic dipoles in the material. In a simple isotropic medium, the field quantities are related as follows:

$$\mathbf{D} = \epsilon \mathbf{E} \quad (2.7)$$

$$\mathbf{B} = \mu \mathbf{H} \quad (2.8)$$

where  $\epsilon$  is the dielectric constant, and  $\mu$  is the permeability.

In addition to the Maxwell's Equations, the Equation of Continuity holds due to the conservation of electric charge:

$$\nabla \cdot \mathbf{J} + \frac{\partial \rho}{\partial t} = 0 \quad (2.9)$$

In the Maxwell's Equations, only two are independent. Usually Equations 2.1 and 2.2 are used with Equation 2.9 to solve for electromagnetic fields.

Maxwell's Equations are first-order differential equations with  $\mathbf{E}$  and  $\mathbf{B}$  coupled. They can be converted into uncoupled second-order wave equations through mathematical manipulations:

$$\left[ \nabla^2 - \mu\sigma \frac{\partial}{\partial t} - \mu\epsilon \frac{\partial^2}{\partial t^2} \right] \begin{Bmatrix} \mathbf{E} \\ \mathbf{B} \end{Bmatrix} = \begin{Bmatrix} \nabla \left( \frac{\rho}{\epsilon} \right) + \mu \frac{\partial \mathbf{J}^s}{\partial t} \\ -\mu \nabla \times \mathbf{J}^s \end{Bmatrix} \quad (2.10)$$

where  $\sigma$  is the conductivity, and  $J^s$  is the source current term. In a source free region, Equations 2.10 become:

$$[\nabla^2 - \mu\sigma \frac{\partial}{\partial t} - \mu\epsilon \frac{\partial^2}{\partial t^2}] \begin{Bmatrix} \mathbf{E} \\ \mathbf{B} \end{Bmatrix} = 0 \quad (2.11)$$

Equations 2.1-2.4 are the time-domain representation of Maxwell's Equations. If the source functions,  $J(\mathbf{r}, t)$  and  $\rho(\mathbf{r}, t)$ , oscillate with a constant angular frequency  $\omega$  in the system, all the fields will oscillate at the same frequency. The Maxwell's equations can be written in time-harmonic form:

$$\begin{cases} \nabla \times \mathbf{E}(\mathbf{r}) = -i\omega\mathbf{B}(\mathbf{r}) \\ \nabla \times \mathbf{H}(\mathbf{r}) = \mathbf{J}(\mathbf{r}) + i\omega\mathbf{D}(\mathbf{r}) \\ \nabla \cdot \mathbf{D}(\mathbf{r}) = \rho(\mathbf{r}) \\ \nabla \cdot \mathbf{B}(\mathbf{r}) = 0 \end{cases} \quad (2.12)$$

In time-harmonic case, Equation 2.10 becomes Helmholtz Equations and Equation 2.11 becomes Helmholtz equations in source-free region:

$$[\nabla^2 + \omega^2 \mu\epsilon^*] \begin{Bmatrix} \mathbf{E} \\ \mathbf{B} \end{Bmatrix} = 0 \quad (2.13)$$

$$\epsilon^* = \epsilon(1 - i\frac{\sigma}{\omega\epsilon}) \quad (2.14)$$

where  $\epsilon^*$  is the complex dielectric constant.

### 2.1.2 Resonant Modes in a Cylindrical Single Mode Cavity

In a cylindrical single mode cavity, there are two types of resonant modes, transverse electric (TE) and transverse magnetic (TM). In TE modes, the electric field components are transverse, and the magnetic field components are parallel to the

direction of wave propagation, which is the axial direction. In TM modes, the electric field components are parallel, and the magnetic field components are transverse to the direction of wave propagation. Three subscripts, n, p, and q, are used to represent the physical appearance of the corresponding mode in an empty cavity, i.e.  $TE_{npq}$  and  $TM_{npq}$ . The subscript n denotes the number of the periodicity in the circumferential direction,  $n=0,1,2,\dots$ ; p denotes the number of field zeroes in the radial direction,  $p=1,2,3,\dots$ ; q denotes the number of half wavelengths of the equivalent circular waveguide,  $q=0,1,2,\dots$  for TM modes and  $q=1,2,3,\dots$  for TE modes.

Theoretically the relationship between the frequency and cavity diameter and length for a given resonant mode can be calculated. The equations for TE and TM modes in an empty cylindrical single mode cavity [2] are:

$$(f)_{npq}^{TE} = \frac{1}{2\pi a \sqrt{\mu\epsilon}} \sqrt{x'_{np}{}^2 + \left(\frac{q\pi a}{h}\right)^2} \quad (2.15)$$

$$(f)_{npq}^{TM} = \frac{1}{2\pi a \sqrt{\mu\epsilon}} \sqrt{x_{np}{}^2 + \left(\frac{q\pi a}{h}\right)^2} \quad (2.16)$$

where f is frequency, a is cavity diameter, h is cavity height,  $x_{np}$  and  $x'_{np}$  are tabulated zeros of the Bessel's function and the derivative of the Bessel's function, respectively.

Images in this dissertation are presented in color. Figure 2.1 and Figure 2.2 show the previous research results at Michigan State University (MSU) about the relation between resonant frequency of some TE and TM modes and cavity length in an empty cavity with a diameter of 17.78 cm.

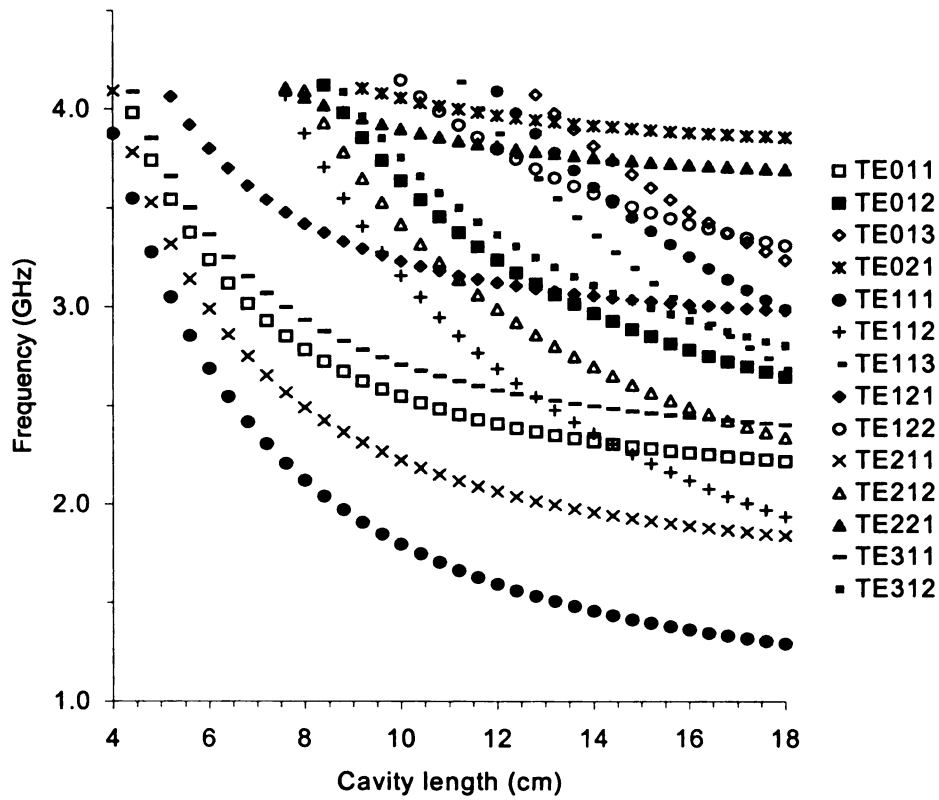


Figure 2.1 TE modes in an empty cavity with a diameter of 17.78 cm

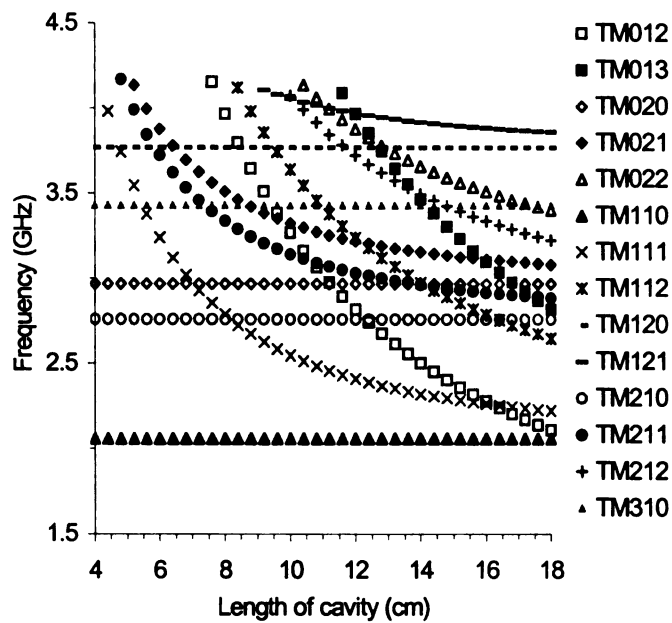


Figure 2.2 TM modes in an empty cavity with a diameter of 17.78 cm

### 2.1.3 Electromagnetic Fields in a Cylindrical Single Mode Cavity

In a homogeneous, source-free cylindrical single mode cavity with perfectly conducting walls, the electromagnetic fields inside the cavity can be derived from Maxwell's equations and boundary conditions.

In TE modes, the electromagnetic field components inside an empty cavity are [2]:

$$\begin{aligned}
 H_{\rho} &= \frac{1}{z} \frac{\partial^2 \psi_{npq}}{\partial \rho \partial z} & E_{\rho} &= -\frac{1}{\rho} \frac{\partial \psi_{npq}}{\partial \phi} \\
 H_{\phi} &= \frac{1}{z} \frac{1}{\rho} \frac{\partial^2 \psi_{npq}}{\partial \phi \partial z} & E_{\phi} &= \frac{\partial \psi_{npq}}{\partial \rho} \\
 H_z &= \frac{1}{z} \left( \frac{\partial^2 \psi_{npq}}{\partial z^2} + k^2 \psi_{npq} \right) & E_z &= 0
 \end{aligned} \tag{2.17}$$

where  $(\rho, \phi, z)$  are the cylindrical coordinates,  $\hat{z} = j\omega\mu$ ,  $k^2 = \omega^2\mu_0\varepsilon$ , and  $\psi_{npq}$  is the wave potential for TE<sub>npq</sub> modes:

$$\psi_{npq} = J_n\left(\frac{x_{np}}{a} \rho\right) \begin{cases} \sin n\phi \\ \cos n\phi \end{cases} \sin\left(\frac{q\pi}{h} z\right) \tag{2.18}$$

where  $a$  is the diameter, and  $h$  is the height of the cavity.

In TM modes, the field components inside an empty cavity are [2]:

$$\begin{aligned}
E_\rho &= \frac{1}{\hat{y}} \frac{\partial^2 \psi_{npq}}{\partial \rho \partial z} & H_\rho &= \frac{1}{\rho} \frac{\partial \psi_{npq}}{\partial \phi} \\
E_\phi &= \frac{1}{\hat{y}} \frac{1}{\rho} \frac{\partial^2 \psi_{npq}}{\partial \phi \partial z} & H_\phi &= -\frac{\partial \psi_{npq}}{\partial \rho} \\
E_z &= \frac{1}{\hat{y}} \left( \frac{\partial^2 \psi_{npq}}{\partial z^2} + k^2 \psi_{npq} \right) & H_z &= 0
\end{aligned} \tag{2.19}$$

where  $\hat{y} = j\omega\epsilon$ , and  $\psi_{npq}$  is the wave potential for  $\text{TM}_{npq}$  modes:

$$\psi_{npq} = J_n\left(\frac{x_{np}}{a}\rho\right) \begin{Bmatrix} \sin n\phi \\ \cos n\phi \end{Bmatrix} \cos\left(\frac{q\pi}{h}z\right) \tag{2.20}$$

When the cavity is loaded with materials, Equations 2.17-2.20 are no longer applicable. For simple materials, analytic methods are useful for calculating the electromagnetic field inside the materials and the cavity. For complex situations (inhomogeneous or anisotropic materials, irregular shapes, etc.), numerical techniques are usually used to solve for the electromagnetic field. The most widely used numerical techniques include the method of moments, the finite-element method, and the finite difference method.

## 2.2 Microwave/Materials Interactions

### 2.2.1 Mechanisms of Microwave/Materials Interactions

Materials are classified into conductors, semiconductors and dielectrics according to their electric conductivity. Conductors contain free charges, which are conducted

inside the material under alternating electric fields so that a conductive current is induced. Electromagnetic energy is dissipated into the materials while the conduction current is in phase with the electric field inside the materials. Dissipated energy is proportional to conductivity and the square of the electric field strength. Conduction requires long-range transport of charges.

In dielectric materials, electric dipoles, which are created when an external electric field is applied, will rotate until they are aligned in the direction of the field. Therefore, the normal random orientation of the dipoles becomes ordered. These ordered polar segments tend to relax and oscillate with the field. The energy used to hold the dipoles in place is dissipated as heat into the material while the relaxation motion of dipoles is out of phase with the oscillation of the electric field. Both the conduction and the electric dipole movement cause losses and are responsible for heat generation during microwave processing. The contribution of each loss mechanism largely depends on the types of materials and operating frequencies. Generally, conduction loss is dominant at low frequencies while polarization loss is important at high frequencies. Most dielectric materials can generate heat via both loss mechanisms.

There are mainly four different kinds of dielectric polarization:

1. Electron or optical polarization occurs at high frequencies, close to ultraviolet range of electromagnetic spectrum [3, 4]. It refers to the displacement of the electron cloud center of an atom relative to the center of the nucleus, caused by an external electric field. When no electric field is applied, the center of positive charges (nucleus) coincides with the center of negative charges (electron cloud). When an

external electric field is present, the electrons are pushed away from their original orbits and electric dipoles are created.

2. Atomic polarization is also referred to as ionic polarization. It occurs in the infrared region of the electromagnetic spectrum. This type of polarization is usually observed in molecules consisting of two different kinds of atoms. When an external electric field is applied, the positive charges move in the direction of the field and the negative ones move in the opposite direction. This mainly causes the bending and twisting motion of molecules. Atomic polarization can occur in both non-ionic and ionic materials. The magnitudes of atomic polarization in non-ionic materials are much less than that in ionic or partially ionic materials.

3. Orientation or dipole alignment polarization occurs in the microwave range of the electromagnetic spectrum. It is the dominant polarization mechanism in microwave processing of dielectrics. Orientation polarization is usually observed when dipolar or polar molecules are placed in an electric field. At the presence of external electric field, the dipoles will rotate until they are aligned in the direction of the field. The dipolar rotation of molecules is accompanied by intermolecular friction, which is responsible for heat generation. Orientation polarization is fundamentally different from electronic and atomic polarization. The latter is due to the fact that the external field induces dipole moments and exerts displacing force on the electrons and atoms, while the orientation polarization is because of the torque action of the field on the pre-existing permanent dipole moments of the molecules.

4. Interfacial or space charge polarization occurs at low frequencies, e.g. radio frequency (RF). It is a fundamental polarization mode in semiconductors. This type

of polarization is caused by the migration of charges inside and at the interface of dielectrics under a large scale field.

### 2.2.2 Dielectric Properties

Most polymers and composites are non-magnetic materials. The electromagnetic energy loss is only dependent on the electric field. Incident electromagnetic fields can interact with conductive and nonconductive materials. The fundamental electromagnetic property of nonmagnetic materials for microwave heating and diagnosis is the complex dielectric constant:

$$\varepsilon = \varepsilon' - j\varepsilon'' \quad (2.21)$$

The real part of the complex dielectric constant is dielectric constant. The higher polarizability of a molecule, the larger its dielectric constant. The imaginary part is dielectric loss factor, which is related to energy dissipated as heat in the materials. Usually, the relative values with respect to the dielectric constant of free space are used:

$$\varepsilon = \varepsilon_0(\varepsilon_r' - j\varepsilon_{eff}'') \quad (2.22)$$

where  $\varepsilon_0$  is the dielectric constant of free space,  $\varepsilon_r'$  is the relative dielectric constant, and  $\varepsilon_{eff}''$  is the effective relative dielectric loss factor. The loss factor of materials consists of both polarization and conduction loss. The polarization loss is further contributed by all four polarization mechanisms mentioned earlier. The effective relative loss factor is expressed as [4]:

$$\varepsilon_{eff}''(\omega) = \varepsilon_d''(\omega) + \varepsilon_e''(\omega) + \varepsilon_a'' + \varepsilon_s'' + \frac{\sigma}{\varepsilon_0\omega} \quad (2.23)$$

where the subscripts d, e, a, and s refer to dipolar, electronic, atomic and space charge polarization, respectively. The loss factor is a function of material structures, compositions, angular frequency, temperature, pressure, etc.

The ratio of the effective loss factor to the dielectric constant is defined as the loss tangent, which is also commonly used to describe dielectric losses:

$$\tan \delta_{eff} = \frac{\epsilon''_{eff}}{\epsilon'_r} \quad (2.24)$$

When introduced into a microwave field, materials will interact with the oscillating electromagnetic field at the molecular level. Different materials will have different responses to the microwave irradiation. Microwave heating of conductive materials, such as carbon fibers and acid solutions, is mainly due to the interaction of the motion of ions or electrons with the electric field. However, conductors with high conductivity will reflect the incident microwaves and can not be effectively heated.

The fields attenuate towards the interior of the material due to skin effect, which involves the magnetic properties of the material. The conducting electrons are limited in the skin area to some extent, which is called the skin depth,  $d_s$ . Defined as the distance into the sample, at which the electric field strength is reduced to  $1/e$ , the skin depth is given by [2]:

$$d_s = \frac{1}{\left(\frac{1}{2}\omega\mu_0\mu'\sigma\right)^{\frac{1}{2}}} \quad (2.25)$$

where  $\omega$  is the frequency of the electromagnetic waves in rad/sec,  $\mu_0$  ( $=4\pi 10^{-7}$  H/m) is the permeability of the free space,  $\mu'$  is the relative permeability, and  $\sigma$  is the conductivity of

the conductor in mhos/m. For example,  $\sigma = 7 \times 10^4$  mhos/m and  $d_s = 38.4 \mu\text{m}$  for graphite at 2.45 GHz in a free space. The skin depth decreases as frequency increases. For a perfect conductor, the electric field is reflected and no electric field is induced inside a perfect conductor at any frequency. Therefore, no electromagnetic energy will be dissipated even though the conductivity of the perfect conductor is infinite.

Microwave heating of nonconductive materials, such as polymers, glass fibers, and Kevlar fibers, is mainly due to the interaction of the motion of dipoles with the alternating electric field. Microwave processing of thermosets is self-adjusting. As the crosslinking occurs, the mobility of dipoles decreases because of the “trapping” or reaction and the dielectric loss factor decreases. Energy absorbed by crosslinking molecules decreases and microwaves are concentrated in unreacted molecules. During microwave processing of thermoplastics, the dielectric loss factor usually increases with temperature and thermal runaway is likely to occur. Thermal runaway can be prevented by decreasing or even turning off power at a temperature close to thermal excursion. Microwave heating selectivity of polymer composites depends on the magnitude of dielectric loss factor of polymers and fibers. When non-conducting fibers, such as glass, are used, microwaves will selectively heat the polymer matrix. When conducting fibers like graphite are used, energy is preferably absorbed by the conductive fibers and heat is conducted from the fiber to the matrix. In this case, loss factor is mainly due to the fiber conductivity and can not be used to diagnose the curing process of the low loss matrix materials.

Dielectric measurement of epoxy curing systems has shown that generally both the dielectric constant and dielectric loss factor increase with temperature and decrease

with extent of reaction [5]. This dependence on temperature and extent of reaction is non-linear. During microwave processing, the dielectric properties of materials change as a result of heating and reaction. This affects the electrical field strength and power absorption in the materials. The change in electric field and power absorption in turn affects the temperature and extent of reaction inside the materials. Thus, the modeling of microwave heating is a coupled non-linear problem, which involves Maxwell's equations for solving the electric field strength, a heat transfer equation for obtaining the temperature distribution inside the material, and a reaction kinetic equation for calculating extent of reaction.

### **2.3 Literature Survey**

Within the portion of the electromagnetic spectrum, frequencies are used for communication and non-communication applications. Major non-communication applications exist in medicine and heating. Two frequencies, 0.915 and 2.45 GHz, are most widely used for microwave heating. However, other frequencies including 5.8, 24.125, 61.25, 122.5, and 245.0 GHz are also reserved by the Federal Communications Commission (FCC) for industrial, scientific, and medical (ISM) applications [6].

Microwave processing is well established in the food, rubber, textile, and wood products industries. Studies of microwave processing of polymeric materials in the early 1960s led to a successful industrial application in the rubber industry. Since the mid-1980's, there has been a great deal of interest in microwave processing of polymeric materials worldwide. The discipline can be categorized in two major fields: microwave-assisted polymer physics (MAPP) and microwave-assisted polymer chemistry (MAPC).

In the field of MAPP, microwave heating is used to assist the dissolution of polymers in such solvents as water and nitric acid. The polymer dissolution is a sample preparation step prior to analysis such as multi-element determination of major elements in polymer additives and polymers, and molecular weight [7-11]. Microwave heating is also used to extract additives from polymers and dry polymers [12-18].

### **2.3.1 Polymer Dielectric Properties**

Dielectric properties of polymers are important for microwave processing, especially the polymers used in electronic components. The dielectric properties change during processing. As thermosets are curing, their dielectric loss factors decrease significantly because of the formation of crosslinking structures. Thus, thermosets absorb less microwave energy so that the reaction is self-quenching. During microwave heating of semicrystalline thermoplastics, heating can be difficult until a critical temperature is reached, where the loss factor increases significantly [19, 20]

Polymers are usually not used as neat materials in commercial applications. Additives are generally used in the resin formulation and the resulting composites may have improved thermal, mechanical, and dielectric properties. The dielectric loss factor of neat polymers is usually small. For example,  $\epsilon''$  of the diglycidyl ether of bisphenol A (DGEBA) epoxy at 2.45 GHz at room temperature microwave is 0.21 [21].  $\epsilon''$  of Nylon 66 at 3 GHz at room temperature is 0.039 and that of polystyrene is 0.00085 [2]. Conducting species have much larger dielectric loss factors than polymers. A small amount of these species can be added into polymers to improve the dielectric loss. In iodine doped polyblends of polystyrene (PS) and polymethylmethacrylate (PMMA),  $\epsilon'$

and  $\epsilon''$  increase as iodine percentage increases. This can be attributed to the complex formation in polymer due to iodine doping [22]. Carbon black is an important conducting material that can increase dielectric properties of polymers [23-27]. Filler materials, e.g. aluminum, copper, and silver, can be also blended with polymers. The dielectric properties of the composite materials have been investigated as a function of volume fraction and frequency. Normally, dielectric properties do not increase readily when a trace amount of fillers are used, but increase significantly as the fillers are further added until a saturation point is reached. Dielectric properties also vary with changing frequency nonlinearly. Furthermore, they were found to depend on inclusion dispersion microstructure as well as constitutive properties [28-33].

Negi et al. prepared low glass-transition-temperature ( $T_g$ ) polymer composites with relatively high dielectric constants, which could be modulated reversibly by voltage variation. Polymers are glassy (hard and brittle) below  $T_g$ , and rubbery (soft and flexible) above  $T_g$ . These polymers could be used in electronic devices [34-36]. The dielectric constant and loss factor of poly (vinylidene fluoride) films decrease as frequency increases from 4 to 13 GHz [37]. The dielectric properties of conductive polyaniline and its composites have been studied [38-40]. Sengwa et al. studied microwave dielectric relaxations in binary mixtures of poly (ethylene glycols) in solution [41-43].

Measuring dielectric properties of polymer composites can be used as a standard nondestructive testing technique to determine the stratified structure of composites [44], molecular orientation and dielectric anisotropy [45], the quality of materials such as porosity and defect dimensions [46-49], and process control [50].

## 2.3.2 Microwave-Assisted Polymer Processing

### 2.3.2.1 Thermosets

Most of research on microwave processing of polymer composites focuses on thermosets. The commonly observed advantages of microwave processing are shortened processing time, and improved properties [51, 52]. Although some studies suggested that microwaves did not change the reaction rate [53], many reports concluded that the cure speed is faster in microwave cure than in thermal cure. Thermosets cured under microwave irradiation include epoxies [54-81], polyesters [82, 83], polyimides [84-87], polyurethanes [88], and others [19, 89-91].

### 2.3.2.2 Reaction Rate and Kinetics

Kinetic models about microwave curing of thermosets are either mechanistic or phenomenological. Mechanistic models are obtained based on reaction mechanisms. The key point is the assumption of free radical polymerization. Several researchers tried to use the concept to model the cure process of thermosetting resins [81]. However, derivation of mechanistic models can be difficult or even impossible because of the complexity of cure reactions. In most cases, phenomenological models are preferred in the studies of curing because they are simpler [81]. Among phenomenological models [74], a semi-empirical has been widely used to represent the cure kinetics of epoxy with unsaturated polyesters:

$$\frac{d\alpha}{dt} = (k_1 + k_2\alpha^m)(1-\alpha)^n \quad (2.26)$$

where  $\alpha$  is the degree of cure,  $t$  is time,  $k_1$  and  $k_2$  are rate constants with Arrhenius temperature dependency, and  $m$  and  $n$  are constants independent of temperature.

Wei et al. at MSU [78, 79] reported that stoichiometric mixtures of DGEBA (diglycidyl ether of bisphenol A) with DDS (diaminodiphenyl sulfone) and mPDA (meta phenylene diamine) were isothermally cured by microwave and conventional heating. Microwave heating enhanced the reaction rates of both systems and a phenomenological model was used to fit the experimental data. Hedreul et al., who studied the reaction kinetics of DGEBA/DDS and rubber-modified epoxy, reached the same conclusion that the phenomenological models fitted the experimental results well [59]. Fang et al. reported the reaction kinetics of a phenylethynyl-terminated imide model compound and an oligomer, and carbon fiber reinforced polyimide composites. Microwave heating gave a much higher reaction rate for both systems than thermal heating [92, 93]. The kinetic studies of the crosslinking of a nadic end-capped imide model compound in microwave heating and thermal heating were investigated. At the same temperature, the reaction rate is about 10 times faster in the microwave heating than in the thermal heating [86]. The kinetics of simultaneous polymerization and degradation of PMMA under microwave radiation were studied. A model was developed to predict the change of molecular weight distribution [94]. Other studies made the same conclusion that the microwave heating can shorten cure time and enhance reaction rate compared to thermal heating [76, 82, 83]. However, Mijovic et al. claimed that there is no difference between microwave and thermal heating methods for processing polymers including epoxies, polyimides, and bismaleimides [53].

Some high dielectric loss materials were added into polymer systems to increase heat absorption during microwave processing. Liu et al. studied glass-graphite-polyimide composites and found that a small quantity of absorber, chopped carbon fiber, can accelerate the cure dramatically. Furthermore, soapstone mold material was found to be an efficient absorber to accelerate the cure process [87]. Thermoplastics that contain even modest polar groups can also be used as additives to accelerate the cure rate of epoxy under microwave heating [67]. In contrast, the effects of carbon black concentration on microwave curing of DGEBA/DDS were studied [95]. The magnitude of the dielectric properties increased drastically and the reaction rate constants decreased as concentration of carbon black increased.

Pultrusion is a continuous manufacturing process and important to industrialize microwave processing of polymer composites. Microwave-assisted pultrusion of a number of glass reinforced epoxy composites was studied and the pulling force was about an order of magnitude smaller than for conventional pultrusion. It is stated that the pulling force reflects a stick-slip mechanism for the crosslinked composites within the MAP die and a slip mechanism for the uncrosslinked composites [70, 71].

### **2.3.2.3 Properties**

Fang et al. reported that higher  $T_g$ , flexible strength, moduli, and shear strength were observed in the microwave-cured composites than in the thermal-cured composites [92]. MSU researchers [58, 78, 79] reported that stoichiometric mixtures of DGEBA/DDS and DGEBA/mPDA were isothermally cured by microwave radiation and conventional heating using thin film sample configurations. While similar  $T_g$  for both

heating methods was obtained at low conversion, higher  $T_g$  was observed in microwave cured samples at an extent of cure larger than 0.6. However,  $T_g$  was similar for microwave and thermal cured poly (methyl methacrylate) (PMMA) [72]. The interfacial properties of Kevlar fiber reinforced epoxy composites post-cured by both conventional and microwave heating were examined [55]. The interfacial shear strengths and critical lengths of the microwave post-cured composites are comparable with those for thermally post-cured ones. Similarly, regarding the impact and flexural strengths, the new microwave-heated polyurethane-based polymer offered no advantage over the existing thermal-heated and microwave-heated PMMA-based denture base polymers. But, it has rigidity comparable to that of the microwave-polymerized PMMA [88]. The average particle size of microwave-heated PMMA was much larger and the particle size distribution was narrow and nearly symmetrical. Morphology of DGEBA/DDS epoxy composites versus microwave heating rate was studied [60]. The heating rate did not have a strong influence on morphology. But morphology of thermoplastic toughened DGEBA/DDS epoxy can be controlled by varying the microwave power [67].

#### **2.3.2.4 Monitor and Heat Transfer Model**

To monitor the cure of polymer composites, a Time-Domain-Reflectometry system was studied [96]. During microwave processing of polymer composites, high temperatures due to exothermic cure reaction can degrade the mechanical properties of the composite. To control the reaction and ensure uniformity of polymer composite materials, temperature was obtained. Using the temperature information, the occurrence of material degradation due to resin over-temperature can be reduced. In addition, a

theoretical model is presented that helps elucidate the influence of the microwave parameters on the temperature profile [97]. The improper control of microwave processing of polymers, especially thick polymer laminates, can lead to quality control problems, such as the formation of voids, non-uniform heating, and over curing. The control system for microwave curing of polymer composites has been studied. In particular, some quality and production issues, and the control of the process parameters, e.g. pressure and temperature, were discussed [98].

Pichon et al. presented a practical electromagnetic-thermal simulation of microwave heating during the curing process of polymer resin. The model is based on finite elements developed for the case of asymmetric geometries and fields [99]. Joly et al. also used the finite element method to model a heat transport phenomenon in a polymer sample heated by microwaves [100, 101]. To understand microwave cure reaction kinetics properly, the results for both microwave and thermal curing polymer were related by obtaining a temperature equivalent value using a phenomenological logarithmic approach [102]. A finite difference numerical simulation was developed to predict the one-dimensional transient temperature profile of the composite laminate during both microwave and thermal heating. Numerical and experimental results were presented for a glass/epoxy laminate with the thickness of 25 mm. It is possible to cure thick laminate composites uniformly and eliminate temperature excursions caused by exothermic reaction [77]. To simulate microwave heating of Nylon-6 inside a ridge waveguide, Maxwell's electromagnetic equations were coupled to the heat transfer equation and solved numerically [86]. A program to control the temperature for microwave curing of an epoxy has also been developed [103].

### **2.3.2.5 Thermoplastics**

The heating characteristics during microwave processing of thermoplastics are different from those of thermosets due to different dielectric behavior during heating. During microwave heating of semicrystalline thermoplastics, heating can be difficult until a critical temperature is reached, at which point the loss factor increases significantly [20]. The critical temperature is related to increased molecular mobility but is not necessarily the same as  $T_g$  of the polymer. If the critical temperature is above  $T_g$ , rapid heating rates can be obtained until the melting temperature of the polymer is reached. Usually, amorphous polymer can be heated more effectively than semicrystalline polymers [104]. The reason might be that the molecules in amorphous polymers are not restricted by the crystal lattice and thus are more mobile. O'Brien et al. used dual beam microwaves to heat glass mat thermoplastic sheets, reducing cycle times up to 60% [105]. Microwaves are also used to process foamable thermoplastics and thermosets [106].

### **2.3.2.6 Composites Bonding**

To bond composite by microwave, a conductive polymer is placed between the parts being joined to serve as a preferential site for electromagnetic energy absorption. Sufficient heat can be generated to weld the joint without heating the entire part, therefore shortening process time and limiting the part distortion [104, 107-109]. Staicovici et al. studied welding and disassembly of high density polyethylene (HDPE) bars, placing an electromagnetic absorbent material polyaniline at the interface. By controlling the amount of remaining polyaniline at the interface, the welded samples can

be placed in the microwave, reheated, and disassembled for recycling and reuse [110-112].

Zhou et al. at MSU studied microwave adhesive bonding, using a glass reinforced ethylene/methacrylic acid copolymer, and a nylon 6 and ethylene/methacrylic acid copolymer as the substrates and an epoxy based material as the adhesive [21, 113]. Significantly shorter bonding times and stronger bonds were obtained. Furthermore, unlike single mode microwaves, variable frequency microwaves (VFM) can obtain uniform heating in microwave adhesive bonding of large-size materials. Similar results were obtained for bonding urethane-based glass fiber composite panels and fiberglass reinforced polyester panels using VFM [114]. VFM can also produce strong bonds for polystyrene and low-density polyethylene [115]. Shanker and Lakhtakia used extended Maxwell Garnett formalism to predict the dielectric constant of a metal-dope composite adhesive for joining polymers [116].

### **2.3.3 Microwave-Assisted Polymer Synthesis**

Traditionally, polymer synthesis can be divided into polycondensation and polyaddition. For polycondensation, the repeating unit of a polymer lacks certain atoms which are present in the monomers. For polyaddition, however, the repeating unit of a polymer has same macromolecular structure as the monomers forming the polymer.

Microwave-assisted polycondensation of benzoguanamine and pyromellitic dianhydride has been studied. It is found that compared with thermal heating method, microwave-assisted polymerization not only had faster heating and complete imidization, but saved time and resources as well [117]. Mallakpour et al. used microwave radiation to

synthesize a number of novel optically active and thermally stable poly (amide-imide)s and poly(ester-imide)s. The microwave-assisted polycondensation proceeded rapidly and resulted in a high yield of products [85, 118-124]. Poly (arylene ether sulfone) functionalized with either hydroxyl or t-butylphenyl end group was synthesized. Microwave processing of the unmodified polymers resulted in fast reaction rates but incompletely cured products. However, in the thermoplastic-modified networks, the addition of the thermoplastic led to vastly improved control over system temperature and therefore fully cured products with high reaction rates. Furthermore, networks generated with a faster cure had much finer morphologies [125]. Phase transfer catalysis (PTC) is frequently used in the synthesis of polymers. The polycondensation of polyethers by microwave-assisted PTC had shortened reaction time, did not require stirring, and resulted in larger molecular-weight products [126]. Microwave radiation was also used in the solid state polyether-ester polyamic acid imidization, resulting in decreased reaction temperature and reaction time [127]. Others achieved a similar result that microwave radiation can reduce the reaction time of the imidization of polyamic acids [128]. A new rapid synthesis of aliphatic polyamides was presented by the microwave-assisted polycondensation of  $\omega$ -amino amides and nylon salts in the presence of a small amount of a polar organic medium as a primary microwave absorber. The reaction proceeded faster than the conventional method [129-131].

Ring-opening polyaddition of  $\epsilon$ -caprolactone was investigated with a microwave furnace at 2.45 GHz. The polymerization was accelerated and improved dramatically by microwave heating [132]. A similar open-ring synthesis of Poly ( $\epsilon$ -caprolactam-co- $\epsilon$ -caprolactone) was carried out with a VFM oven. Compared with the thermal heating

products, microwave-assisted copolymers had equivalent molecular weight, but higher yield, amide composition, and  $T_g$  [93]. Jacob, Chia, and Boey studied microwave-assisted polymerization of poly (methyl acrylate) (PMA), polystyrene (PS), and polymethylmethacrylate (PMMA). Microwave heating can accelerate reaction rates and the “microwave effect” increased as the power increased [133].

Cationic polymerization of epoxies under microwave irradiation was studied by Stoffer et al. Reaction selectivities, and reaction temperature shifts at different microwave powers were observed [134, 135]. Solid state polymerization of poly (ethylene terephthalate) (PET) and nylon 66 was studied. Theoretical analysis and experimental data show that the increase in the reaction rate under microwave radiation was not caused by an increase in the bulk temperature, but by enhanced diffusion rates due to direct heating of condensate [68]. Microwave can reduce the reaction time and help obtain good yields of products used to synthesize conjugated polymers such as polyphenylacetylene, which has interesting optical and electrical properties [136]. Microwave is also used in the field of solution polymerization [137, 138]. A study of emulsion polymerization of PS in a polar solvent concluded that the reaction could be carried out rapidly using microwave radiation [139].

Copolymerization mechanism of dibutyltin maleate and allyl thiourea was studied. The copolymer may be used as soluble polymer agents for metal ions. Effect of composition of the feed, the power and time of microwave radiation on conversion and intrinsic viscosity was investigated [140-142]. Graft copolymerization of hydroxyethyl methacrylate onto wool fabrics was studied. Microwave heating could improve the reactivity of the monomer. The influence of various parameters of reaction including

time, microwave intensity, catalyst, and monomer concentration on reaction were investigated [143]. Microwave was used to initiate the copolymerization of methyl methacrylate and 2-hydroxyethyl methacrylate monomers. The product was obtained in a very short time and the molecular weight was almost double the values obtained by thermal heating reactions [144]. Microwave can be used to obtain porous biodegradable polymer composites with adequate micro- and macro-porosity and promising mechanical properties, which may be used in the biomaterials field [145].

#### **2.3.4 Microwave Plasma Modified Polymer Surface**

Polymer materials are inexpensive and normally easy to process. They have excellent physical and chemical properties and can be used in such industries as plastics, rubber, fiber, adhesive, medicine, etc. But, polymers may not have surface properties needed for some special applications, e.g. stability, adhesion, special surface energy, wettability, and biocompatibility. Therefore, research on technologies to modify polymer surface is important for polymer applications. The ultimate goal of plasma modification is to produce polymer materials with chosen bulk properties and with particular surface properties. Microwave plasma at low temperatures has become an interesting and effective method to modify polymer surface. Different types of gases are used to produce plasma. The depth of modified polymer surface is usually several hundred angstroms and the bulk properties of the polymers are not changed [146-148].

The microwave plasma is used to modify the surface properties of polymers, such as durable surface, adhesion, surface tension, wettability, wear resistance, and biocompatibility.

In order to obtain a durable, functional surface of poly (tetrafluoroethylene) (PTFE), water microwave plasma has been used to modify PTFE films. The water plasma introduces functional groups and radicals, serving as reactive species for the gas phase graft polymerization of acrylic acid. A homogeneous and stable poly (acrylic acid) (PAAC) layer with a thickness of about 70 nm was generated on the surface of PTFE foils [149]. A study of vacuum plasma and atmospheric pressure plasma modifying polymer surface showed that VFM-assisted nonequilibrium plasmas (APNEPs) at atmospheric pressure could be effective in modifying polymer surfaces. The source gases were air, nitrogen, argon, helium and gas mixtures. Polymers were LDPE, HDPE, PMMA, polypropylene (PP), and PET. VFM APNEP can clean polymer surface, form durable surface, and, thus, enhance surface energy [150]. Oxidation of polymer surface is an effective method to protect polymers from oxidative degrading. A facile method of the surface oxidation of PE and PP in the solid phase was developed, using potassium permanganate as an oxidizing agent. The oxidation did not affect thermal properties of the polymer [120, 122]. Polydimethylsiloxane (PDMS) is usually used as outdoor high-voltage composite insulator. Exposure of PDMS to oxygen can cause a loss of hydrophobicity and thus accelerate aging. To simulate the aging mechanism, oxygen microwave plasma was used to treat PDMS materials. The oxidized surface layer with a thickness of 130-160 nm was thinner after longer plasma exposure [151]. Hollander et al. studied the mechanism of oxidation of PP and PE by oxygen plasma and concluded that short wavelength radiation contributed appreciably to the surface modification [152]. Lianos et al. also studied the mechanisms of modification by remote oxygen microwave

plasma on LDPE, PS, and PMMA. The relative density of ground state atomic oxygen in the plasma initiated the oxidation [153].

A coating of polymers is often required to provide additional functional properties, such as a barrier against permeation of gases, controlled optical properties, and abrasion resistance. The permeation of water and other gases leads to aging of plastic packaging materials. To enhance the stability of PEC and polycarbonate (PC), a new multilayer coating system using microwave plasma was investigated and proved effective to prevent oxygen and water from diffusing into the polymers [154]. A dual microwave/radio frequency (MW/RF) reactor was designed to deposit an optical thin film on polymer substrates [155]. The deposition of silicon alloys for protective and optical coatings on polymers is an interesting topic. The influence of  $N_2$ ,  $H_2$ , and  $O_2$  plasma modification on pure and commercial PC was investigated to enhance the adhesion of plasma deposited silica films. The major influence of plasma on pure PC was chain scission and that on commercial PC was crosslinking, in which additives in commercial PC played a major role [156]. Adhesion of amorphous hydrogenated silicon nitride ( $SiN_{1.3}$ ) and oxide ( $SiO_2$ ) films on PC and on silicon substrates, by using a dual-mode MW/RF plasma system, has also been studied. The goal was to get a controllable adhesion and optical properties of the interface. The adhesion strength was a function of the substrate material and the energy of bombarding ions, and related to the mechanical properties of the films [157]. The plasma-treated PC contains a crosslinked surface layer with a depth of 50 nm and a less dense transition region between the polymer and the film. The thickness of this interface layer was about 100 nm [158].

The study of adhesion at metal-polymer interfaces is of great interest. In general, modification of the polymer surface with inert gas plasma prior to metal deposition can improve the adhesion properties of the metal-polymer interfaces. A study of surface modification of fluoropolymers including PTFE by the remote hydrogen plasma showed that the treatment can improve adhesion of copper metal and the polymers [159].

Surface wettability and adhesive properties of polyamides were improved by ammonia and nitrogen/oxygen microwave plasma [160]. To improve adhesion of PET and metals, such as Ag, nitrogen and argon plasmas were deposited on a PET substrate [161]. Low pressure plasmas were used to improve adhesion of a fluoropolymer and Cu. Nitrogen was most efficient among all the gases used, e.g. N<sub>2</sub>, O<sub>2</sub>, N<sub>2</sub>/H<sub>2</sub>, O<sub>2</sub>/H<sub>2</sub>, and H<sub>2</sub>. The reasons of the improvement may be surface cleaning, increased wettability, and the formation of chemical linkages at the interface [162]. Argon plasma treatment on PC could improve adhesion of PC with metals, possibly caused by crosslinking in the plasma treated surface [163].

Mechanical properties and T<sub>g</sub> of composites of cellulose and polymers such as PS, PP, and chlorinated polyethylene (CPE) were improved if cellulose fibers were treated by ammonia, nitrogen, and methacrylic acid (MMA) plasmas [164]. Microwave plasma can treat polymer fillers, such as, CaCO<sub>3</sub>, TiO<sub>2</sub>, and carbon black, to improve adhesion of fillers with polymer matrix, and therefore improve mechanical properties of the composites [165]. The wettability of PE can be modified by oxygen plasma and the radio frequency can achieve much faster treatment than microwave plasma [166]. The wettability of poly (ether ether ketone) (PEEK), PC, PMMA [167], and poly

(phthalazinone ether sulfone ketone) (PPESK) [168] were improved by microwave plasma treatment.

The wear resistance of PMMA was improved by microwave plasma treatment of the surface. The agent was plasma of CH<sub>4</sub> diluted in Ar gas, which foamed a transparent polymer-like carbon film on the PMMA surface [169]. Scratch-resistant PC films were achieved by remote argon plasma modification on the PC surface. A good sticking interface polymer layer grew with argon discharging [170]. MW/RF plasma technology can also be used to remove polymers effectively from a material surface in the semiconductor industry [171].

Polymers can be used as biomaterials. In the field of tissue engineering, poly (3-hydroxybutyrate) (PHB), produced by many types of microorganisms, has become commercially available. But, it is hydrophobic while biomaterials should be hydrophilic. Ammonia plasma can be used to modify the surface properties of PHB. A durable conversion of the hydrophobic material into hydrophilic was obtained and no significant changes in the morphology of the surface was observed. Furthermore, there were amides and amino groups on the surface, which will be useful in the necessary biochemical reaction [172]. PTFE is one of the common polymers applied in medical devices and long-term blood-contacting implants. However, the hydrophobic property of PTFE is a drawback because PTFE can adsorb protein strongly. In order to change PTFE into a hydrophilic material, poly (ethylene oxide)-poly(propylene oxide)-poly(ethylene oxide) (PEO-PPO-PEO) triblock copolymers were immobilized on the surface of fluoropolymer using argon plasma method successfully [173]. MW/RF plasmas have been used to modify biomedical polyurethane and silicone. Feed gases were CO<sub>2</sub>, H<sub>2</sub>O, and NH<sub>3</sub>. The

plasmas can improve the stability of the materials but have no significant improvement regarding antibiotic properties. Furthermore, MW-plasma system was better than RF-plasma system in terms of deposition rate, barrier properties, and introduction of amine functional groups onto the surface [174]. Schroder et al. concluded that ammonia plasma treatment is a fairly universal method to introduce amino biofunctional groups onto the surfaces of polymeric biomaterials including PE, PS, PC, PEEK, PET, PMMA, polyethylenephthalate (PEN) [175]. To improve biocompatibility of PE, microwave plasma polymerization of allyl alcohol can be used to introduce hydroxyl groups into the polymer surface [176]. In order to be applied in biomedical fields, the surface modification of polyimides by H<sub>2</sub>O and D<sub>2</sub>O plasma was studied [177].

Microwave plasma modification mechanism is an interesting topic for many researchers. Kobayashi et al. studied the mechanism of polyacrylonitrile (PAN) modification by oxygen plasma [178]. A Langmuir probe can be used to detect the end point of polymer etching by plasma [179]. The reaction of imidazole molecules plasma with poly (vinyl chloride) (PVC) was investigated and a mechanism was proposed [180]. Bichler et al. investigated the adhesion mechanisms of aluminum, aluminum oxide, and silicon oxide on biaxially oriented polypropylene (BOPP), poly (ethyleneterephthalate) (PET), and poly(vinyl chloride) (PVC) [181]. The microwave plasma method had a drawback of surface degradation and the degradation rate was high when the polymer materials were directly immersed in the plasma because of ion and electron bombardments. Therefore, modifying polymers in the flowing afterglow of the discharge may decrease the degradation. The mechanisms of surface modifications of polymers, such as PP, PE, and PC, by the flowing afterglow of oxygen plasma were studied [182].

The mechanism of Al and Cu metallization of untreated and oxygen plasma treated PE and PET was investigated [183]. Spin-coated specimens of crosslinked polydimethylsiloxane modified by oxygen plasma were investigated [151].

### **2.3.5 Microwave Plasma Polymerization**

Microwave-activated monomer plasma can be used to synthesize polymers, which have unique features. Transparent and fluorescent polymer films were synthesized and deposited on to glass slides at 10 Pa by microwave plasma using three types of volatile aromatics: benzene, toluene, and styrene [184]. The microwave plasma assisted deposition of hexamethyldisiloxane [HMDSO-(CH<sub>3</sub>)<sub>3</sub>SiOSi(CH<sub>3</sub>)<sub>3</sub>] films for corrosion protection of Al metal sheet surfaces was synthesized [185]. A plasma polymer from acrylic acid deposited on PE by a pulsed plasma method was studied and a mechanism was proposed to explain experimental data [186]. Ultrathin (<5 nm) fluorinated polymer films of homogeneous thickness were synthesized using CF<sub>4</sub>/H<sub>2</sub> plasma. The surface energy of the films was more than four times that of PTFE. The deposition can be separated into two phases, a growth phase and a treatment phase. The depth of the films was limited by plasma parameters. The thickness limiting behavior can be explained by the dualism of etching and polymerization occurring in fluorocarbon discharges. The films showed the excellent anti-adhesion to PC and good adhesion to the Ni substrate [187]. The properties of polymers from n-hexane and n-heptane plasma were studied [188]. A book about plasma polymerization has been published [189].

### 2.3.6 Polymer Degradation

To protect the environment, petroleum-based polymer wastes should be recycled. A study of microwave pyrolysis of HDPE and aluminum/polymer laminates showed that microwave method had the same features as conventional pyrolytic method and can also treat laminates. Clean aluminum can be recycled after the microwave treatment [190]. Devulcanization is one new method of recycling waste rubber products, meaning that the cleavage of cross-linking sulfur bonds without destroying the polymer chain bonds. Microwave can be used in the rubber devulcanization process and was proved effective [191]. Microwave has also proven to be an effective energy source in the solvolysis of polyamide-6 [192], and PET [193]. The depolymerizations were finished in 4-20 minutes.

Some polymers containing silicon can convert to ceramic when heated at temperatures higher than 800°C. Six preceramic polymers were pyrolyzed into ceramics using microwave and thermal heating methods. The heating method could affect the amount and size of the  $\beta$ -SiC nanocrystals and the graphitization of residual carbon [194]. A polymeric method based on the Pechini process was investigated in synthesizing alpha-alumina. Different polymers were prepared using the microwave and thermal heating methods in the polyesterification reaction. Microwave heating at 2.45 GHz can reduce the polyesterification time dramatically and the mechanism of the reaction did not change [195]. The electrochemical properties of superfine spinel  $\text{LiMn}_2\text{O}_4$  ceramics synthesized by microwave polymer method were studied [196].

### **2.3.7 Nanomaterials**

Nanomaterials have been a great interesting interdisciplinary field of material science in the past ten years. Microwave can be used in production of nanomaterials. A concentrated uniform PS nanoparticle in solution was obtained under microwave radiation and a structural model was proposed to predict the resultant particle size [197]. Microwave heating method helped obtain monodisperse TiO<sub>2</sub> nanoparticles from inverse polystyrene-poly(ethylene oxide) diblock copolymer micelles in toluene by hydroxylation of titanium alkoxide [198]. PS-coated Fe nanoparticles were obtained by microwave plasma polymerization and their magnetic properties were studied. PS coating plays an important role in the underlying magnetic response of the particles [199]. Uniform polymer-stabilized metal nanoparticles can be produced continuously under microwave irradiation [200]. Microwave plasma method can also be used to produce polymer/ceramics nanoparticles [200-204].

### **2.3.8 Applications**

The use of microwave energy can be classified as either a communication or non-communication application. Since the discovery of electromagnetic waves, it has been widely used in communications. The earliest reported non-communication use of microwaves in polymer processing was an attempt to cure plywood cement in 1940 [205]. In the 1960s, microwave processing was successfully applied in the vulcanization of the rubber in the tire industry [206]. By now, the vulcanization of extruded rubber weather-stripping for the automotive and construction industries has been one of the most successful applications of microwave heating in industry [207]. Microwave heating has

also been used in forest industry and food industry [206, 208-213]. Examples of industrial applications of microwave processing include curing of Flip-Chip underfill and pultrusion of wood products [214]. In Flip-Chip process, the silicon chip is attached to the Printing Circuit Board (PCB) via solder bumps to reduce the assembly size. Recently organic PCBs are used to replace the expensive ceramic boards. Underfills are used to reduce the mismatch of coefficient of thermal expansion between the silicon chips and the substrates. Microwave techniques are applied in this process to selectively heat the underfills without heating up the PCBs and to reduce the cure cycles.

Microwave has also been used in pultrusion of wood products. The pultrusion process is a continuous manufacturing method that can be used to produce composites. The shape of the product is determined by continuously pulling the composite material through a die to produce uniform profile parts. The key step in a pultrusion process is to control the solidification process within the die.

## **CHAPTER 3 MICROWAVE CURING MECHANISM OF EPOXY RESINS**

### **3.1 Introduction**

The previous research results at Michigan State University have shown that microwaves reduced the curing times of epoxy resins [215-220]. These results motivate further investigation on microwave heating mechanisms to provide explanations for reaction rate enhancement by microwaves. The enhancement of polymer curing rate has been demonstrated in a number of studies [78, 89, 221-223]. Some investigators suggested that the reaction rate enhancement was because of microwave thermal effect, which is localized superheating [78, 221]. Some other investigators attributed it to specific microwave non-thermal effects, such as accelerated reaction of the secondary amine group [222], and improved diffusion rate of reactive species [223].

Fu et al. studied the microwave thermal or non-thermal effect by comparing continuous-power and pulsed-power microwave curing of epoxy resins [56]. Experimental results showed that continuous-power microwave curing had only slightly higher reaction rates and ultimate extents of cure than pulsed-power curing. The results seemed to support the theory of thermal effect. But non-thermal effect could not be disproved because the power level in pulsed-power curing was much higher than that in continuous-power curing. Microwave power has large influence on both microwave thermal and non-thermal effects. Further, it has been pointed out that microwave heating of materials depends largely on dielectric properties [4]. Microwaves can be more efficiently coupled into components with larger dielectric loss factor. Fillers with high dielectric properties can be added into resins to modify microwave thermal effect without

significantly affecting the non-thermal alignment of polar groups in the electromagnetic field.

In this chapter, microwave heating mechanism is investigated via studying microwave curing kinetics of epoxy resins.

### **3.2 Mechanisms of Epoxy Resin Curing Reactions**

The conversion of thermosetting resins to rigid solid is brought about by small chain polymer molecules reacting with curing agents or each others to form a crosslinked molecular network. Thermosets, such as phenolics, amino resins, polyesters, polyurethanes, poly-isocyanurates, silicones, and polyimides, react in a similar fashion as epoxy resins. However, epoxy resins have great versatility, low shrinkage, good chemical resistance, high mechanical properties, outstanding adhesion, and reaction without the evolution of byproducts. Epoxy resin curing may accomplish at room temperature or require the addition of external heat, depending on the type of the curing agent. For example, the epoxy/amine resins used in this study required heat to initiate.

Epoxy groups react with amine via a ring-opening mechanism. Functionality of epoxy resin or curing agent is determined by the number of reactive groups per molecule. The three-step epoxy reaction is shown in Figure 3.1 [224]. In the first step, an epoxy group reacts with a primary amine to form a secondary amine. In the second step, another epoxy group reacts with the secondary amine to form a tertiary amine. The third step is etherification, which is reaction of a formed hydroxyl group and an epoxy group to form an ether crosslinking epoxy. However, etherification is insignificant for stoichiometric

mixtures. The progress of the reaction is defined in terms of extent of cure or percentage of available epoxy groups reacted.

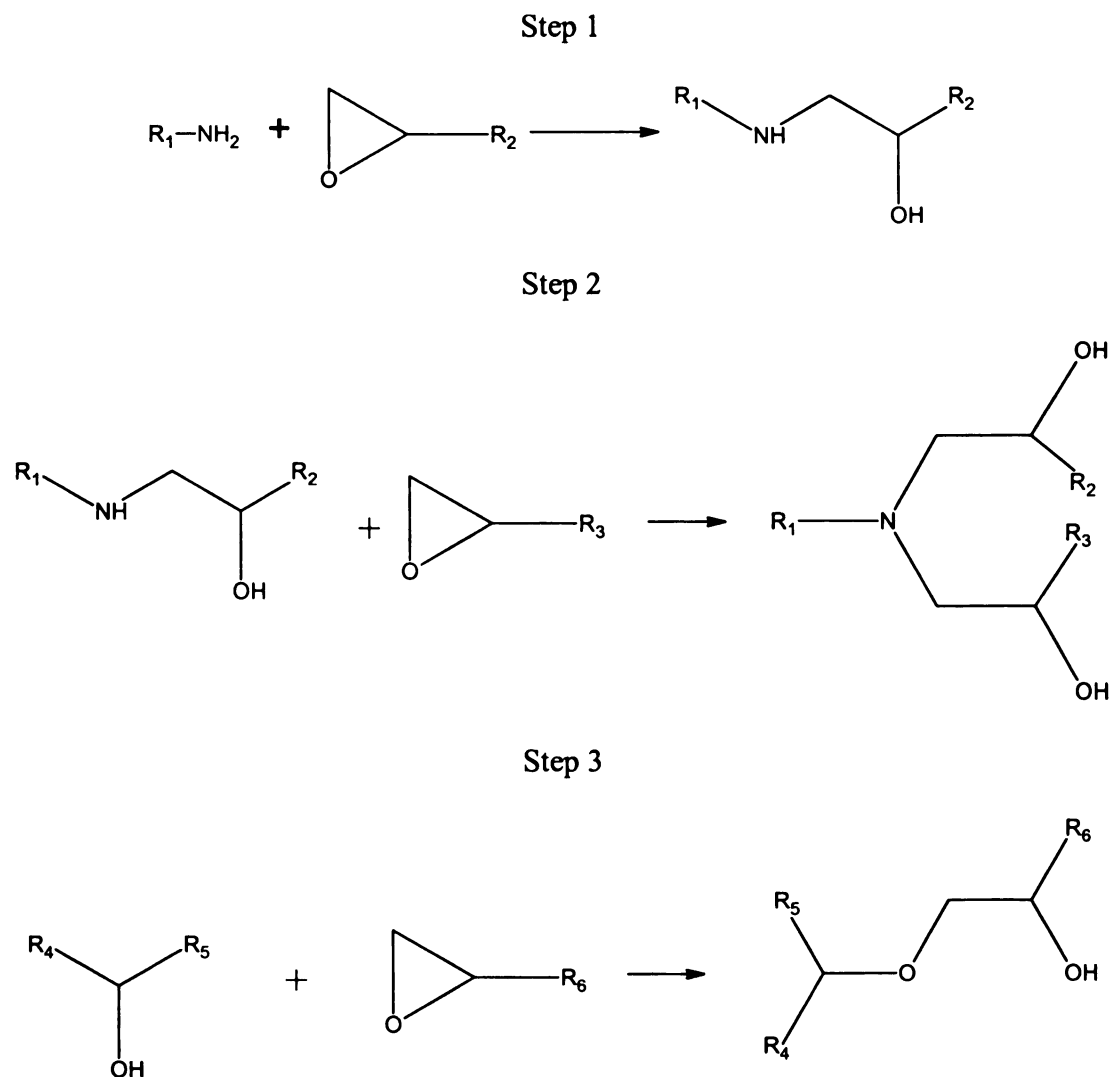


Figure 3.1 Three-step epoxy curing mechanism

The hydroxide groups, formed during the reaction, can act as catalysts so that the reaction is autocatalytic, which is shown in Figure 3.2 [215]. The electron pair of the amine group bonds to the chain terminating carbon in the epoxy group, causing a bond

breakage of the carbon-oxygen bond. The hydrogen atom detaches itself from the amine group and reattaches to the oxygen atom to form a hydroxide. The hydroxide group catalyzes further epoxy/amine addition by providing a hydrogen bond to the epoxy group.

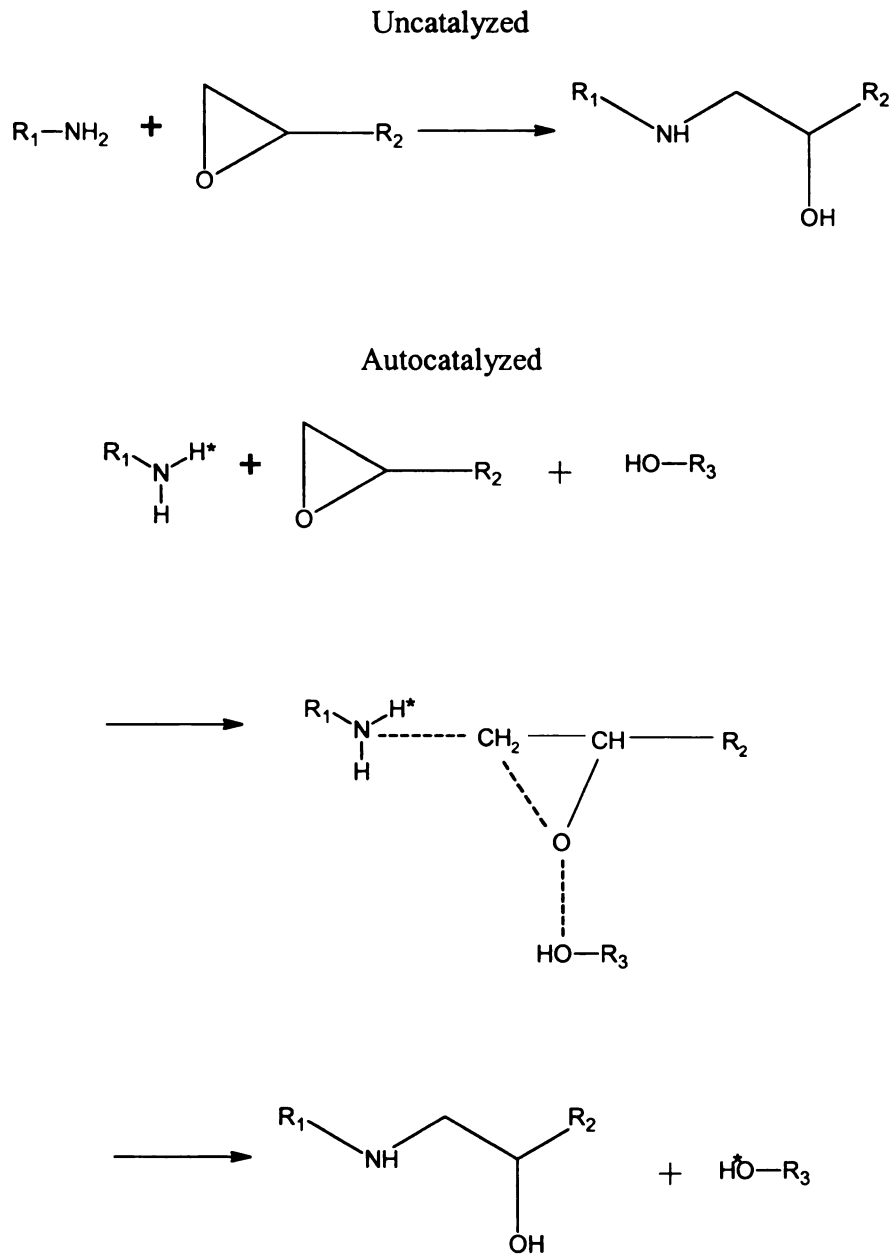


Figure 3.2 Uncatalyzed and autocatalyzed epoxy curing reaction mechanisms

### **3.3 Epoxy Resin Curing Kinetics**

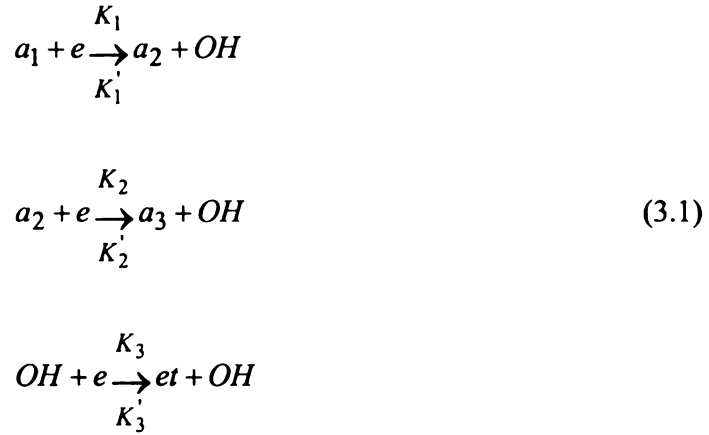
Epoxy resins are the most widely used matrix materials for advanced composites. A large amount of work has been performed in the curing of the general class of epoxy resins. A variety of models, proposed for curing of neat epoxy resins, have been further applied to thermal curing of doped resins and microwave curing of neat resins. Research efforts on the curing kinetics of epoxy and other commonly used resins, such as vinylester and polyester, are reviewed.

#### **3.3.1 Thermal Curing**

There are mainly two categories of kinetic models for the curing process [81]. Mechanistic model is obtained based on reaction mechanisms while phenomenological model is developed without considering the details of cure reactions. Although mechanistic models offer the advantages of better prediction and interpretation without conducting cure experiments for each new variable in the cure system, the phenomenological models usually have simpler forms with less kinetic parameters. In addition, the complexity of cure reactions sometimes makes the derivation of mechanistic models very difficult or even impossible. Therefore, phenomenological models have been used in most studies of cure kinetics. A summary of mechanistic and phenomenological models for cure reactions is presented as follows.

##### **3.3.1.1 Mechanistic Models**

The proposed reaction kinetic mechanism for epoxy-aromatic diamine system is shown in Equation 3.1 [225],



where  $a_1$ ,  $a_2$ ,  $a_3$ ,  $e$ , and  $et$  are primary amine, secondary amine, tertiary amine, epoxy, and ether group, respectively;  $K_i$  and  $K_i'$ ,  $i=1, 2, 3$ , are specific reaction rate constants for the catalytic and non-catalytic reactions, respectively. From the kinetic mechanism, mechanistic models for the curing process can be derived.

For the simplified case of no etherification, steric hindrance or OH impurity, a cure kinetic expression for epoxy has been derived as follows [226]:

$$\frac{d\alpha}{dt} = (k_1 + k_2\alpha)(1-\alpha)(B-\alpha) \tag{3.2}$$

where  $B$  is the ratio of the initial hardener equivalents to epoxy equivalents,  $B=1$  for a stoichiometric mixture;  $\alpha$  is the extent of cure;  $k_1$  and  $k_2$  are the catalytic and non-catalytic polymerization reaction rate constants, respectively.

The above equation holds well up to the gelation point. To model the whole curing reaction, the following kinetic model has been proposed [227]:

$$\begin{aligned}
\frac{d\alpha}{dt} &= (k_1 + k_2\alpha)(1-\alpha)(B-\alpha), \quad \text{when } \alpha < \alpha_{gel} \\
\frac{d\alpha}{dt} &= k_3(1-\alpha), \quad \text{when } \alpha > \alpha_{gel}
\end{aligned} \tag{3.3}$$

where  $k_3$  is the first order reaction rate constant with Arrhenius temperature dependency, and  $\alpha_{gel}$  is the extent of cure at the gelation point.

The etherification of a stoichiometric mixture of epoxy and amine can be neglected at low curing temperatures [79, 228-231]. However, it can no longer be ignored at high curing temperatures or with excess epoxy [79, 215]. In addition, the reaction rate constant for primary and secondary amine is not always the same. For the generalized case of epoxy curing with etherification, steric hindrance and an OH impurity, the curing kinetics has been derived for a stoichiometric mixture of epoxy and amine [79]. The kinetic models are shown in the following equations:

$$\frac{d\alpha}{dt} = \left[ \frac{2(1-n)\phi + n\phi^{n/2}}{2-n} + LF(\phi) \right] (1-\alpha) [k_1 + k_2 F(\phi)] \quad (3.4)$$

$$F(\phi) = 1 + \frac{[OH]_0}{e_0} \frac{(1-n)\phi + \phi^{n/2}}{2-n} \quad (3.5)$$

$$\alpha = \frac{(1-\phi)(1-n)(2-L) + 2(1-\phi^{n/2})(1-\frac{L}{n}) - (2-n)L(1 + \frac{[OH]_0}{e_0}) \ln \phi}{2(2-n)} \quad (3.6)$$

where  $n$  is the reaction rate constant ratio between the secondary amine-epoxy reaction and the primary amine-epoxy reaction,  $n = K_2/K_1 = K_2'/K_1'$ ;  $L$  is the reaction rate constant ratio between the etherification and the primary amine-epoxy reaction,  $L = K_3/K_1 = K_3'/K_1'$ ;  $[OH]_0$  is the initial concentration of OH impurity;  $\phi = a_1/e_0$ ;  $e_0$  is the initial epoxy concentration;  $k_1 = e_0 K_1'$ ; and  $k_2 = e_0^2 K_1$ .

If  $L=0$  (i.e. no etherification),  $n=1$  (i.e. no steric hindrance) and  $[OH]_0=0$  (i.e. no OH impurity), the above reaction kinetics simplifies into the following equation for a stoichiometric epoxy-amine mixture:

$$\frac{d\alpha}{dt} = (k_1 + k_2\alpha)(1-\alpha)^2 \quad (3.7)$$

This kinetic equation is consistent with Equation 3.2 because of B=1 for a stoichiometric mixture in Equation 3.2.

### 3.3.1.2 Phenomenological Models

The simplest phenomenological model is the n<sup>th</sup> order reaction kinetic model [74, 232], which assumes that the kinetics can be expressed as:

$$\frac{d\alpha}{dt} = k(T)f(\alpha) \quad (3.8)$$

where  $\alpha$  is the extent of cure,  $t$  is the time, the function  $f(\alpha)$  is expressed as  $(1-\alpha)^n$ , and  $k(T)$  is the overall reaction rate constant which obeys the Arrhenius relation:

$$k(T) = A \exp\left(-\frac{E}{RT}\right) \quad (3.9)$$

The n<sup>th</sup> order reaction kinetics is computationally simple. According to this model, the maximum reaction rate should occur at the beginning of the reaction. However, in real cases,  $\alpha=0.3 \sim 0.4$  at maximum reaction rate, which is better explained by the autocatalyzed reaction mechanism [233, 234]. The reactions between amines and epoxy are autocatalyzed by the hydroxide groups formed in the reactions. The initial rate should be slow due to lack of catalytic hydroxide groups. The cure kinetic expression of autocatalyzed reaction for a stoichiometric reactant mixture is given by:

$$\frac{d\alpha}{dt} = (k_1 + k_2\alpha^m)(1-\alpha)^n \quad (3.10)$$

where  $k_1$  is the non-catalytic polymerization reaction rate constant,  $k_2$  is the autocatalytic polymerization reaction rate constant,  $m$  is the autocatalyzed polymerization reaction order, and  $n$  is the non-catalyzed polymerization reaction order. This model has been widely used to represent adequately the cure kinetics of epoxy and unsaturated polyester cure systems [233-241].

### 3.3.1.3 Microwave Curing Kinetic Model

Thermal cure kinetic models have been used in modeling the reaction kinetics of microwave cured epoxy resins [56, 79, 218]. It was demonstrated that the microwave cure kinetics of epoxy resin systems could be described by the autocatalytic kinetic model up to vitrification [79, 218]. In the study of continuous-power and pulsed-power microwave curing of epoxy resins [56], a semi-empirical kinetic model was used:

$$\frac{d\alpha}{dt} = (k_1 + k_2\alpha^m)(\alpha_u - \alpha)^n \quad (3.11)$$

where  $\alpha$  is the extent of cure,  $k_1$  and  $k_2$  are rate constants,  $m$  and  $n$  are constants, and  $\alpha_u$  is the ultimate extent of cure. This model is similar to Equation 3.10 except that the ultimate extent of cure  $\alpha_u$  is included in the equation. This is because, at certain stage of the reaction, gelation and vitrification take place and, thus, the reaction rates are controlled by physical deposition. The ultimate extent of cure is usually less than 100%.

### 3.3.2 Kinetic Model Used in This Study

The phenomenological kinetic model in Equation 3.10 is used in this study. The reaction rate constants  $k_1$  and  $k_2$  obey the Arrhenius relation:

$$k_i(T) = A_i \exp\left(-\frac{E_i}{RT}\right) \quad (3.12)$$

where  $i=1$  for non-catalytic polymerization reaction or 2 for autocatalytic polymerization reaction,  $A_i$  is the Arrhenius frequency factor, and  $E_i$  is the activation energy.  $E_i$  and  $A_i$  can be obtained from the reaction rate constants at different temperatures.

### **3.4 Experimental**

#### **3.4.1 Experimental Equipment**

##### **3.4.1.1 Experimental Circuit**

The experimental circuit was assembled for microwave processing. The circuit directs microwaves into the applicator, allows the measurement of temperature, incident and reflected powers, and reduces the power reflected back to the power source to prevent damage to the power source. The microwave circuit is illustrated in Figure 3.3.

Microwave signal generator is a sweep oscillator (HP8350B) connected with a RF plug-in (HP86235A). A variable frequency amplifier (Lambda LT-1000) is used to amplify the signal. The amplified power signal is in the range from 0 to 200 Watts. Microwave frequency can be adjusted from 2 GHz to 4 GHz either manually or automatically. A 3-port circulator is used to prevent the reflected power from damaging the power source. The input and reflected microwave powers are decoupled with 20db directional couplers (Narda 3043-20) and measured with power meters (HP435B). A dummy load is used to absorb most of the reflected power. A multi-channel LUXTRON fluoroptic thermometer and a multi-channel Nortech NoEMI-TS fiberoptic thermometer

are used for sample temperature measurement. The probes are electrically nonconductive so that they do not perturb or be perturbed by the microwave fields.

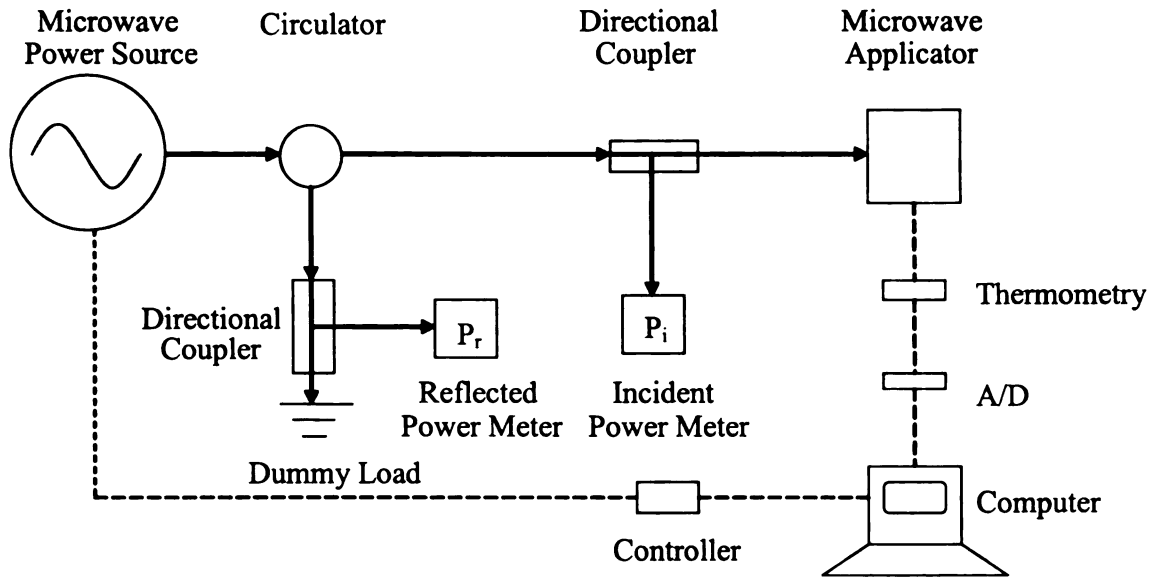


Figure 3.3 Circuit of the microwave curing system

A cylindrical single mode cavity with a diameter of 17.78 cm is used. The coupling probe is side mounted 3 cm above the bottom of the cavity. The cavity length ( $L_c$ ) and the probe depth ( $L_p$ ) are adjusted to be 13.2 cm and 2.0 cm, respectively. A sample is loaded at the center of the cavity.

### 3.4.1.2 Temperature Sensing Systems

Two types of thermometers are used in this study. One is multi-channel LUXTRON fluoroptic thermometer. The Luxtron thermometer uses Decay Time Technology to measure the temperature of the sensor [242]. Luxtron sensors contain a

small amount of magnesium fluorogermate. The sensors are attached at the tip of the optic fiber. The optical system excites the sensor with blue light. In turn the sensor fluoresces a red light, the intensity of which decays exponentially with time. The time constant of the decay is inversely proportional to the temperature. Therefore, the temperature can be obtained by measuring the decay time. The temperature probes are electrically nonconductive, which will not perturb or be perturbed by the microwave fields. The other one is multi-channel NoEMI-TS fiberoptic thermometer. The working principle is based on the absorption of light by a semi-conducting crystal bonded to the end of an optical fiber [243]. The crystal is in well contact with the materials to be processed with microwaves. As the crystal temperature increases, more low-energy photons are captured and absorbed by the band. The absorption edge is moved towards the longer wavelengths. Therefore, measuring the position of the absorption shift gives a measurement of the crystal's temperature and, thus, the temperature of the materials. The sensor is immune to and does not perturb the electromagnetic field.

#### **3.4.1.3 Microwave Applicators**

The most commonly used microwave applicators include waveguide, commercial *multimode* microwave ovens, and single mode applicator. Waveguides are hollow metal *tubes*, the *high-reflectivity* walls of which allow microwaves to propagate. Commercial *multimode* microwave ovens have large dimensions compared to the operating *wavelength*, allowing the establishment of multi modes at the same time. The EM field *inside multimode* ovens is not uniform and shows many peaks and valleys. Turntables are *usually used* to rotate the materials to be processed for more uniform heating. Single

mode cavity supports one mode at one time and has well-defined electric field pattern. The single mode cavity system has higher energy efficiency to transfer microwave power into the processed materials. A cylindrical single mode cavity is used in this study. Since one mode heating is not uniform with high field intensity confined to small regions, variable frequency techniques can be used to excite several modes with complementary heating patterns sequentially to obtain more uniform heating.

A sketch of the cylindrical single-mode cavity used in this study is shown in Figure 3.4.

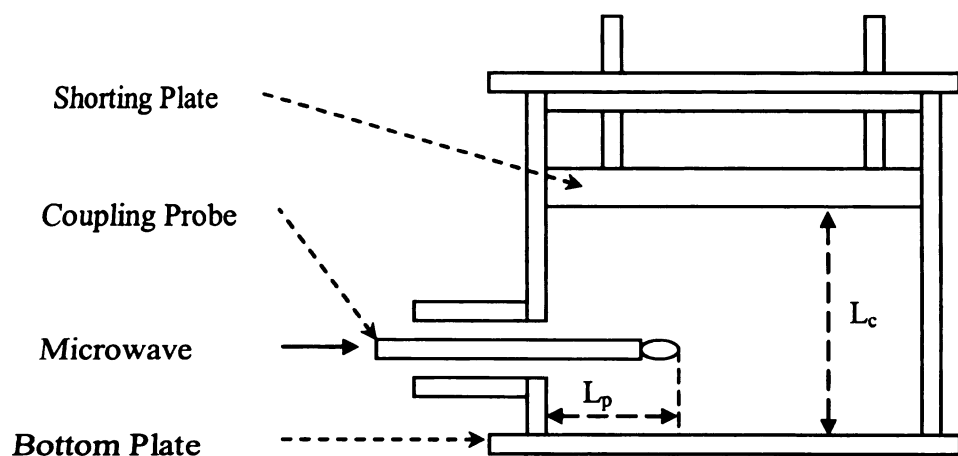


Figure 3.4 A cylindrical single-mode resonant cavity

The cavity is made out of a length of metal circular waveguide with both ends shorted by brass. The cavity has an inner diameter of 17.78 cm with cavity length adjustable from 10 cm to 30 cm. Microwave energy is introduced into the cavity by a coaxial coupling probe. The coupling probe is side mounted 3 cm above the base of the

cavity. The probe is adjustable in the radial direction so that the coupling probe depth  $L_p$  can be changed for locating critical coupling conditions. The range of the probe depth is from 0 mm to 50 mm. The top shorting plate is adjustable so that the cavity length  $L_c$  can be changed. The bottom plate is removable for sample loading. Both the top and the bottom plates are shorted with the cavity wall by metallic finger stocks.

#### **3.4.1.4 Cavity Characterization and Process Control**

Before microwave curing, the loaded cavity was characterized to locate the heating modes. The mode spectrum, as shown in Figure 3.5, was obtained with measuring the incident power ( $P_i$ ) and the reflected power ( $P_r$ ) as a function of frequency. The frequency with minimum reflectance ( $P_r/P_i$ ) was the resonant frequency of a mode. Among many available electromagnetic modes, two center heating modes TM020 and TM021 were selected because the material sample was loaded at the center of the cavity. For the experimental setup in this study, the resonant frequency of TM020 was around 2.89 GHz and the resonant frequency of TM021 was around 3.17 GHz. Figures 3.6 and 3.7 describe the theoretical electric field of TM020 and TM021 in a empty cavity with *FEMLAB*, respectively.

Traditional proportional-integral-differential (PID) method was used to control *the curing temperature* by adjusting the incident power level. The PID controller was *programmed* with LabView as a subroutine. The three parameters  $K_c$ ,  $T_i$  and  $T_d$  were *obtained with* Ziegler-Nichols frequency response method. The details of the method are *described in literature* [244].

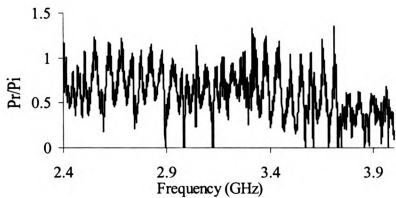


Figure 3.5 Mode spectrum of the loaded cavity for microwave curing

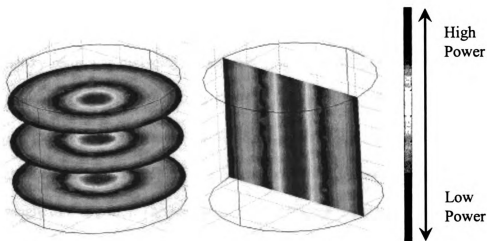


Figure 3.6 Electrical field of  $TM_{020}$  mode

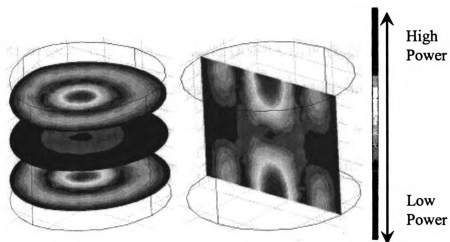


Figure 3.7 Electrical field of TM 021 mode

### 3.4.2 Experimental Materials and Procedure

The epoxy resin was diglycidyl ether of bisphenol A (DGEBA), and the curing agent was 3, 3'-diaminodiphenyl sulfone (DDS). DGEBA was DER332 from Dow Chemical with an epoxy equivalent weight of 173 and a molecule weight of 346 g/mol. The curing agent DDS was from TCI America with an amine equivalent weight of 62 and a molecule weight of 248 g/mol. The properties of the reactants are shown in Table 3.1.

Table 3.1 Properties of the reactants at 25°C

Materials	Chemical Structure	Density (g/cm <sup>3</sup> )	$\epsilon'$	$\epsilon''$
DGEBA		1.16	4.31	0.383
DDS		1.33	4.04	0.116



All of the materials were used as received without further purification. In preparing the neat epoxy resin, stoichiometric DGEBA/DDS (2.79: 1 by weight) were mixed at 130°C. The mixture was well stirred by hand in a 130°C oil bath until DDS was completely dissolved (in approximately 5-10 minutes). The resins were degassed at 0.02 bar and 100°C for 5 minutes. Fresh samples were kept in a -20°C freezer and used within 2 weeks.

For each microwave curing experiment,  $0.1 \pm 0.003$  grams of resin was loaded into a cylindrical Teflon holder with 2 cm high, the inner diameter of which was 1.25 cm. The thickness of the resin was around 0.6 mm. Because of the small dimensions of the sample, the temperature within the resin was assumed as uniform. The cylindrical Teflon holder with fresh DGEBA/DDS mixture was loaded on the bottom of the cavity and heated under microwave radiation from room temperature to the cure temperature 145°C for a certain time, ranging from 5 to 100 min.

After the completion of each experiment, extents of cure were determined by Differential Scanning Calorimetry (DSC). The samples were scanned in the DSC pan at a heating rate of 5°C/min from 20 to 320°C. The extents of cure were then calculated with the following equation:

$$\alpha = \frac{H_t - H_r}{H_t} \quad (3.13)$$

where  $\alpha$  is the extent of cure,  $H_t$  is the total heat of reaction per gram of the uncured sample,  $H_r$  is the residual heat of reaction per gram of the cured sample.

### 3.5 Results and Discussion

#### 3.5.1 Temperature and Power Deposition Profiles

During microwave curing, data acquisition of temperature, incident and reflected powers was performed every second. With the PID controller used, the curing temperature was controlled within 1°C of the set point temperature. The typical temperature profiles during microwave heating and curing of epoxy resins are shown in Figure 3.8. The power deposition was calculated as the difference between the incident and reflected powers. The reflected power was close to zero for the experimental setup in this study. The typical power deposition profile during microwave curing at 145°C is shown in Figure 3.9. The temperatures in Figure 3.8 and deposition powers in Figure 3.9 are the average numbers in every 15 seconds.

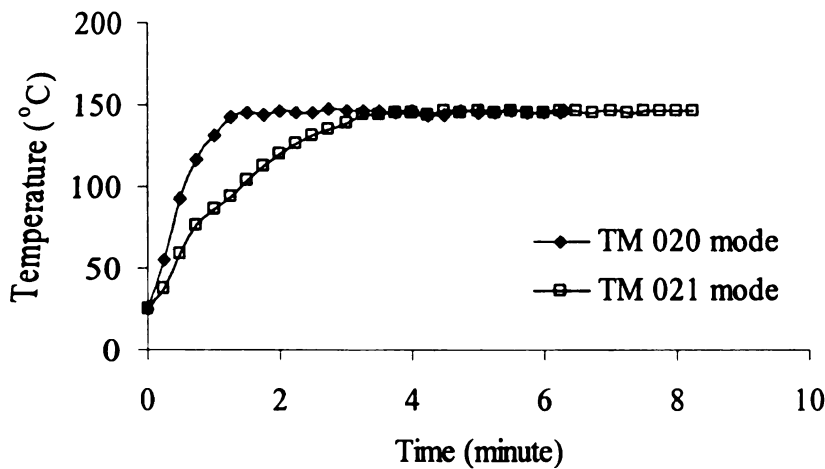


**Figure 3.8** Temperature profiles during microwave cure at 145 °C

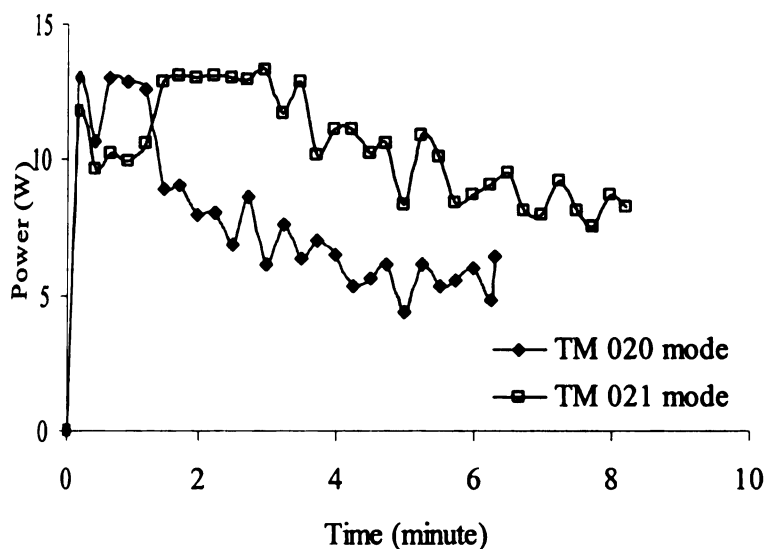


Figure 3.9 Power profiles during microwave cure at 145°C

The temperature profiles of the two modes in Figure 3.8 are similar. The temperature increased with heating time until 145°C and then fluctuated around 145°C. The difference is that it took longer time to heat DGEBA/DDS mixture to the curing temperature in TM 021 mode than TM 020 mode.

The power deposition curves for two modes in Figure 3.9 are similar. At the beginning, initial high power levels dropped to set power level 10 W. Then, high power levels were required to heat up the materials from room temperature to the isothermal curing temperature. After the isothermal curing temperature was reached, the power level was stable for a while and then dropped. This phenomenon can be explained by that the exothermal heat generated and dielectric property changed during the curing process. The curing of DGEBA/DDS was governed by an autocatalyzed reaction mechanism and the maximum curing rate usually occurred at the extent of cure of 0.3-0.4. Therefore, at the

beginning of curing, the curing rate kept increasing until the maximum rate was reached. During this period, high power level was needed. Correspondingly the rate of heat generation from the exothermal curing reaction increased. This tended to lower the power requirement. Then, the increase of curing extent in DGEBA/DDS mixtures tended to decrease the power requirement and the decrease in dielectric properties in cross-linking process tended to increase the power requirement. Therefore, power was still required to maintain the curing reaction but not as much as at the beginning of curing. However, the overall power requirements in two modes are not same, more power is required in TM 021 mode than in TM020. This is consistent with the phenomenon of temperature profile in Figure 3.8.

Table 3.2 shows times used to heat DEGBA/DDS reacting system from room temperature to 145°C and average power depositions in the two modes. Less time and power depositions were required in TM 020 mode than TM 021 mode.

Table 3.2 Time and average power required in the two modes

Curing Time (minutes)	Heating time from room temperature to 145°C (min)		Average power deposition (W)	
	TM 021	TM 020	TM 021	TM 020
5	3.9	1.2	10.5	7.8
10	6.9	2.4	12.7	5.4
20	3.2	2.5	10.7	8.5
30	6.0	0.9	17.3	3.4
40	1.6	1.6	7.7	6.4
60	2.6	0.9	11.7	6.1
80	3.0	2.8	20.6	11.0
100	2.4	2.0	13.9	11.0
<b>Average</b>	<b>3.7</b>	<b>1.8</b>	<b>13.1</b>	<b>7.4</b>

Based on the above experimental results and analysis, it is concluded that TM 020 mode is more effective and efficient than TM 021 mode. This can be explained by the theoretical electric field distribution of the two modes in Figures 3.6 and 3.7. The highest power concentration of TM 020 mode is located in the center of the cylindrical cavity while that of TM 021 mode is located in the centers of the top and bottom circles of the cylindrical cavity. Since the sample was put in the cylindrical center a little above the bottom circle, the power, that the sample can be absorbed, is not as much in the electromagnetic field of TM 021 mode as in that of TM 020 mode.

### 3.5.2 Kinetics

Microwave curing of the epoxy resins were performed at 145°C. The average resonant frequencies and standard deviations of microwave modes used in the experiments are shown in Table 3.3. The extent of cure of the resins was tested with DSC as a function of curing time. At least three samples were measured for each time point. The experiment data are shown in Table 3.4. The extent of cure as a function of curing time is shown in Figure 3.10.

Table 3.3 Resonant frequencies of the two microwave modes

Mode	TM 020	TM 021
Resonant Frequency (GHz)	3.123	2.887
Standard Deviation	0.002	0.006

Table 3.4 DSC results of cured epoxy resins

Time (min)	TM 020			Time (min)	TM 021		
	Absorption Heat (J/g)	Extent of Cure	Standard Error		Absorption Heat (J/g)	Extent of Cure	Standard Error
0	407	0%	5.1%	0	406	0%	3.6%
5	382	6%	4.4%	5	346	15%	2.4%
20	203	50%	1.0%	10	260	36%	1.4%
30	156	62%	3.7%	20	209	49%	1.3%
40	117	71%	6.6%	30	156	62%	2.6%
60	22	95%	0.4%	60	56	86%	0.4%
80	13	97%	0.3%	80	35	91%	2.1%
100	14	96%	0.3%	100	15	96%	0.2%

From Table 3.4 and Figure 3.10, it can be seen that curing curves under both modes, TM 020 and TM 021, have the typical shape of autocatalytic reaction. The initial curing rate was slow due to lack of catalytic hydroxide groups. As the reaction proceeded, hydroxide groups were generated and the maximum curing rate occurred at the extent of cure of around 30 to 40%.

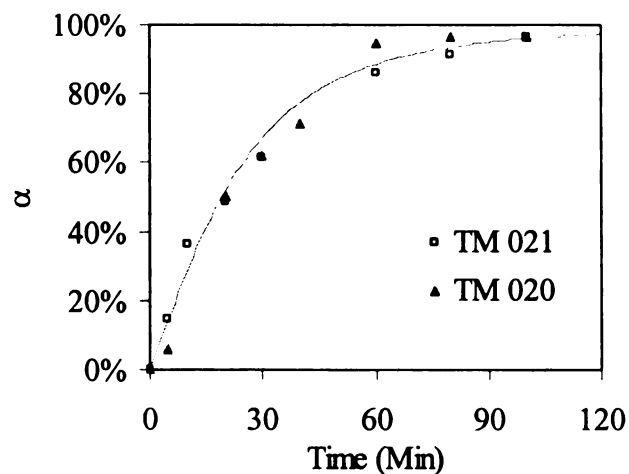


Figure 3.10 Extent of cure vs. curing time

POLYMATH was used in data regression to determine the kinetic parameters. The Levenberg-Marquardt algorithm was used to find the parameter values, which minimizes the sum of squares of the errors. The kinetic parameters in Equation 3.10 were first assigned initial values.

$$\frac{d\alpha}{dt} = (k_1 + k_2\alpha^m)(1-\alpha)^n \quad (3.10)$$

where  $k_1$  is the non-catalytic polymerization reaction rate constant,  $k_2$  is the autocatalytic polymerization reaction rate constant,  $m$  is the autocatalytic polymerization reaction order, and  $n$  is the non-catalytic polymerization reaction order. The calculated values of parameters are shown in Table 3.5.  $k_2$  is higher than  $k_1$ . This verifies that the epoxy curing is mainly governed by autocatalytic reaction mechanism.

Table 3.5 Values of the kinetic parameters

m	0.67
n	1.30
$k_1$	0.026
$k_1/k_2$	0.7

### 3.6 Conclusions

The curing of DGEBA/DDS epoxy resin system under microwave radiation at 145 °C was governed by an autocatalyzed reaction mechanism. A kinetic model can be used to describe the curing progress.

$$\frac{d\alpha}{dt} = (k_1 + k_2\alpha^m)(1-\alpha)^n$$

where  $k_1$  is the non-catalytic polymerization reaction rate constant,  $k_2$  is the autocatalytic polymerization reaction rate constant,  $m$  is the autocatalyzed polymerization reaction order, and  $n$  is the non-catalyzed polymerization reaction order.

## **CHAPTER 4 DIELECTRIC ANALYSIS OF CURING EPOXY RESINS**

### **4.1 Introduction**

The study of the dielectric properties during polymerizations of epoxy resins under microwave irradiation has both fundamental and practical interests. It provides useful information about details of the curing reactions and, thus, has been developed as a nondestructive testing technique to monitor the curing processes.

A microwave cavity technique is used here to obtain dielectric data and to diagnose the microwave (MW) curing of epoxy/amine resins at 2.45 GHz. Dielectric properties of epoxy/amine resins are not from the ionic contribution, but due to the presence of polar groups in the molecules. Microwave energy can be directly absorbed by these polar groups to cause localized heating, which initiates the curing processing. The absorption occurs primarily at epoxy and amine groups during the early stages of heating. These polar groups are consumed during cure while hydroxyl groups are formed, which also absorb microwave radiation and, subsequently, react with epoxy groups. The mobility of polar chains decreased as the crosslinking reaction proceeds. The effect of changing mobility and population of these polar groups on the dielectric properties of the system can be determined by dielectric measurement. The rate of absorption of microwave energy is determined by dielectric loss factor and electric field strength. The crosslinked molecules, normally with low dielectric properties, do not absorb microwave energy as readily as the monomers with high dielectric properties. Therefore, dielectric properties can be an index of energy dissipation in the resins and an index of extents of reaction. The advantages of using microwave heating and dielectric diagnostics to initiate

and monitor the curing process are: (1) selective and controlled direct heating due to absorption of microwave energy by polar groups; (2) increased control of materials temperature-time profile and input power to decrease thermal degradation and optimize the cure cycle. These advantages may cause microwave cured materials to have superior mechanical characteristics by chemically modifying the polar groups or by intelligently selecting the microwave power cycle conditions.

Epoxy resin is one of the most versatile materials used in such areas as general purpose, electrical, and aerospace. In the general-purpose area, the diglycidyl ether of bisphenol A (DGEBA) epoxy resin is the preferred material and has been used as pipes, adhesives, protective coatings, and electrical insulations. Until now, the studies on DGEBA epoxy resins primarily focus on measuring dielectric properties as a function of frequency at a constant temperature. However, microwave heating apparatus usually operates at a constant frequency, e.g. 2.45 GHz for all domestic microwave ovens. The Federal Communications Commission (FCC) allocated a number of microwave frequencies for Industrial, Scientific and Medical applications (ISM), among which 2.45 GHz is the major operating frequency worldwide. In order to improve industrial applications of microwave processing of epoxy resins, understanding the dielectric properties and relaxation during cure at an ISM microwave frequency is essential. The objective of this chapter is to do the dielectric analysis of the curing systems of DGEBA and different curing agents at 2.45 GHz over a temperature range. The dielectric properties changing with the reaction were fit by models and the evolutions of dielectric parameters, e.g. dielectric strength, shape parameter, and relaxation activation energy, were analyzed.

## 4.2 Background on Dielectric Analysis

### 4.2.1 Fundamental Theories for Dielectric Relaxation

In linear systems a response and a stimulus are proportional to one another in equilibrium. Relaxation is a delayed response to a changing stimulus in such a system. Dielectric relaxation is relaxation occurring in dielectrics. The stimulus is always an electrical field, and the response is a polarization [245]. If a material is under a dynamic electric field, the linear response to this field is defined as complex dielectric constant. Complex dielectric constant of the material has dipolar contribution and ionic contribution. For non-conducting materials, complex dielectric constant is mainly contributed by presence of the dipoles [218].

#### 4.2.1.1 Complex Dielectric Constant

The complex dielectric constant (or permittivity) is expressed as follows:

$$\epsilon^* = \epsilon' - \epsilon'' j = (\epsilon'_r - \epsilon''_r j) \epsilon_0 \quad (4.1)$$

where the unit is F/m,  $\epsilon'$  is the dielectric constant,  $\epsilon''$  is the dielectric loss factor,  $\epsilon_0$  ( $=8.85 \times 10^{-12}$  F/m) is the permittivity of free space,  $\epsilon'_r$  is the relative dielectric constant, and  $\epsilon''_r$  is the relative dielectric loss factor. Although  $\epsilon'_r$  is referred to as the dielectric constant in many papers, it is a function of temperature, pressure, humidity, and other conditions. In this paper,  $\epsilon'$  refers to  $\epsilon'_r$  while  $\epsilon''$  refers to  $\epsilon''_r$ .

The first effort to explain absorption of electromagnetic power by polar materials was that of Peter Debye [246]. Absorption occurs when dipoles, ordered with respect to an electric field, relax to a random orientation. The energy required to hold the dipoles in

an ordered orientation is released as thermal energy when the dipoles relax. The relaxation time is an indication of the amount of time required for a collection of dipoles in an electric field to revert to a random orientation once the field is removed. Following is the Debye model:

$$\begin{aligned}\varepsilon^* &= \varepsilon_\infty + \frac{(\varepsilon_0 - \varepsilon_\infty)}{1 + \omega\tau j} \\ \varepsilon' &= \varepsilon_\infty + \frac{(\varepsilon_0 - \varepsilon_\infty)}{1 + \omega^2\tau^2} \\ \varepsilon'' &= \frac{(\varepsilon_0 - \varepsilon_\infty)\omega\tau}{1 + \omega^2\tau^2}\end{aligned}\tag{4.2}$$

where  $\varepsilon'$  is the dielectric constant,  $\varepsilon''$  is the dielectric loss factor,  $j$  is the imaginary unit,  $\omega$  ( $=2\pi f$ ,  $f$  is the oscillator frequency in Hz) is the radial frequency of the electric field in  $s^{-1}$ ,  $\tau$  is the relaxation time in s,  $\varepsilon_0$  is the low frequency dielectric constant, and  $\varepsilon_\infty$  is the high frequency dielectric constant. The functions represented by Equation 4.2 are illustrated in Figure 4.1, for the specific values  $\varepsilon_0=8$  and  $\varepsilon_\infty=2$ .

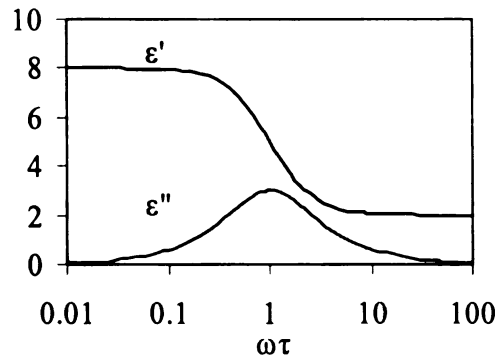


Figure 4.1 Schematic diagram of the Debye model

Experimentally, one usually measures the quantities  $\epsilon'$  and the loss tangent, which is defined in Equation 4.3. Loss tangent can also be expressed as Equation 4.4, according to the Debye equations.

$$\tan \delta = \frac{\epsilon''}{\epsilon'} \quad (4.3)$$

$$\tan \delta = \frac{(\epsilon_0 - \epsilon_\infty)\omega\tau}{\epsilon_0 + \epsilon_\infty\omega^2\tau^2} \quad (4.4)$$

Although Debye model works well for systems containing small molecules in gas media or media with low viscosity, it does not work for complicated systems including polymers. Therefore, Cole and Cole proposed an empirical equation for a distribution of the relaxation time process which considered that each dipole had its own relaxation [247]. This distribution of dielectric relaxation time process can be represented and derived using a generalized Maxwell relaxation model. Davidson and Cole proposed another empirical equation from the experimental observation of the asymmetric dielectric dispersion curve due to interaction of neighboring dipoles [248]. The Cole-Cole model and Davidson-Cole model are shown in Equations 4.5 and 4.6, respectively.

$$\begin{aligned} \epsilon^* - \epsilon_\infty &= \frac{(\epsilon_0 - \epsilon_\infty)}{[1 + (j\omega\tau)^{1-\alpha}]} \\ \epsilon' &= \epsilon_\infty + \frac{(\epsilon_0 - \epsilon_\infty) [1 + (\omega\tau)^{1-\alpha} \sin(\frac{\alpha\pi}{2})]}{1 + 2(\omega\tau)^{1-\alpha} \sin(\frac{\alpha\pi}{2}) + (\omega\tau)^{2(1-\alpha)}} \\ \epsilon'' &= \frac{(\epsilon_0 - \epsilon_\infty)(\omega\tau)^{1-\alpha} \cos(\frac{\alpha\pi}{2})}{1 + 2(\omega\tau)^{1-\alpha} \sin(\frac{\alpha\pi}{2}) + (\omega\tau)^{2(1-\alpha)}} \end{aligned} \quad (4.5)$$

$$\begin{aligned} \varepsilon^* - \varepsilon_\infty &= \frac{(\varepsilon_0 - \varepsilon_\infty)}{(1 + j\omega\tau)^\beta} \\ \varepsilon' &= \varepsilon_\infty + \frac{(\varepsilon_0 - \varepsilon_\infty)\cos(\beta\theta)}{(1 + (\omega\tau)^2)^{\frac{\beta}{2}}} \\ \varepsilon'' &= \frac{(\varepsilon_0 - \varepsilon_\infty)\sin(\beta\theta)}{(1 + (\omega\tau)^2)^{\frac{\beta}{2}}} \\ \theta &= \arctan(\omega\tau) \end{aligned} \tag{4.6}$$

where  $\alpha$  and  $\beta$  are the shape parameters with a range from 0 to 1. The functions represented by the Davidson-Cole model in Equation 4.6 are illustrated in Figure 4.2, for the specific values,  $\varepsilon_0=8, \varepsilon_\infty=2$ , and  $\beta=0.2$ .

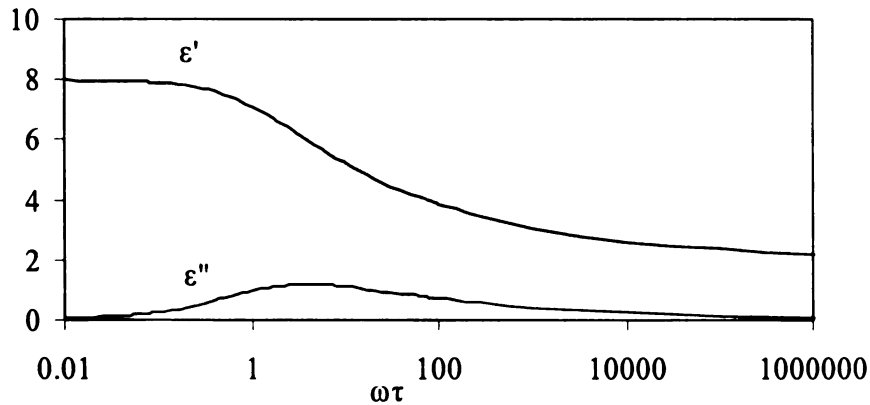


Figure 4.2 Schematic diagram of the Davidson-Cole model

Havriliak and Negami combined the Davidson-Cole and Cole-Cole models, and proposed a general empirical model, which is known as Havriliak-Negami (H-N) model [249, 250]:

$$\varepsilon^* - \varepsilon_\infty = \frac{(\varepsilon_0 - \varepsilon_\infty)}{[1 + (j\omega\tau)^{1-\alpha}]^\beta} \quad (4.7)$$

where  $\alpha$  is dispersion width parameter with the range  $0 \leq \alpha \leq 1$ , and  $\beta$  is dispersion skewness parameter with the range  $0 \leq \beta \leq 1$ . If  $\beta$  equals to 1, the H-N model is Cole-Cole model; If  $\alpha$  equals to 0, the H-N model is Davidson-Cole model. Using the complex identity in Equation 4.8 and DeMoivre's theorem, the H-N model in Equation 4.7 can be separated into the real part and the imaginary part, described in Equation 4.9.

$$j^P = e^{\frac{jP\pi}{2}} \quad (4.8)$$

$$\varepsilon' = \varepsilon_\infty + \frac{(\varepsilon_0 - \varepsilon_\infty)\cos(\beta\theta)}{[1 + 2(\omega\tau)^{1-\alpha}\sin(\frac{\alpha\pi}{2}) + (\omega\tau)^{2(1-\alpha)}]^\frac{\beta}{2}}$$

$$\varepsilon'' = \frac{(\varepsilon_0 - \varepsilon_\infty)\sin(\beta\theta)}{[1 + 2(\omega\tau)^{1-\alpha}\sin(\frac{\alpha\pi}{2}) + (\omega\tau)^{2(1-\alpha)}]^\frac{\beta}{2}} \quad (4.9)$$

$$\theta = \arctan \left[ \frac{(\omega\tau)^{(1-\alpha)}\cos(\frac{\alpha\pi}{2})}{1 + (\omega\tau)^{(1-\alpha)}\sin(\frac{\alpha\pi}{2})} \right]$$

### 4.2.1.2 Typical Graphs

Complex dielectric constant is a function of frequency, temperature, pressure, and material structure and composition. Two most important factors in the dielectric spectrum are temperature and frequency. Four types of graphs based on these two variables are usually used to present dielectric data:

(1) Cole-Cole plot (Arc diagram). The Cole-Cole plot is obtained by plotting the dielectric loss factor versus dielectric constant. The Debye model is a semicircle in the Cole-Cole plot. This plot is usually used to verify the above dielectric models. The following figures are typical Cole-Cole plots for the Debye model and the Davidson-Cole model, for the specific values,  $\epsilon_0=8, \epsilon_\infty=2$ , and  $\beta=0.2$ .

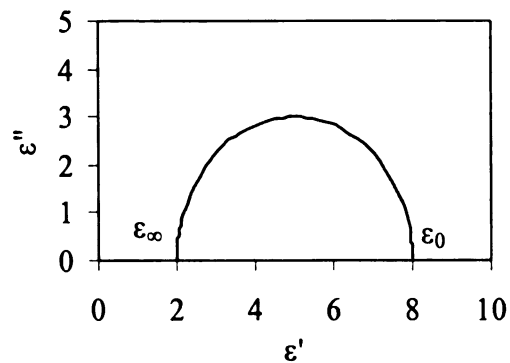


Figure 4.3 Schematic diagram of Cole-Cole plot of the Debye model

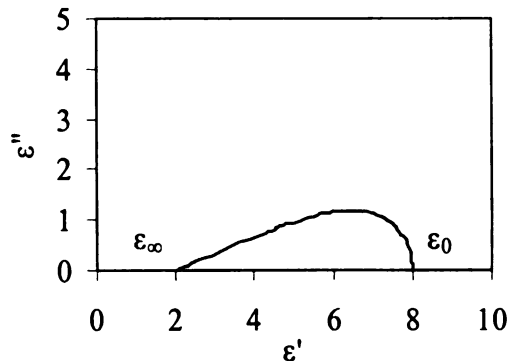


Figure 4.4 Schematic diagram of Cole-Cole plot of the Davidson-Cole model

(2) Complex dielectric constant versus frequency. Plotting complex dielectric constant versus frequency at constant temperature is to illustrate the time-temperature superposition.

(3) The relaxation time at maximum loss versus the reciprocal of temperature. The purpose of this graph is to identify the type of the molecular relaxation motions and to calculate activation energy for the relaxation transition. In practice, frequency is usually used as a parameter and temperature as a variable.

(4) Complex dielectric constant versus temperature. Complex dielectric constant versus temperature is plotted at a fixed frequency. Thus, the dielectric spectra can be easily compared with mechanical relaxation spectra, and thermomechanical, dilatometric, and differential scanning calorimetric curves which are also measured as a function of temperature.

#### 4.2.1.3 Dielectric Relaxation Time

Debye gave the relaxation time for a spherical polar molecule as

$$\tau = \frac{3V\eta}{kT} \quad (4.10)$$

where V is the molecular volume,  $\eta$  is the viscosity, k is Boltzmann's constant, and T is the temperature [246].

Kauzmann and Eyring [251, 252] expressed the relaxation process of local molecular transitions as a first-order reaction with an activation energy, which fitted to the Arrhenius expression

$$\tau = A \times e^{\left(\frac{E_a}{RT}\right)} \quad (4.11)$$

where  $E_a$  is the activation energy in J/mol,  $R$  is the gas constant in J/mol·K,  $T$  is the temperature in K, and  $A$  is the relaxation time in the high temperature limit in s.

Normally, the dipoles will have a short relaxation time at high temperatures, in low viscous medium (low intermolecular attraction), and with small molecular sizes (or small dipole sizes). Large molecules in highly viscous (or solid or networked) media can be expected to have large relaxation times, and the relaxation time would decrease as the temperature increases.

For structural transitions, it is generally recognized that the temperature dependence of the relaxation time above glass transition temperature is governed by WLF equation [253]

$$\tau = \tau(T_g) e^{\left( \frac{A(T-T_g)}{B+T-T_g} \right)} \quad (4.12)$$

where  $T$  is temperature,  $T_g$  is glass transition temperature,  $A$  and  $B$  are constants.

#### 4.2.1.4 Typical Dielectric Relaxation Processes

Three major types of molecular relaxation processes are classified in the structural transition region of materials [218]:

- (1)  $\alpha''$  process is the motion of larger crystallite on the melting phase.
- (2)  $\alpha'$  process is the motion of macromolecules in crystalline region at the beginning of the melting process.
- (3)  $\alpha$  process. This process randomizes the dipole moments through random Brownian motion of large segments of a polymer chain. These relaxations take place at low frequencies and, therefore, with long relaxation times. The characteristic relaxation

time increased over that of the liquid state due to reduced molecular motion in the solid state.  $\alpha$  process is a principal relaxation process.

Several secondary types of molecular motions below the principal relaxation process are defined in the local molecular transition regions:

(4)  $\beta$  process. This process occurs at higher frequency. It randomizes the dipole moments by reorientation of individual dipoles in the molecule chain, involving segmented motion of a small section of the polymer chain than  $\alpha$  process. A plot of the loss tangent versus temperature would yield a broad, flat distribution due to the fact that there are a number of different dipoles involved in a  $\beta$  process, each with its own characteristic absorption.  $\beta$  process occurs at higher frequencies than  $\alpha$  process.

(5)  $\gamma$  process is motion of individual groups of atoms in or attached to the backbone chains at higher frequencies in the microwave region.

(6)  $\gamma'$  process is motion of groups of atoms in branches or at the ends.

#### **4.2.2 Literature Review**

Dielectric techniques under microwave irradiation have been applied extensively to monitor thermal curing of thermosetting resins and composites by several investigators [254-262]. These dielectric measurements are usually performed by measuring an admittance of the materials placed between two conducting electrodes under microwave irradiation over frequencies less than 10 MHz. Significant data variations in dielectric measurement due to the interference of electrode polarization at low frequency or glass transition at high cure temperatures have been reported in the literatures [261, 262].

Studies on the dielectric properties of epoxy resins have received considerable attention [5, 263-281]. One main relaxation,  $\alpha$ , and two secondary relaxations,  $\beta$  and  $\gamma$ , were found in DGEBA [263]. The structural  $\alpha$  relaxation, which takes place at low frequencies and high temperatures, was due to the Brownian motions of the polymer chain [264-269]. The secondary  $\beta$  process, occurring at higher frequencies and lower temperatures, was assigned to a smaller section of the polymer chain than the  $\alpha$  process, e.g. the hydroxyether group  $-\text{CH}_2\text{-CHOH-CH}_2\text{-O-}$  [270]. The secondary  $\gamma$  relaxation, which is found located at higher frequencies than the  $\beta$  process, was the motion of individual groups of atoms, such as, epoxide groups, amine groups, and hydroxyl groups [5, 266-269]. The evolution of the dielectric constant and the dielectric loss factor during cure is related to the disappearance of dielectric dipoles in the reactants [273, 276-278] while the changes in the relaxation time depend on the viscosity of the reacting mixture [258, 259, 279-281].

Koike et al. studied the dielectric properties of a series of epoxy prepolymers including DGEBA [264, 265].  $\alpha$  relaxation was found in all studied prepolymers and fits to the empirical H-N equations. The WLF equation can be used to describe the relationship between the relaxation time and the temperature higher than the glass transition temperature.

Researchers at University of Pisa, Italy studied the dielectric properties of DGEBA and CGE (a monoepoxide, cresyl-glycidyl-ether) at different temperatures and frequencies [266-269, 274-277]. Two relaxation processes were found [275]. One is the structural  $\alpha$  relaxation process, freezing at the glass transition. The glass transition temperature of DGEBA is  $-16^\circ\text{C}$ . The other one is a secondary  $\gamma$  relaxation. When the

temperature increases,  $\alpha$  relaxation shifts toward higher frequencies and, eventually, merged with the  $\gamma$  relaxation. The spectra of the two relaxations show a non-Debye and asymmetric behavior. The experimental data fit a superposition of two H-N equations for the two relaxation processes [266]. The relaxation time of  $\gamma$  relaxation process were fitted by the Arrhenius equation, while that of  $\alpha$  relaxation process was non-Arrhenius and can be described by the empirical Vogel-Fulcher-Tammen equation [266].

### **4.3 Experimental**

#### **4.3.1 Experimental Systems**

The microwave diagnostic and processing system at MSU was developed by Dr. Jow. The details of the system and the single mode perturbation method can be found in his dissertation [218]. A switch between the heating and diagnostic systems was developed by Mr. Charvat [282]. A software program, called Diane which was developed by Dr. Jow at MSU, is used to calculate the dielectric constant and dielectric loss factor of materials. Here is a brief description of the system.

The microwave diagnostic and processing system consists of a microwave external circuit (an energy source, transmission lines, and the coupling probe), diagnostic elements (e.g. an X-Y oscilloscope, power meters, the E-field diagnostic probe, and a temperature sensor device), and the loaded cavity (e.g. the cavity and the loaded material). The system is shown in Figure 4.5. A cylindrical TM 012 mode cavity is used to process epoxy resins at a frequency of 2.45 GHz. A fluoroptic temperature sensing device (Luxtron 750), which does not absorb electromagnetic energy or interfere with

electromagnetic fields, is used to on-line monitor the material temperature. The fluoro optic probe is protected by a 3 mm O.D. pyrex capillary tube. A cylindrical Teflon sample holder is also required to contain the liquid samples. The cylindrical geometry of both the cavity and loaded materials is selected in order to facilitate diagnosis, modeling, and theoretical analysis.

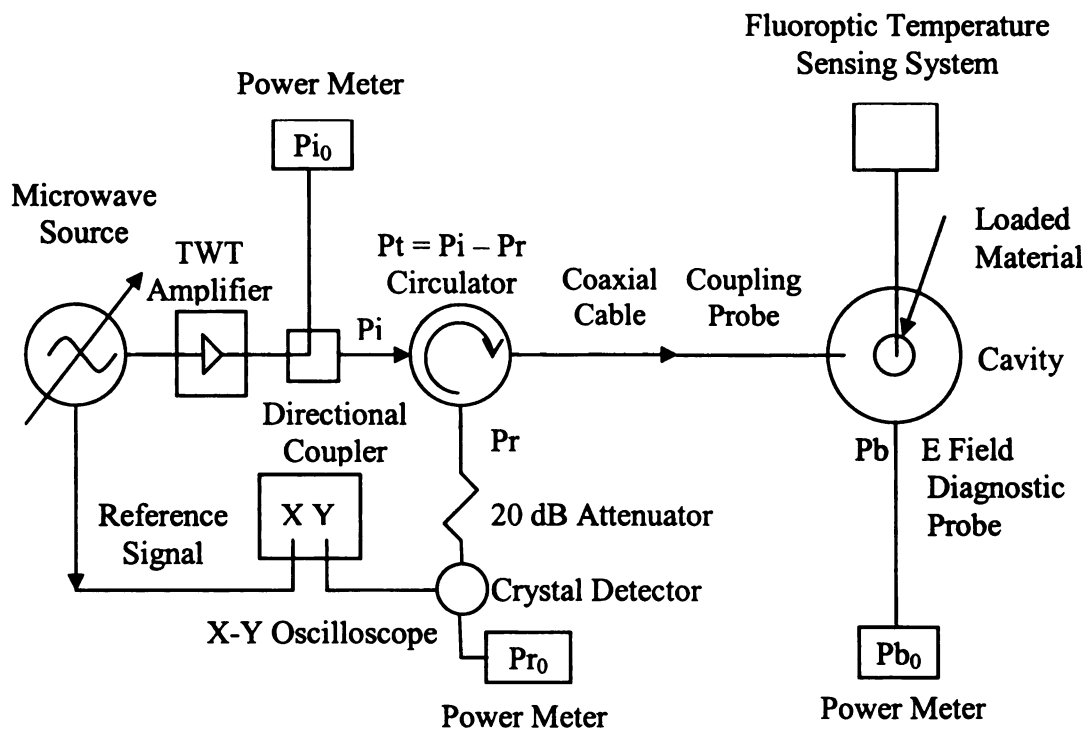


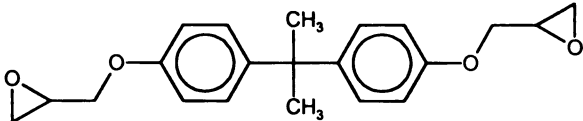
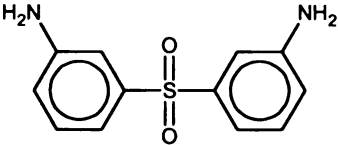
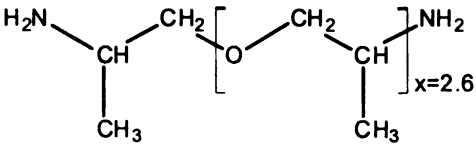
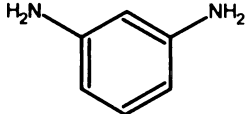
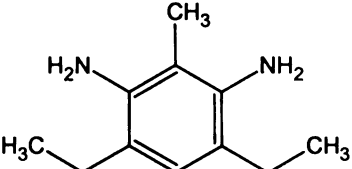
Figure 4.5 Schematic illustration of the microwave processing and diagnostic system

#### 4.3.2 Experimental Materials

The epoxy resin used in this study was diglycidyl ether of bisphenol A (DGEBA, DER 332 by Dow Chemical). The curing agents were 3,3-diaminodiphenyl sulfone (DDS by TCI America), a difunctional primary amine (Jeffamine D-230 by Huntsman), m-

phenylenediamine (mPDA by Sigma-Aldrich), and diethyltoluenediamine (Epikure W by Resolution Performance Product). The chemical structures and properties of the reactants are shown in Table 4.1.

Table 4.1 Properties of the epoxy resin and curing agents

Name	Chemical Structure	Epoxy/amine equivalent weight	Density at 25°C (g/ml)
DGEBA		171-175	1.16
DDS		62	1.33
Jeffamine D-230		60	0.948
mPDA		27	1.14
Epikure W		43-46	1.02

### 4.3.3 Sample Preparation

All of the materials were used as received without further purification. In preparing neat DGEBA/DDS epoxy resins, stoichiometric DGEBA and DDS (2.79:1 by weight) were mixed in a glass beaker. The mixtures were well stirred by hand in a 130°C

oil bath until the DDS was completely dissolved (in approximately five minutes). Finally, the resins were degassed at 0.02 bar at 100°C for five minutes.

In order to prepare neat DGEBA/Jeffamine epoxy resins, DGEBA was first preheated in a glass beaker at 50°C to melt any crystals and then a stoichiometric Jeffamine (weight ratio of DGEBA:Jeffamine 2.88:1) was added. The mixture was stirred for five minutes with a magnetic bar at room temperature and degassed at 0.02 bar at room temperature for five minutes.

To prepare neat DGEBA/mPDA epoxy resins, stoichiometric DGEBA and mPDA (6.4:1 by weight) were mixed in a glass beaker. The mixtures were well stirred with a magnetic bar at 65°C for five minutes and then degassed at 0.02 bar at room temperature for five minutes.

To prepare neat DGEBA/W epoxy resins, stoichiometric DGEBA and W (3.89:1 by weight) were mixed in a glass beaker. The mixtures were well stirred with a magnetic bar at 50°C for five minutes and then degassed at 0.02 bar at room temperature for five minutes.

#### **4.3.4 Measurements**

An empty Teflon holder with a fluoroptic probe was located at the position of the strongest electric field in the TM 012 mode cavity by a cotton thread. This cavity was critically coupled with a microwave external circuit and initial measurements were made by single and swept frequency methods at 2.45 GHz. The Teflon holder was removed from the cavity.

The degassed liquid epoxy resins were poured into the Teflon holder. The sample volumes (about 2.00 cm<sup>3</sup>) of epoxy resins were experimentally determined so that the resonant frequency shift was much less than the resonant frequency throughout the entire process. The Teflon holder with a fluoro optic probe and epoxy resin sample was relocated at the position of the highest electric field for the TM012 cavity mode at 2.45 GHz.

The single frequency microwave curing and diagnostic system was used to heat the liquid samples in the Teflon holder. The fresh DGEBA/DDS samples were heated to react at 145°C for specified reaction time periods, e.g. 1, 5, and 20 minutes, with the exception of those for the 0% cured epoxy resin, which were heated to 100°C. The curing temperatures for the DGEBA/Jeffamine, DGEBA/mPDA, DGEBA/W systems were 90, 110, and 160 °C, respectively. And the peak temperatures for the unreacted epoxy resins were 80, 90, and 100°C. Thereafter, the single frequency microwave curing system was switched to a low-power swept frequency diagnostic system by changing the switch position. Measurements of temperature and dielectric properties using the swept frequency method were made during free convective cooling of the samples. The cooled samples were analyzed with a Differential Scanning Calorimeter (DSC) to determine the residual heat of reaction per gram and thus the extents of cure. The calculation of extent of cure of epoxy resins is illustrated in Chapter 3.4.1. The reported extent of cure data is an average value at least three samples.

#### **4.4 Results and Discussion**

#### 4.4.1 DGEBA/DDS System

Dielectric properties of DGEBA, DDS, and uncured DGEBA/DDS mixture at 2.45 GHz and different temperatures are shown in Figure 4.6.

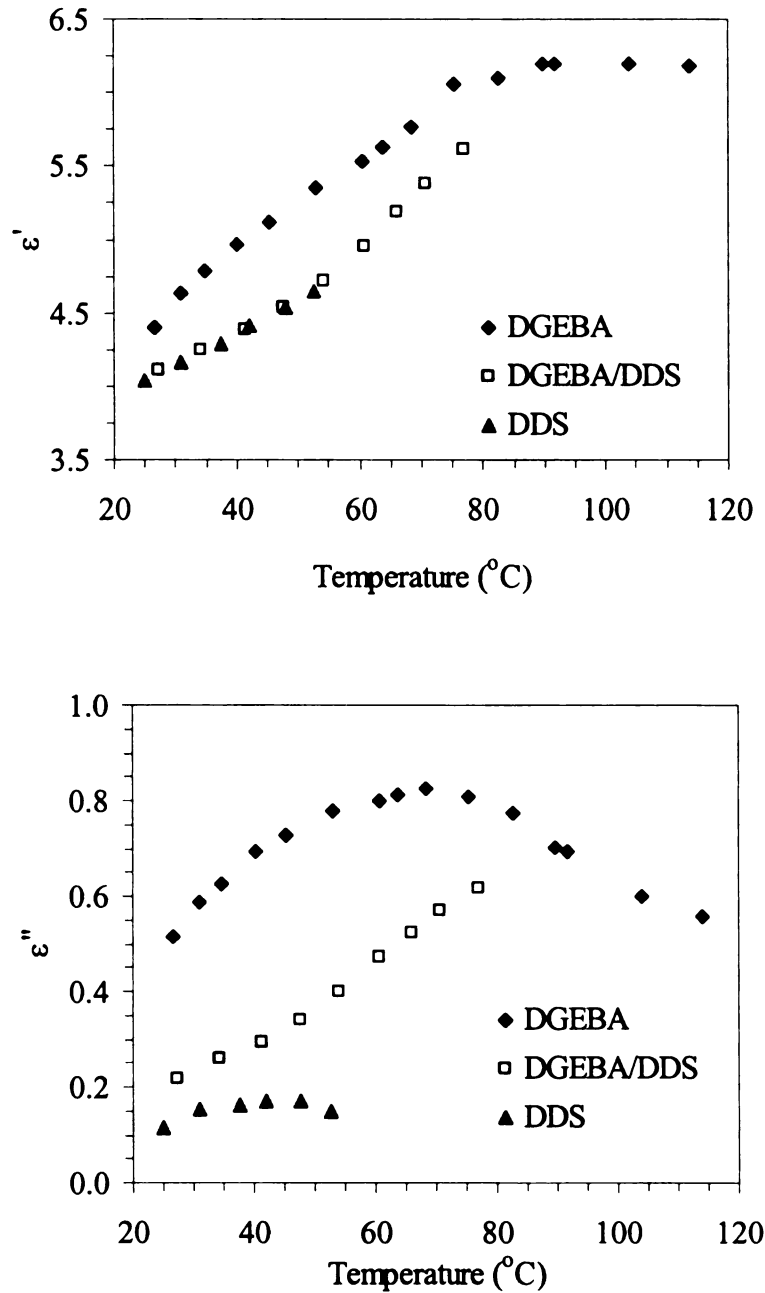


Figure 4.6 Dielectric properties vs. temperature for DGEBA, DDS, and uncured DGEBA/DDS mixture

The dielectric constant of DGEBA increases as the temperature increases from 20 to 80°C, remains stable around 80 to 100°C, and then decreases. The dielectric loss factor increases first and then decreases with a peak value around 70 to 80°C. The dielectric constant and dielectric loss factor of DDS and uncured DGEBA/DDS mixture increase as the temperature increases. The dielectric constant of DGEBA/DDS is smaller than that of DGEBA but similar to that of DDS while the dielectric loss factor of DGEBA/DDS is between that of DGEBA and DDS. The added DDS increases the viscosity of DGEBA matrix and hinders the relaxation time of DGEBA. Furthermore, the dielectric properties of DDS are smaller than those of DGEBA. Therefore, the dielectric properties of DGEBA/DDS are less than those of DGEBA.

The dielectric constant and dielectric loss factor of reacting DGEBA/DDS epoxy resins at different temperatures are shown in Figure 4.7. The extents of cure were calculated from DSC data, which are shown in Table 4.2. Due to the ununiformity of microwave heating, a distribution of extents of cure exists in the samples. From Figure 4.7, it is found that both dielectric constant and dielectric loss factor increase as the temperature increases and decrease as the curing reaction proceeds. According to the Debye model in Equation 4.2, the dielectric properties increase as the relaxation time decreases. Generally, the relaxation time decreases as the temperature increases. Hence, the dielectric properties should increase as the temperature increases.

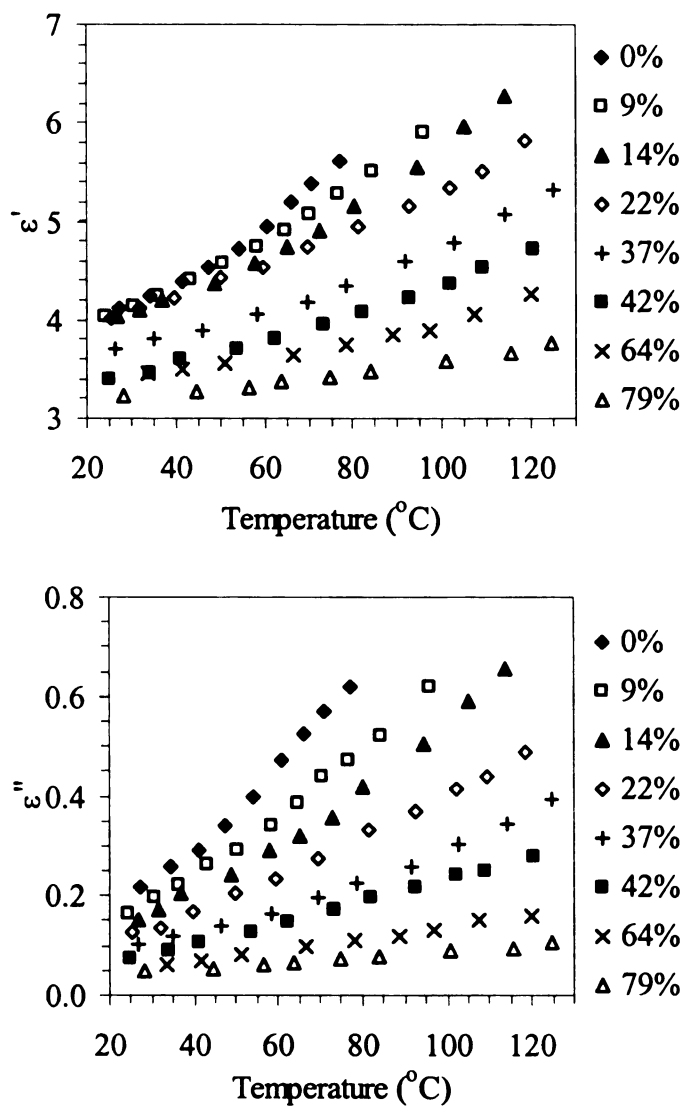


Figure 4.7 Temperature dependence of dielectric properties for the DGEBA/DDS epoxy resins at different extents of cure (%)

Table 4.2 DSC results of the curing DGEBA/DDS system

Reaction Heat (J/g)	432	387	395	324	249	168	203	72
	448	436	415	350	253	299	153	109
	419	403	360	362	269	262	58	63
	439	370	330	370	294	222	57	64
	429	365	363	290	308	297	319	157
Average	433	392	372	339	275	250	158	93
Extent of Cure	0%	9%	14%	22%	37%	42%	64%	79%
Standard Error	1%	3%	3%	3%	3%	6%	11%	4%

The reaction mechanism of the DGEBA/DDS epoxy resin system is shown in Figure 4.8 [224]. DGEBA reacts with amines via a ring-opening mechanism. Two-step reactions occur during cure. In the first step, an epoxy group reacts with a primary amine to form a hydroxyl group and a secondary amine. In the second step, the formed secondary amine reacts with another epoxy group to produce a hydroxyl group and a tertiary amine [281]. The progress of the reaction is defined in terms of extent of cure. The viscosity of the reacting systems rise as the polymerization goes on [281] and two distinguishable transitions, i.e. the gelation and the vitrification, are crossed.

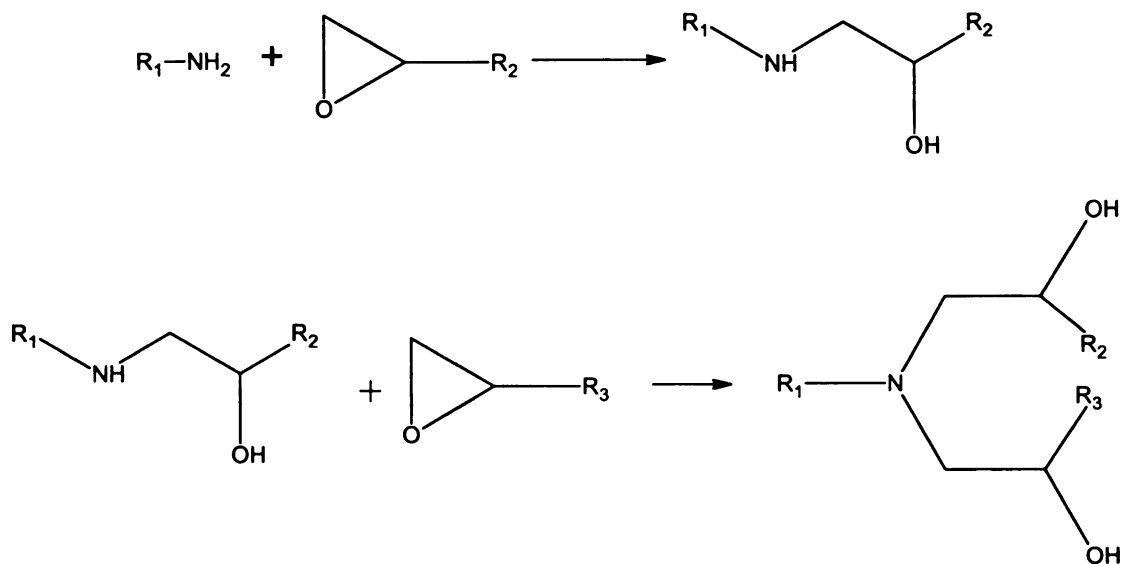


Figure 4.8 DGEBA resin curing mechanism

In general, three relaxation processes,  $\alpha$ ,  $\beta$ , and  $\gamma$ , may occur [263-281]. The  $\alpha$  relaxation, which takes place at low frequencies, randomizes the dipole moments through the Brownian motion of whole molecules [266]. Due to the high frequency used in the experiments and crosslinking between DGEBA and DDS, the whole molecules of the

system may not relax. Therefore, the  $\alpha$  relaxation does not dominate in the reacting system. The  $\beta$  relaxation occurs at a higher frequency, being attributed to the hydroxyl groups attached to the backbone of polymers [263]. Considering the low concentration of the hydroxyl groups in the reacting system, the  $\beta$  relaxation gives a negligible contribution to the relaxation processes. Therefore, the relaxations that occurred in the subject material are mainly  $\gamma$  relaxation.

To interpret the evolution of the dielectric properties during the curing reaction, one should know the dielectric behavior of all involved dipolar groups, which are, however, too complicated to differentiate. Since the dipolar groups within the reacting system and their dynamics are substantially similar, the dielectric properties of the reacting system reflect the combination of all the dipolar groups involved in the reaction.

The  $\gamma$  relaxation is the motion of dipolar groups of atoms, which should include: epoxy and amine groups with the unreacted DGEBA and DDS; dipolar groups with the intermediate products and final polymers, e.g., -NH- and -OH. As the reaction goes on, epoxy dipoles disappear, amine dipoles change to -NH- and =N-, and new dipoles, such as hydroxyl groups, appear. Overall, the total number of the dipolar groups within the reacting system is stable. Taking into account decreasing dielectric properties during cure, it is reasonable to suppose that the contribution of different dipolar groups to the relaxation is different. The unreacted epoxy groups, -O-, and amine groups, -NH<sub>2</sub>-, within the reaction system are the main driving forces for the apparent combined  $\gamma$  relaxation observed in this study. The disappearance of the epoxy and amine groups during the reaction is one reason accounting for the changes of the dielectric properties. Other researchers reported similar results [273, 276-278]. However, it may not be the only

reason. According to the classical Debye theory, the dielectric dipoles are regarded as spheres in a continuous medium having a macroscopic viscosity [246]. Schonhals and Schlosser studied the dielectric relaxation in polymeric solids and argued that the environment with high viscosity hindered the diffusion process of dipolar groups, causing the dielectric behavior of polymers far from ideal Debye materials [283]. In this study the transitions from liquid to gel and then to solid was observed during the cure reactions for all the four reacting systems. The increasing viscosity of the reacting systems should hinder the mobility of the dipolar groups associated with the relaxation and cause the relaxation time to increase [258, 259, 279-281]. The two reasons accounting for the evolution of the dielectric constant and the dielectric loss factor are a decrease in the number of the dipolar groups in the reactants and an increase in the viscosity during the reaction.

The Davidson-Cole model [248] can be used to describe the dielectric behavior of DGEBA epoxy resins:

$$\begin{aligned} \epsilon^* - \epsilon_\infty &= \frac{(\epsilon_0 - \epsilon_\infty)}{(1 + j\omega\tau)^n} \\ \epsilon' &= \epsilon_\infty + \frac{(\epsilon_0 - \epsilon_\infty)\cos(n\theta)}{(1 + (\omega\tau)^2)^{\frac{n}{2}}} \\ \epsilon'' &= \frac{(\epsilon_0 - \epsilon_\infty)\sin(n\theta)}{(1 + (\omega\tau)^2)^{\frac{n}{2}}} \\ \theta &= \arctan(\omega\tau) \end{aligned} \tag{4.13}$$

where n is the shape parameter with a range of  $0 \leq n \leq 1$ .

Consideration of the experimental dielectric data leads to a simplifying assumption. The observation that the dielectric constant and loss factor increased as the temperature increases happens only when the product  $(\omega\tau)$  is greater than unity, as shown in Figures 4.1 and 4.2. Therefore, it is logical to assume that the value of  $(\omega\tau)^2$  is much greater than one. In that case, the expressions of  $\epsilon'$  and  $\epsilon''$  in Equation 4.13 reduce to:

$$\epsilon' = \epsilon_{\infty} + \frac{(\epsilon_0 - \epsilon_{\infty}) \cos(n \frac{\pi}{2})}{(\omega\tau)^n} \quad (4.14)$$

$$\epsilon'' = \frac{(\epsilon_0 - \epsilon_{\infty}) \sin(n \frac{\pi}{2})}{(\omega\tau)^n}$$

Combining the calculation rules of complex numbers in Equations 4.15 and 4.16, the complex dielectric constant can be derived in Equation 4.17.

$$\frac{1}{r} [\cos(-t) + j \sin(-t)] = \frac{1}{r [\cos(t) + i \sin(t)]} \quad (4.15)$$

$$[\cos(t) + j \sin(t)]^n = \cos(nt) + j \sin(nt) \quad (4.16)$$

$$\begin{aligned} \epsilon^* &= \epsilon' - \epsilon'' j \\ &= \epsilon_{\infty} + \frac{(\epsilon_0 - \epsilon_{\infty})}{(\omega\tau)^n} [\cos(n \frac{\pi}{2}) - j \sin(n \frac{\pi}{2})] \\ &= \epsilon_{\infty} + \frac{(\epsilon_0 - \epsilon_{\infty})}{(\omega\tau)^n} \frac{1}{\cos(n \frac{\pi}{2}) + j \sin(n \frac{\pi}{2})} \\ &= \epsilon_{\infty} + \frac{(\epsilon_0 - \epsilon_{\infty})}{(\omega\tau)^n} \frac{1}{[\cos(\frac{\pi}{2}) + j \sin(\frac{\pi}{2})]^n} \\ &= \epsilon_{\infty} + \frac{(\epsilon_0 - \epsilon_{\infty})}{(j\omega\tau)^n} \end{aligned} \quad (4.17)$$

The proposed simplified Davidson-Cole expression to describe the dielectric properties of DGEBA/DDS system is shown in Equation 4.18.

$$\begin{aligned}\varepsilon^* &= \varepsilon_\infty + \frac{(\varepsilon_0 - \varepsilon_\infty)}{(j\omega\tau)^n} \\ \varepsilon' &= \varepsilon_\infty + \frac{(\varepsilon_0 - \varepsilon_\infty)\cos(n\frac{\pi}{2})}{(\omega\tau)^n} \\ \varepsilon'' &= \frac{(\varepsilon_0 - \varepsilon_\infty)\sin(n\frac{\pi}{2})}{(\omega\tau)^n}\end{aligned}\quad (4.18)$$

where  $\varepsilon^*$  is the complex dielectric constant,  $\varepsilon'$  is the dielectric constant,  $\varepsilon''$  is the dielectric loss factor,  $j$  is the imaginary unit,  $\omega$  ( $=2\pi f$ ,  $f$  is the oscillator frequency in Hz) is the radial frequency of the electric field in  $s^{-1}$ ,  $\tau$  is the relaxation time in s,  $\varepsilon_0$  is the low frequency dielectric constant,  $\varepsilon_\infty$  is the high frequency dielectric constant, and  $n$  is the shape parameter with a range of  $0 \leq n \leq 1$ .

It is observed that Equation 4.19 can be derived from Equation 4.18.

$$\tan(n\frac{\pi}{2}) = \frac{\varepsilon''}{\varepsilon' - \varepsilon_\infty} \quad (4.19)$$

The proposed simplified Davidson-Cole expression in Equation 4.18 is similar to, but more specific than, a model proposed by Schonhals and Schlosser (S-S) [283, 284]:

$$\begin{aligned}\varepsilon''(\omega) &\sim \omega^m \quad (\omega \ll \omega_0) \\ \varepsilon''(\omega) &\sim \omega^{-n} \quad (\omega \gg \omega_0)\end{aligned}\quad (4.20)$$

where  $m$  and  $n$  are shape parameters, and  $\omega_0$  is the angular frequency at maximum  $\varepsilon''$ . If Equation 4.18 is correct, a plot of  $\varepsilon''$  versus  $\varepsilon'$  should yield a straight line. Figure 4.9

shows  $\epsilon''$  versus  $\epsilon'$  at different extents. Straight lines represent the calculated data from the proposed simple model and points represent experimental data.

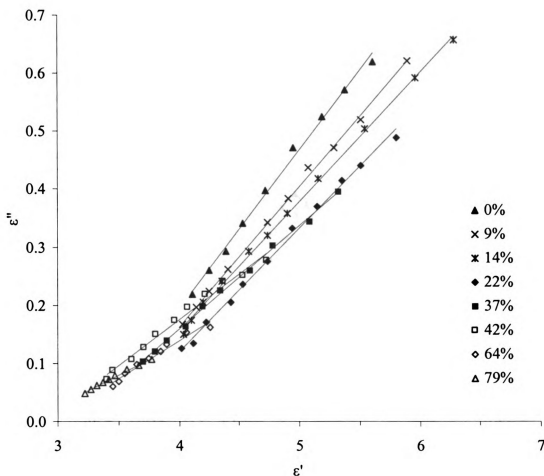


Figure 4.9  $\epsilon''$  vs.  $\epsilon'$  for the DGEBA/DDS epoxy resins at different extents of cure (%)

The  $\gamma$  relaxation time should fit the Arrhenius expression, shown in Equation 4.11. Combined with Equation 4.11, Equation 4.18 can be rewrite in Equation 4.21. If the proposed simple model is correct and the Arrhenius expression is applicable to the  $\gamma$  relaxation, plots of  $\ln(\epsilon' - \epsilon'_\infty)$  and  $\ln(\epsilon'')$  versus  $1/T$  should yield straight lines. Figures 4.10 and 4.11 demonstrate that this is indeed the case.

$$\ln(\varepsilon' - \varepsilon_{\infty}) = \ln \left[ \frac{(\varepsilon_0 - \varepsilon_{\infty}) \cos(n \frac{\pi}{2})}{(\omega A)^n} \right] - n \frac{E_a}{RT}$$

(4.21)

$$\ln(\varepsilon'') = \ln \left[ \frac{(\varepsilon_0 - \varepsilon_{\infty}) \sin(n \frac{\pi}{2})}{(\omega A)^n} \right] - n \frac{E_a}{RT}$$

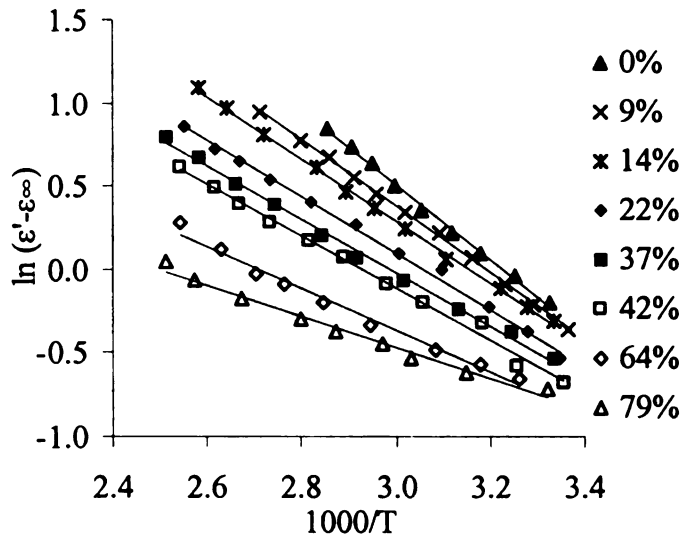


Figure 4.10  $\ln(\varepsilon' - \varepsilon_{\infty})$  vs.  $1000/T$  for the curing DGEBA/DDS system

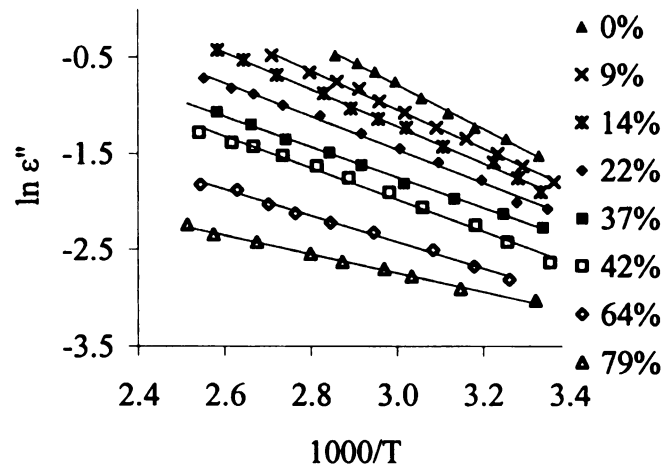


Figure 4.11  $\ln(\varepsilon'')$  vs.  $1000/T$  of the curing DGEBA/DDS system

$\epsilon_\infty$ ,  $n$ ,  $E_a$ , and a relation between  $A$  and  $\epsilon_0$  in Equations 4.11 and 4.18 can be figured out from the slopes and intercepts of straight lines in Figures 4.9-4.11. The value of  $\epsilon_0$  was estimated from the references [266, 269] and then  $A$  was calculated. Figure 4.12 shows the comparison of the experimental and calculated data of the reacting DGEBA/DDS system, where curves represent the calculated data from the simplified Davidson-Cole expression and points represent experimental data.

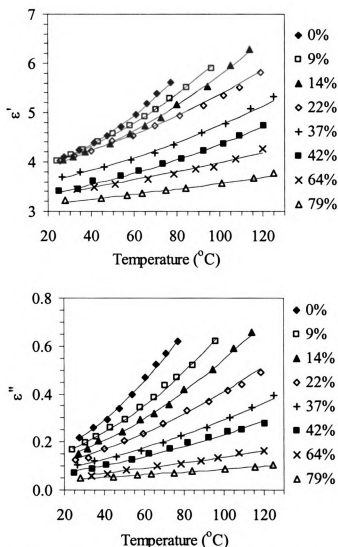


Figure 4.12 Comparison between the experimental and calculated dielectric properties of the curing DGEBA/DDS system

The proposed simple model fits experimental results exactly. The difference between the experimental and the calculated data is caused by the calculation error based on the approximation functions and the experimental error due to fluctuation of measured data including temperature, resonant frequency, and half-power frequency bandwidth.

To verify the assumption of the proposed expression, comparison of the experimental data and Cole-Cole plots of the calculated data is shown in Figure 4.13, where curves represent the calculated data by the Davidson-Cole model and points represent experimental data. The experimental data are located in the left side of the spectra, where tangent lines can be used to represent curves approximately. The tangent lines are related to the simplified Davidson-Cole expression.

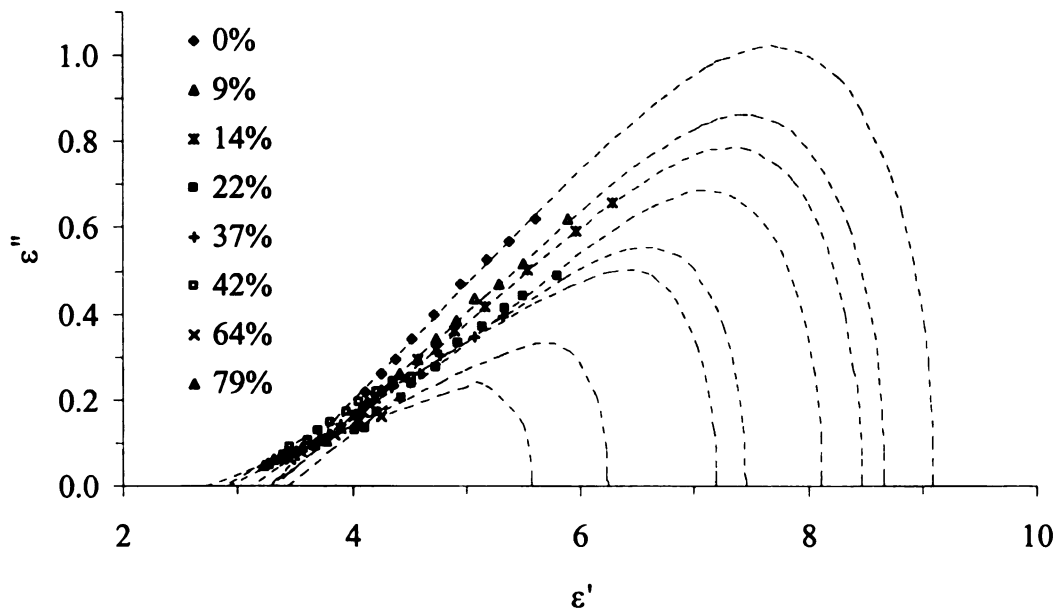


Figure 4.13 Cole-Cole plots for the curing DGEBA/DDS system

Table 4.3 shows the calculated values of all parameters the simplified Davidson-Cole expression, and the Arrhenius rate law. The parameter  $n$  describes the skewness of the dispersion of the relaxation times, which increases as  $n$  ranges from unity to zero. The value of  $n$  for an ideal Debye material is unity while that for polymeric solutions is around 0.5 [285]. As the reaction goes on, the parameter  $n$  decreases linearly, from 0.17 down to 0.07 (see Figure 4.14). The parameter  $n$ , according to Schonhals and Schlosser, is related to the intramolecular movement for the main  $\alpha$  relaxation of polymers [283, 284]. However, in this experiment it is shown that  $n$  is mainly connected with motion of dipolar groups for the secondary  $\gamma$  relaxation. During the reaction the motion of dipolar groups is hindered by the medium with increasing viscosity caused by curing epoxy resins. Therefore,  $n$  decreases. The rationale is similar to the argument that  $n$  is connected with the local chain dynamics of a polymer and decreases in the range of 0-0.5 with an increase of hindrance of orientational diffusion in the polymer [283]. Another similar result is that  $n$  for DGEBA prepolymers decreases as the molecule weight increases [265].

Table 4.3 Values of the parameters for the curing DGEBA/DDS system

Extent of Cure	$n$	$\epsilon_0$ [266, 269]	$\epsilon_\infty$	$(\epsilon_0 - \epsilon_\infty)$	$E_a$ (kJ/Mol)	$A$ (s)
0%	0.17	9.10	3.29	5.81	110	4.2E-25
9%	0.15	8.67	3.33	5.34	110	1.7E-24
14%	0.14	8.47	3.30	5.16	112	2.1E-24
22%	0.13	8.12	3.43	4.69	107	5.2E-23
37%	0.11	7.45	3.11	4.34	119	8.6E-24
42%	0.10	7.19	2.89	4.30	133	7.1E-25
64%	0.08	6.24	2.93	3.31	129	5.4E-23
79%	0.07	5.57	2.73	2.83	121	7.2E-20

The parameter  $\epsilon_0$  represents the equilibrium behavior while  $\epsilon_\infty$  represents the instantaneous behavior. Therefore,  $(\epsilon_0 - \epsilon_\infty)$  is the effective moment of the orienting dipoles [249]. The  $\gamma$  relaxation strength  $(\epsilon_0 - \epsilon_\infty)$  was found to decrease during the polymerization (see Fig 4.14), which is consistent with the decreasing number of the epoxy and amine groups of the reactants. Researchers at University of Pisa reached same results for similar reacting systems [267, 269] while Sheppard and Senturia reported that the relaxed dielectric constant  $\epsilon_\infty$  decreased as the reaction progressed and could be linearly related to the extent of cure for DGEBA/DDS reacting system [273]. In addition, the relaxation strength was found to diminish with increasing molecular weight of DGEBA prepolymers [265].

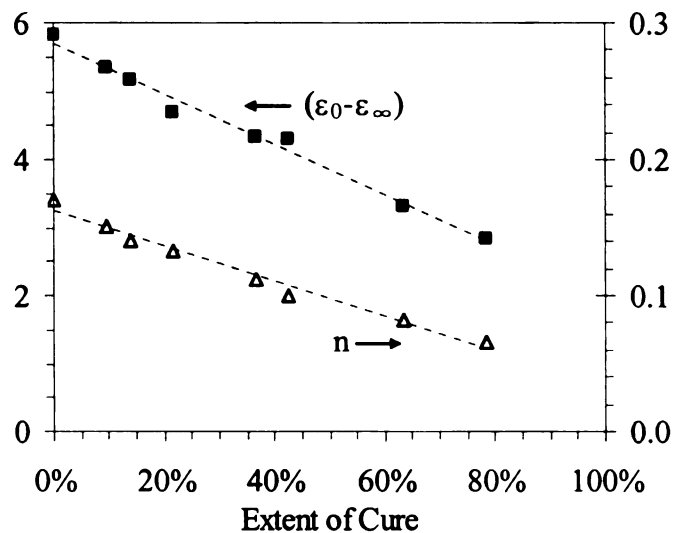


Figure 4.14 n and  $(\epsilon_0 - \epsilon_\infty)$  vs. extent of cure for the curing DGEBA/DDS system

The activation energy of the  $\gamma$  relaxation first increases, and then decreases during cure in Figure 4.15. The activation energy is the mean value of a distribution of activation

energies [251] and changes with the polymerization [259]. The phenomenon of increasing activation energy is consistent with the fact that the viscosity increases as the polymerization progresses. However, after the extent of cure reaches around 50%-60% the activation energy start to decrease. It may be explained by that the hindrance ability of the existing polymer chains may be weaker than that of dipoles in the reactants and thus less energy is needed for dipolar groups to relax after the peak point. Inasmuch as the gel point for the DGEBA/DDS system is 58% [281], the peak around 50-60% extent may be related to the gel point of the curing system.

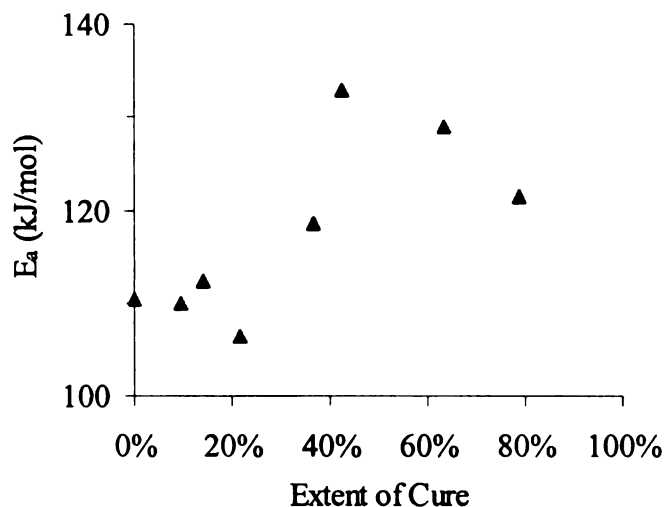


Figure 4.15  $E_a$  vs. extent of cure for the curing DGEBA/DDS system

Figure 4.16 shows the calculated  $\gamma$  relaxation time of DGEBA/DDS epoxy resin at different temperatures and extents. The relaxation time increases as the temperature decreases and the curing reaction goes on. The main reason for the remarkable increase of the relaxation time during the reaction is the rise of the medium viscosity.

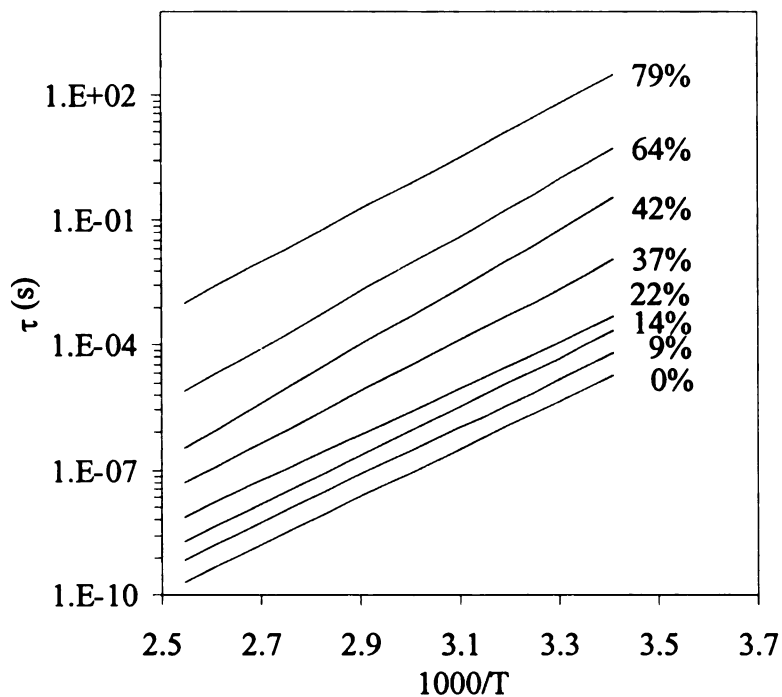


Figure 4.16  $\tau$  vs.  $1000/T$  for the curing DGEBA/DDS system

**Conclusion:** The dielectric properties of a crosslinking DGEBA/DDS system as a function of temperature in a range of 20-120°C at 2.45 GHz have been investigated. The dielectric properties of DGEBA/DDS mixture are less than those of DGEBA. The dielectric constant and dielectric loss factor of the DGEBA/DDS system increase as the temperature increases while they decrease during the reaction. The experimental data fitted the proposed simplified Davidson-Cole expression well. The  $\gamma$  relaxation has been identified. The Arrhenius expression is applicable to the  $\gamma$  relaxation. The evolution of all parameters as the reaction proceeds was related to the facts that the number of the dipolar groups involved in the reaction decreases and medium viscosity increases.

#### 4.4.2 DGEBA/Jeffamine D-230 System

Dielectric properties of DGEBA, Jeffamine D-230 (Jeffamine hereafter), and uncured DGEBA/Jeffamine mixture at 2.45 GHz versus temperature is shown in Figure 4.17.

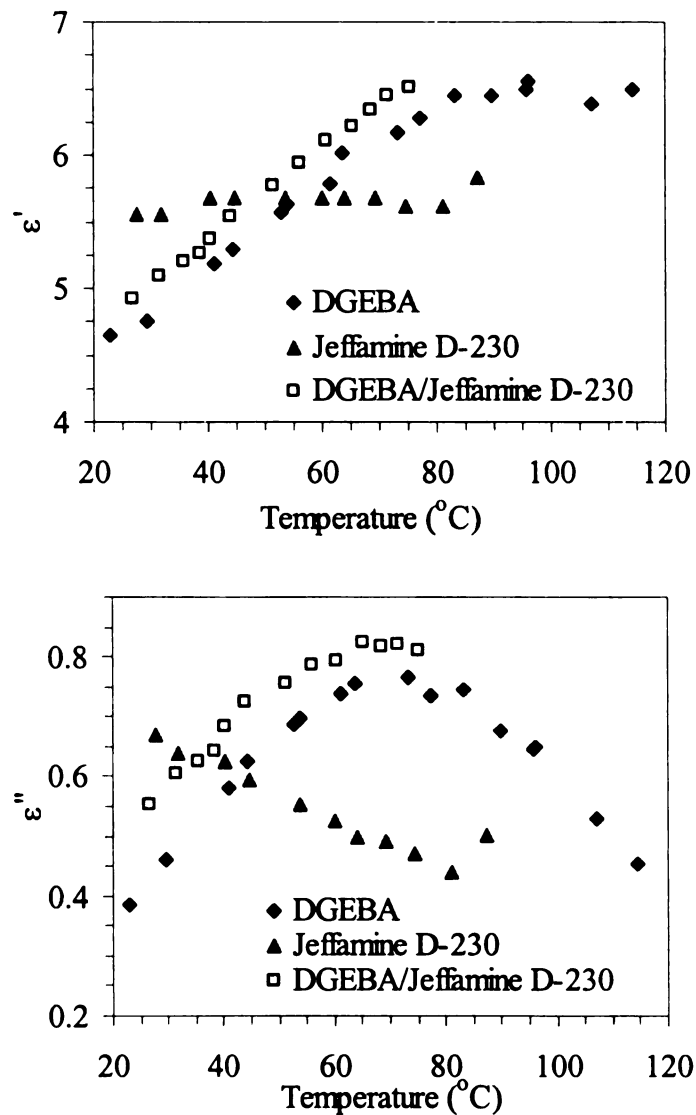


Figure 4.17 Dielectric properties vs. temperature for DGEBA, Jeffamine D-230, and uncured DGEBA/Jeffamine D-230 mixture

The dielectric constant of DGEBA increases with an increase in temperature from 20°C to 80°C, remains stable around 80°C to 100°C, and then decreases. The dielectric loss factor increases first, and decreases with a peak value around 70°C. The dielectric constant of Jeffamine is stable while its loss factor decreases as the temperature increases. Changes of the dielectric properties of uncured DGEBA/Jeffamine mixture are similar to those of DGEBA over a temperature range of 20 to 80°C. The dielectric constant and loss factor of the mixture are similar to those of DGEBA. Compared with DDS (see Table 4.1), Jeffamine has longer molecular chains. The long molecular chains, which act as lubricant, may decrease the viscosity of DGEBA matrix. Since the mixture is easier to relax than DGEBA, the dielectric properties of the mixture are larger than those of DGEBA.

The extents of cure were calculated from DSC data, which are shown in Table 4.4. Dielectric constant and dielectric loss factor of reacting DGEBA/Jeffamine epoxy resins at a temperature range of 20-90°C are shown in Figure 4.18, where points represent the experimental data and lines represent calculated data.

Table 4.4 DSC results of the curing DGEBA/Jeffamine system

Absorbed Heat (J/g)	260	296	298	222	177	160	119	62
	313	253	229	185	208	143	125	44
	299	238	192	205	156	161	82	50
Average	291	262	240	204	180	154	109	52
Extent of Cure	0%	10%	18%	30%	38%	47%	63%	82%
Standard Error	5%	6%	11%	4%	5%	2%	5%	2%
Physical State	Liquid	Liquid	Liquid	Liquid	Gel	Solid	Solid	Solid

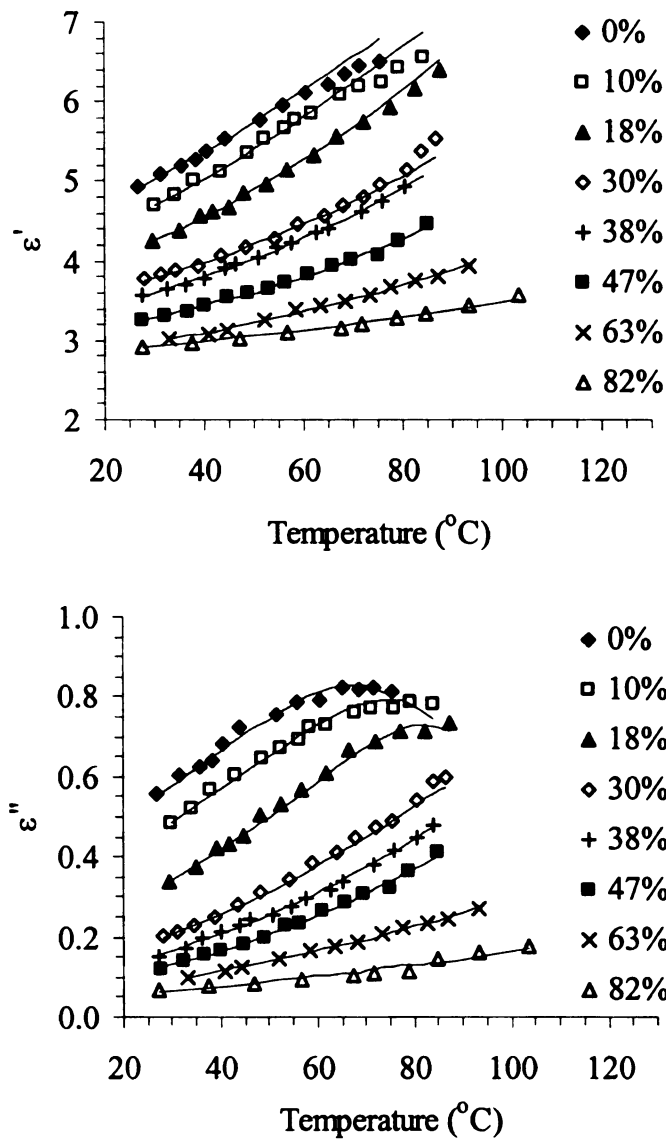


Figure 4.18 Temperature dependence of dielectric properties for the curing DGEBA/Jeffamine system

The dielectric properties of DGEBA/Jeffamine epoxy resins decrease as the extent of cure increases and increase with temperature except  $\epsilon''$  at 0 and 10% extents at high temperatures. The explanation of the phenomena is similar to that of DGEBA/DDS system. The reaction mechanism of the DGEBA epoxy resin system is shown in Figure 4.8. The two reasons accounting for the decrease in the dielectric constant and loss factor

during the reaction are a decrease in the number of the dipolar groups in the reactants and an increase in the viscosity.

The Davidson-Cole model was used to describe the dielectric behavior of DGEBA/Jeffamine epoxy resins while the simplified Davidson-Cole expression is used to calculate the parameters. Furthermore, the expression is applicable to dielectric data at the extent of cure over 30% and low temperature parts at the extent of cure from 0 to 30%. The Davidson-Cole model is given by Equation 4.13 while the simplified Davidson-Cole expression is shown in Equation 4.18.

Figure 4.19 shows plots of  $\epsilon''$  versus  $\epsilon'$ , which yield straight lines. The values of  $\epsilon''$  and  $\epsilon'$  of DGEBA/Jeffamine at 0%, 10%, 18%, and 30% extents are low temperature values in Figure 4.18, since the values at high temperatures did not yield straight lines.

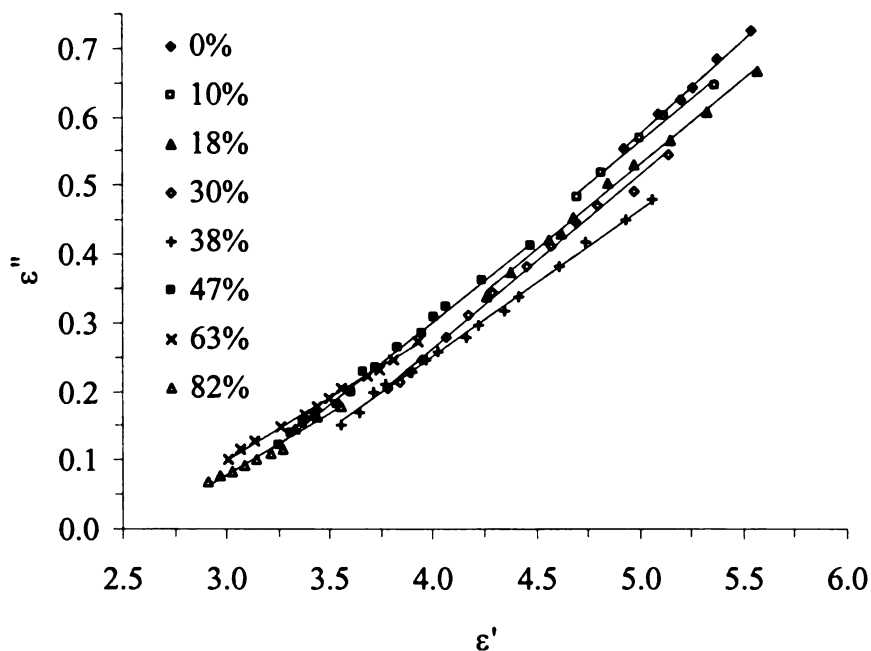


Figure 4.19  $\epsilon''$  vs.  $\epsilon'$  for the curing DGEBA/Jeffamine system

Similar to the DGEBA/DDS system, the predominant relaxation in the DGEBA/Jeffamine system is the  $\gamma$  relaxation [5], which should fit the Arrhenius expression. According to Equation 4.21, plots of  $\ln(\epsilon' - \epsilon_\infty)$  versus  $1/T$  and  $\ln(\epsilon'')$  versus  $1/T$  of experimental data in Figure 4.19 yield straight lines, shown in Figures 4.20 and 4.21. Curves represent fit of the proposed expression to the experimental data points.

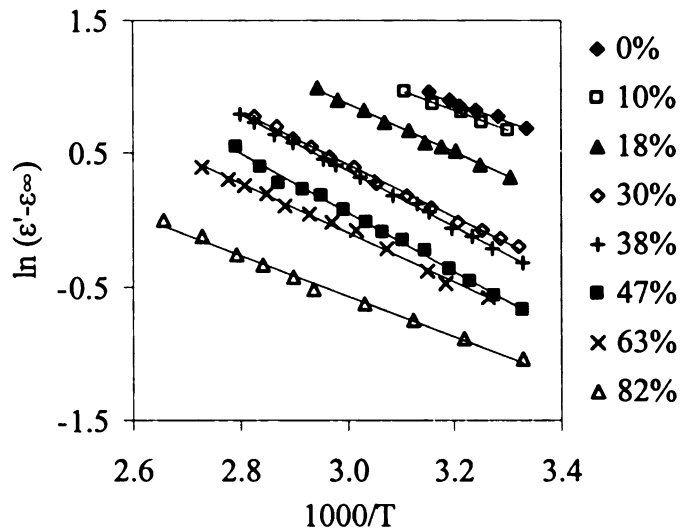


Figure 4.20  $\ln(\epsilon' - \epsilon_\infty)$  vs.  $1000/T$  for the curing DGEBA/Jeffamine system

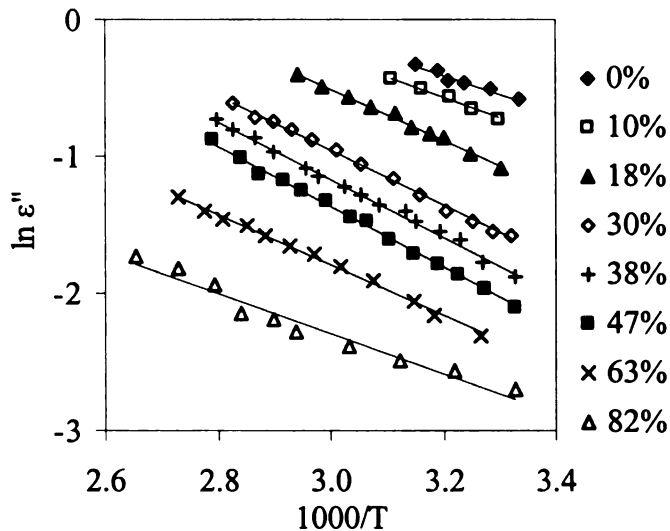


Figure 4.21  $\ln(\epsilon'')$  vs.  $1000/T$  for the curing DGEBA/Jeffamine system

The parameters  $n$  and  $\varepsilon_{\infty}$  of the curing DGEBA/Jeffamine epoxy resins were calculated from slopes and intercept of Figure 4.19.  $E_a$  and a relation between  $\varepsilon_0$  and  $A$  can be calculated based on Figures 4.20 and 4.21. The values of  $\varepsilon_0$  at 0%, 10%, 18%, 30% extents were modified until the calculated data from the Davidson-Cole model fitted the experimental data well.  $\varepsilon_0$  at 38%, 47%, 63%, and 82% extents were estimated based on the modification and the rule that  $(\varepsilon_0 - \varepsilon_{\infty})$  decreases during curing.

Comparison of the experimental data with the calculated data is shown in Figure 4.18. The calculated data at 0%, 10%, 18%, and 30% extents were calculated from the Davidson-Cole model while the others were calculated using the simplified Davidson-Cole expression.

Figure 4.22 shows the comparison of the experimental data with the calculated Cole-Cole arcs from the Davidson-Cole model. According to Figures 4.18 and 4.22, the calculated values fitted the experimental data well. The difference between the experimental data and the calculated data is caused by the calculation error based on the approximation functions and the experimental error due to fluctuation of measured data including temperature, resonant frequency, and half-power frequency bandwidth.

The simplified Davidson-Cole expression is applicable to part of the experimental data of the DGEBA/Jeffamine system while it is applicable to all measured data for the DGEBA/DDS system. Compared with Jeffamine, DDS has a rigid chain which hinders the relaxation of dipolar groups. Therefore, the dielectric behavior of DGEBA/DDS epoxy resins for low extents of cure under 2.45 GHz is similar to that of polymers, which can be described by the simplified Davidson-Cole expression, while that of

DGEBA/Jeffamine is similar to that of low molecular weight chemicals, e.g. glycerol, which can be described by the Davidson-Cole model.

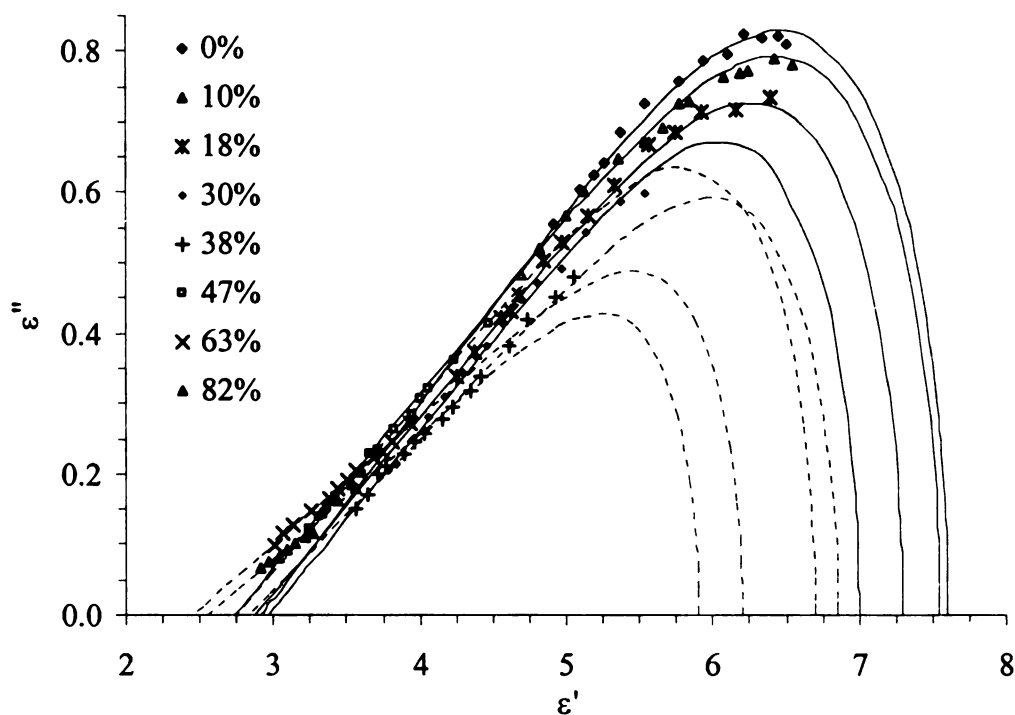


Figure 4.22 Cole-Cole plots for the curing DGEBA/Jeffamine system

Table 4.5 shows the calculated values of all parameters in the models. The gel point of the reacting DGEBA/Jeffamine system is between 30% and 40% extents. Before the extent of cure reaches 30%, the reacting system is not viscous and the relaxation time is small. Therefore, the simplified Davidson-Cole expression is not suitable to describe its dielectric behavior.

As the reaction goes on, the parameter  $n$  decreases from 0.172 down to 0.112 (see Figure 4.23). The parameter  $n$  is mainly connected with the motion of dipolar groups for the secondary  $\gamma$  relaxation. During the reaction the motion of dipolar groups is hindered

by crosslinking epoxy resins. Therefore, the parameter  $n$  decreases. The parameter  $\epsilon_0$  represents the equilibrium behavior while  $\epsilon_\infty$  represents the instantaneous behavior. Therefore,  $(\epsilon_0 - \epsilon_\infty)$  is the effective moment of the orienting unit. The  $\gamma$  relaxation strength  $(\epsilon_0 - \epsilon_\infty)$  was found to decrease during the polymerization, as shown in Figure 4.23. This is consistent with the decreasing number of the dipolar groups in the reactants.

Table 4.5 Values of the parameters for the curing DGEBA/Jeffamine system

Extent of cure	$n$	$\epsilon_0$	$\epsilon_\infty$	$(\epsilon_0 - \epsilon_\infty)$	$E_a$ (kJ/mol)	$A$ (s)
0%	0.172	7.60	2.92	4.68	69	8.6E-21
10%	0.155	7.55	2.74	4.81	80	2.6E-22
18%	0.156	7.30	2.88	4.42	99	8.9E-25
30%	0.158	7.00	2.96	4.04	105	8.7E-25
38%	0.134	6.85	2.83	4.02	131	3.0E-28
47%	0.150	6.70	2.74	3.96	123	2.0E-26
63%	0.114	6.20	2.45	3.75	135	9.8E-27
82%	0.112	5.90	2.56	3.34	110	2.2E-21

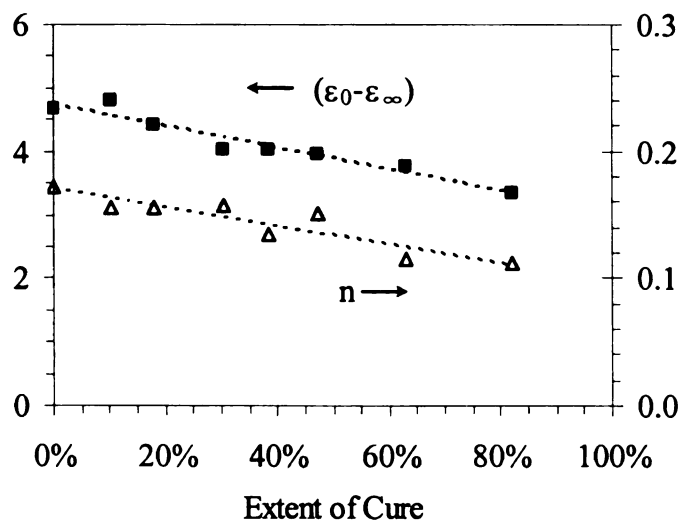


Figure 4.23  $n$  and  $(\epsilon_0 - \epsilon_\infty)$  vs. extent of cure for the curing DGEBA/Jeffamine system

The activation energy of the  $\gamma$  relaxation first increases and then decreases during the reaction in Figure 4.24. The increasing activation energy during cure is consistent with the fact that the viscosity of the reacting system increases as the polymerization progresses. However, after the extent of cure reaches around 60% the activation energy start to decrease. It may be explained by that the hindrance ability of the existing polymer chains may be weaker than that of dipoles in the reactants and thus less energy is needed for dipolar groups to relax after the peak point.

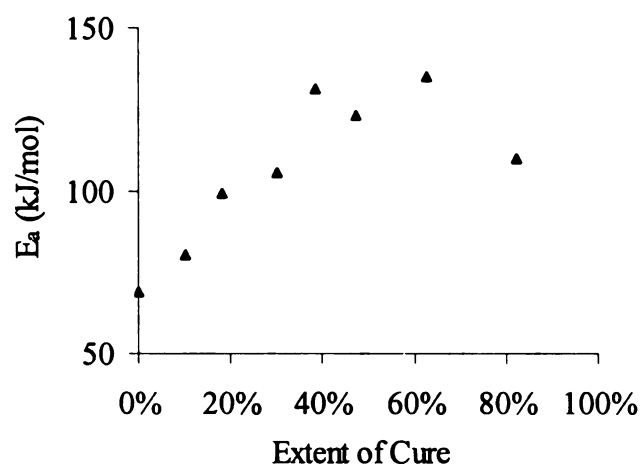


Figure 4.24  $E_a$  vs. extent of cure for the curing DGEBA/Jeffamine system

Figure 4.25 shows the calculated  $\gamma$  relaxation time of DGEBA/Jeffamine epoxy resin at different temperatures and extents. The relaxation time increases as the temperature decreases and the curing reaction goes on. The main reason for the remarkable increase of the relaxation time during the reaction is the rise of the medium viscosity.

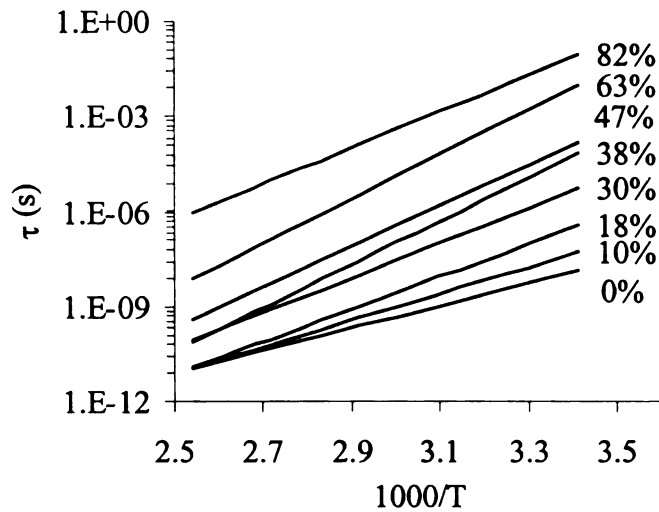


Figure 4.25  $\tau$  vs.  $1000/T$  for the curing DGEBA/Jeffamine system

**Conclusion:** The dielectric properties of a crosslinking DGEBA/Jeffamine D-230 epoxy resin system as a function of temperature in a range of 20-90°C at 2.45 GHz have been investigated. The dielectric constant and dielectric loss factor of the uncured DGEBA/Jeffamine D-230 mixture are larger than those of DGEBA. Normally, the real and the imaginary part of the complex dielectric constant increased with temperature while they decreased as the extent of cure increased. The Davidson-Cole model can be used to describe the experimental data. The simplified Davidson-Cole expression is used to calculate the parameters in the Davidson-Cole model. It is also applicable to the experimental data of extent of cure larger than 30%. The Arrhenius-like dependent  $\gamma$  relaxation has been identified. The evolution of the parameters in the models, e.g. the shape parameter  $n$ , the relaxation strength  $(\epsilon_0 - \epsilon_\infty)$ , the activation energy  $E_a$ , and the relaxation time  $\tau$ , was related to the facts that the dipolar groups in the reactants decrease in number and medium viscosity increases during the polymerization.

#### 4.4.3 DGEBA/mPDA System

Dielectric properties of DGEBA, mPDA, and uncured DGEBA/mPDA mixture at 2.45 GHz versus temperature are shown in Figure 4.26.

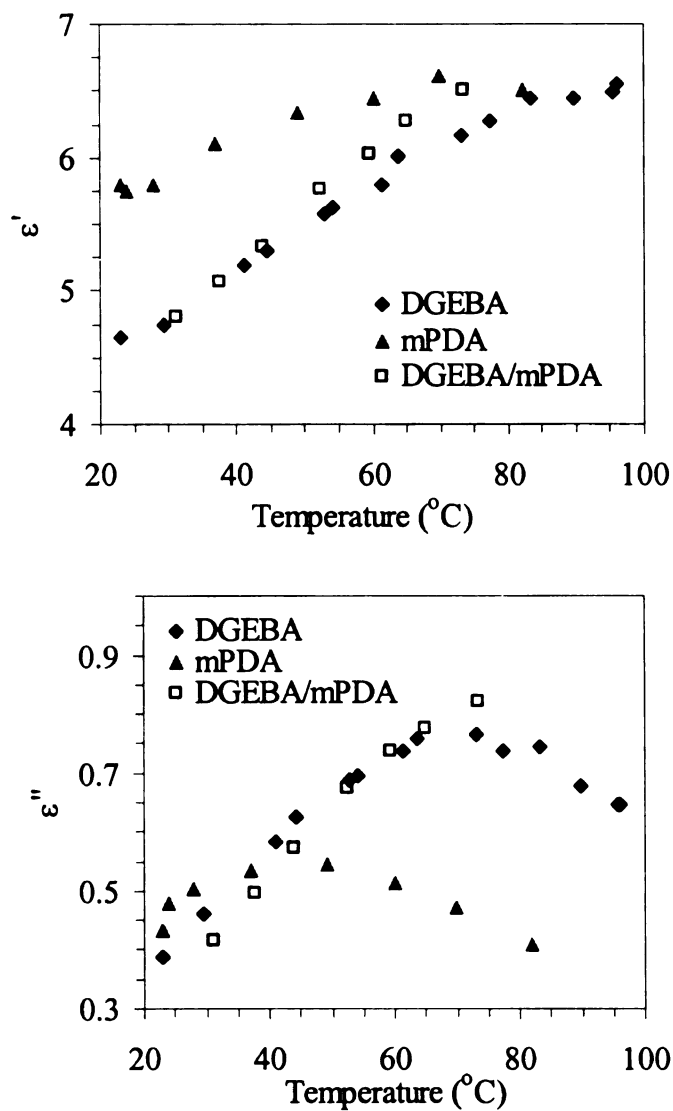


Figure 4.26 Dielectric properties vs. temperature for DGEBA, mPDA, and uncured DGEBA/mPDA mixture

The dielectric constant of DGEBA increases as the temperature increases from 20°C to 80°C, remains stable around 80°C to 100°C, and then decreases. The dielectric loss factor increases first, and then decreases with a peak value around 70°C. The dielectric constant of mPDA increases while its loss factor has a peak around 40°C as the temperature increases. The dielectric properties of uncured DGEBA/mPDA mixture are almost same as those of DGEBA over temperatures ranging from 20 to 80°C. Compared with DDS (see Table 4.1), mPDA has small molecules and low amine equivalent weight. Added mPDA did not change the dielectric properties of DGEBA too much due to its small molecules, which may not change the viscosity of DGEBA.

Dielectric constant and dielectric loss factor of reacting DGEBA/mPDA epoxy resins over a temperature range of 20-100°C are shown in Figure 4.27, where points represent the experimental data and lines represent calculated data. The extents of cure were calculated from DSC data, which are shown in Table 4.6.

Table 4.6 DSC results of the curing DGEBA/mPDA system

Absorbed Heat (J/g)	467	488	319	311	211	89	72
	492	370	297	215	192	93	60
	477	403	302	223	198	112	81
Average	479	420	306	249	200	98	71
Extent of Cure	0%	11%	35%	47%	58%	79%	85%
Standard Error	2%	7%	1%	6%	1%	1%	1%
Physical state	Liquid	Liquid	Liquid	Solid	Solid	Solid	Solid

The dielectric properties of DGEBA/mPDA epoxy resins decrease as the extent of cure increases and increase with temperature except  $\epsilon''$  at 11% extent of cure at high temperatures. The explanation of the phenomena is similar to that of DGEBA/DDS and

DGEBA/Jeffamine systems. The reaction mechanism of the DGEBA epoxy resin system is shown in Figure 4.8. The predominant relaxation in the DGEBA epoxy resins at 2.45 GHz is the  $\gamma$  relaxation [5]. The two reasons accounting for the decrease in the dielectric constant and loss factor during the reaction are a decrease in the number of the dipolar groups in the reactants and an increase in the viscosity.

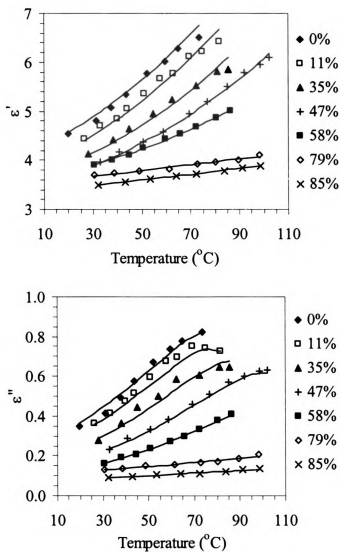


Figure 4.27 Temperature dependence of dielectric properties for the curing DGEBA/mPDA system

The Davidson-Cole model was used to describe the dielectric behavior of DGEBA/mPDA epoxy resins while the simplified Davidson-Cole expression can be used to calculate the parameters. The simplified Davidson-Cole expression is also applicable to dielectric properties of DGEBA/mPDA epoxy resins over 47% extents and low-temperature dielectric parts of those from 0% to 47% extents. The Davidson-Cole model is given by Equation 4.13 while the simplified Davidson-Cole expression is shown in Equation 4.18. The dominant  $\gamma$  relaxation in this system should fit the Arrhenius expression in Equation 4.11.

Figure 4.28 shows plots of  $\epsilon''$  versus  $\epsilon'$ , which yield straight lines. The values of  $\epsilon''$  and  $\epsilon'$  at 11, 35, and 47% extents are low-temperature data in Figure 4.27.

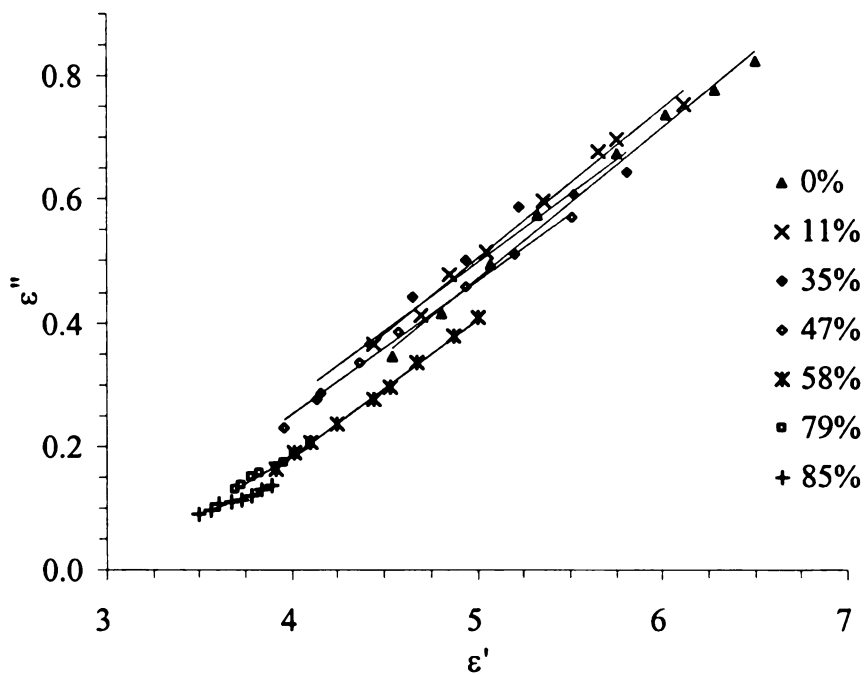


Figure 4.28  $\epsilon''$  vs.  $\epsilon'$  for the curing DGEBA/mPDA system

According to Equation 4.21, plots of  $\ln(\epsilon' - \epsilon_\infty)$  versus  $1/T$  and  $\ln(\epsilon'')$  versus  $1/T$  of experimental data in Figure 4.28 yield straight lines, shown in Figures 4.29 and 4.30.

Curves represent fit of the proposed expression to the experimental data points.

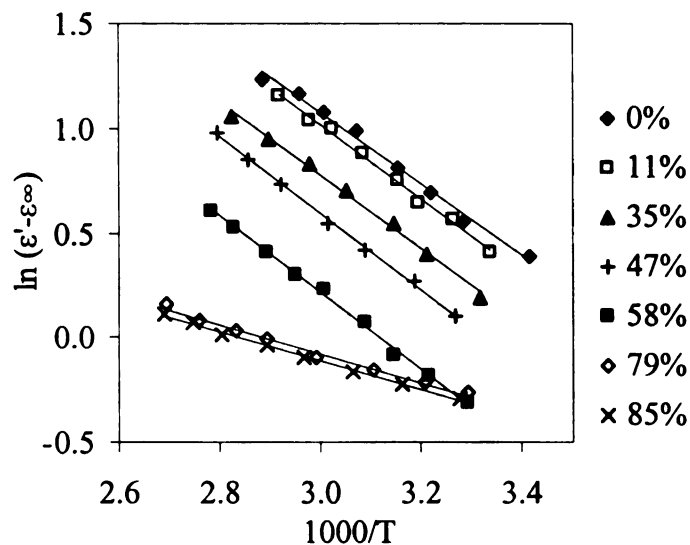


Figure 4.29  $\ln(\epsilon' - \epsilon_\infty)$  vs.  $1000/T$  for the curing DGEBA/mPDA system

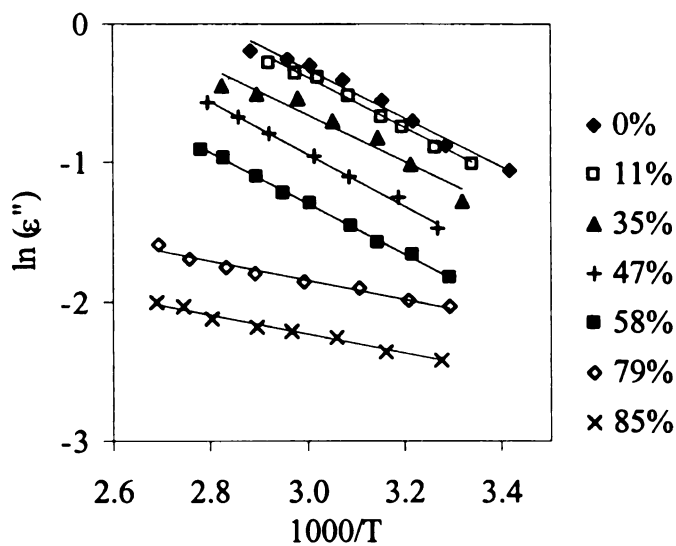


Figure 4.30  $\ln(\epsilon'')$  vs.  $1000/T$  for the curing DGEBA/mPDA system

The parameters  $n$  and  $\epsilon_{\infty}$  of the curing DGEBA/mPDA epoxy resins were calculated from slopes and intercept of Figure 4.28.  $E_a$  and a relation between  $\epsilon_0$  and  $A$  can be calculated based on Figures 4.29 and 4.30. The values of  $\epsilon_0$  at 0%, 11%, 35%, 47% extents were modified until the calculated data from the Davidson-Cole model fitted the experimental data well.  $\epsilon_0$  at 58%, 79%, and 85% extents were estimated based on the modification and the rule that  $(\epsilon_0 - \epsilon_{\infty})$  decreases during curing.

Comparison of the experimental data with the calculated data is shown in Figure 4.27. The calculated data of 0% to 47% extents were calculated from the Davidson-Cole model while the others were calculated using the simplified Davidson-Cole expression. Figure 4.31 shows the comparison of the experimental data with the calculated Cole-Cole plots from the Davidson-Cole model.

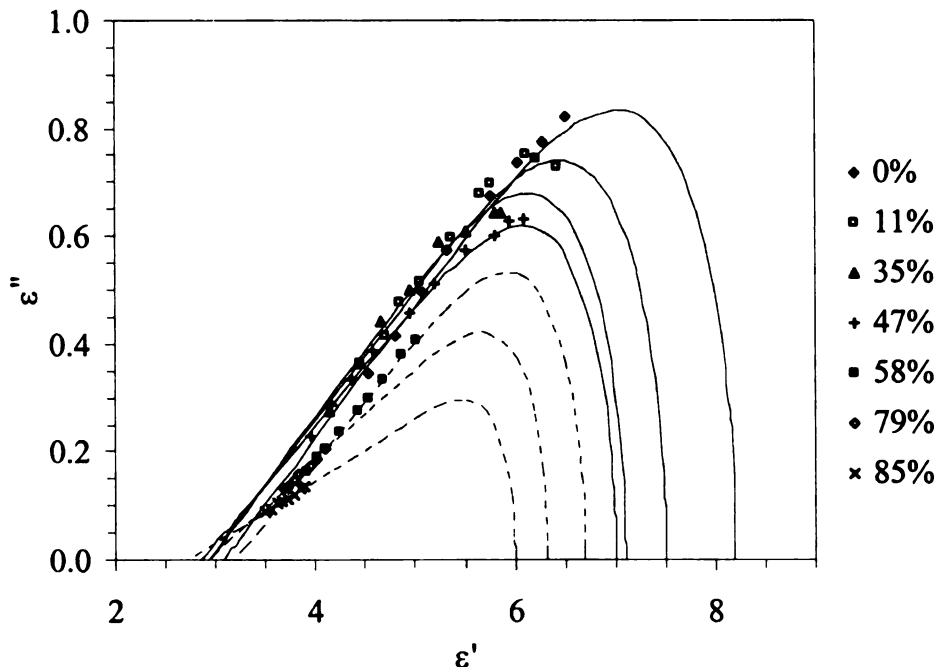


Figure 4.31 Cole-Cole plots for the curing DGEBA/mPDA system

Table 4.7 shows the calculated values of the parameters of the Davidson-Cole model and the Arrhenius expression. As the reaction goes on the parameter  $n$  decreases from 0.153 down to 0.073 (see Figure 4.32). The parameter  $n$  is mainly connected with the motion of dipolar groups for the secondary  $\gamma$  relaxation. During the reaction the motion of dipolar groups is hindered by curing epoxy resins. Therefore, the parameter  $n$  decreases.  $\epsilon_0$  represents the equilibrium behavior while  $\epsilon_\infty$  represents the instantaneous behavior. Therefore,  $(\epsilon_0 - \epsilon_\infty)$  is the effective moment of the orienting unit. The  $\gamma$  relaxation strength  $(\epsilon_0 - \epsilon_\infty)$  was found to decrease during the polymerization in Figure 4.32. This is consistent with the decreasing number of the dipolar groups in the reactants.

The activation energy of the  $\gamma$  relaxation first increases and then decreases during the reaction, shown in Figure 4.33. The increasing activation energy during cure is consistent with increasing viscosity of the reacting system during curing. However, after the extent of cure reaches around 40%, gel point shown in Table 4.6, the activation energy start to decrease. It may be explained by that the hindrance ability of the existing polymer chains may be weaker than that of dipoles in the reactants and thus less energy is needed for dipolar groups to relax after the peak point.

Table 4.7 Values of the parameters for the curing DGEBA/mPDA system

Extent of cure	$n$	$\epsilon_0$	$\epsilon_\infty$	$(\epsilon_0 - \epsilon_\infty)$	$E_a$ (kJ/mol)	$A$ (s)
0%	0.153	8.20	3.07	5.13	93	4.6E-24
11%	0.152	7.50	2.94	4.56	98	7.1E-25
35%	0.153	7.10	2.93	4.17	101	6.2E-25
47%	0.137	7.00	2.85	4.15	113	6.3E-26
58%	0.139	6.70	3.18	3.52	109	8.4E-25
79%	0.108	6.32	2.92	3.40	53	4.3E-14
85%	0.073	6.00	2.73	3.27	79	9.2E-16

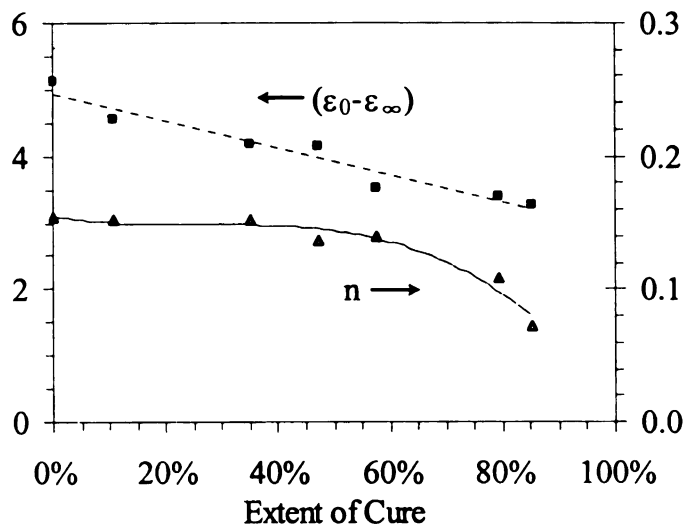


Figure 4.32 n and ( $\epsilon_0 - \epsilon_\infty$ ) vs. extent of cure for the curing DGEBA/mPDA system

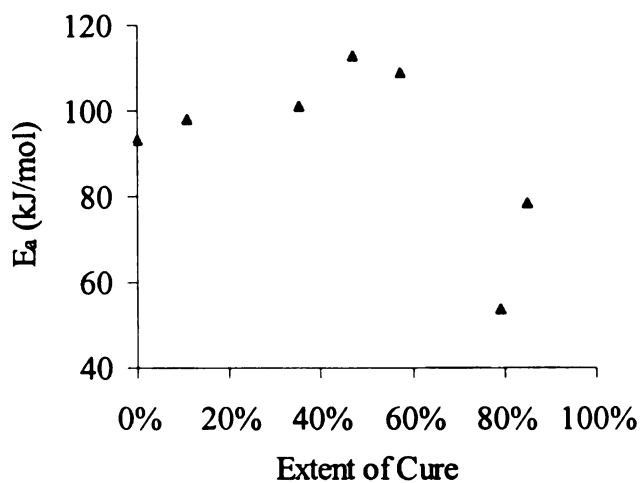


Figure 4.33  $E_a$  vs. extent of cure for the curing DGEBA/mPDA system

Figure 4.34 shows the calculated  $\gamma$  relaxation time of DGEBA/mPDA epoxy resin at different temperatures and extents. The relaxation time increases as the temperature decreases and the curing reaction goes on. The main reason for the remarkable increase of the relaxation time during the reaction is the rise of the medium viscosity.

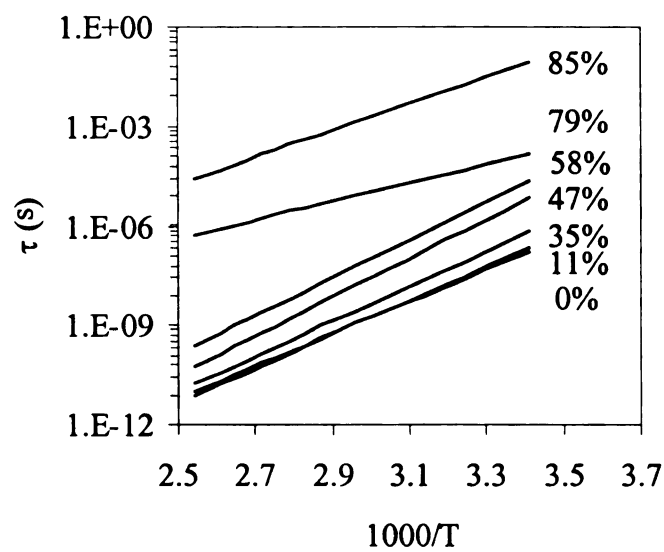


Figure 4.34  $\tau$  vs.  $1000/T$  for the curing DGEBA/mPDA system

**Conclusion:** The dielectric properties of a crosslinking DGEBA/mPDA epoxy resin system as a function of temperature in a range of 20-100°C at 2.45 GHz have been investigated. The dielectric constant and dielectric loss factor of the uncured DGEBA/mPDA mixture are similar to those of DGEBA. Normally, the real and the imaginary part of the complex dielectric constant increased with temperature while they decreased as the extent of cure increased. The Davidson-Cole model can be used to describe the experimental data. The simplified Davidson-Cole expression is used to calculate the parameters and is also applicable to the experimental data of extent of cure larger than 47%. The Arrhenius-like dependent  $\gamma$  relaxation has been identified. The evolution of the parameters in the models, e.g. the shape parameter  $n$ , the relaxation strength ( $\epsilon_0 - \epsilon_\infty$ ), the activation energy  $E_a$ , and the relaxation time  $\tau$ , can be related to facts that the dipolar groups in the reactants decrease in number and medium viscosity increases during the polymerization.

#### 4.4.4 DGEBA/Epikure W System

Dielectric properties of DGEBA, Epikure W (W hereafter), and uncured DGEBA/W mixture in a temperatures range of 20 to 120°C are shown in Figure 4.35.

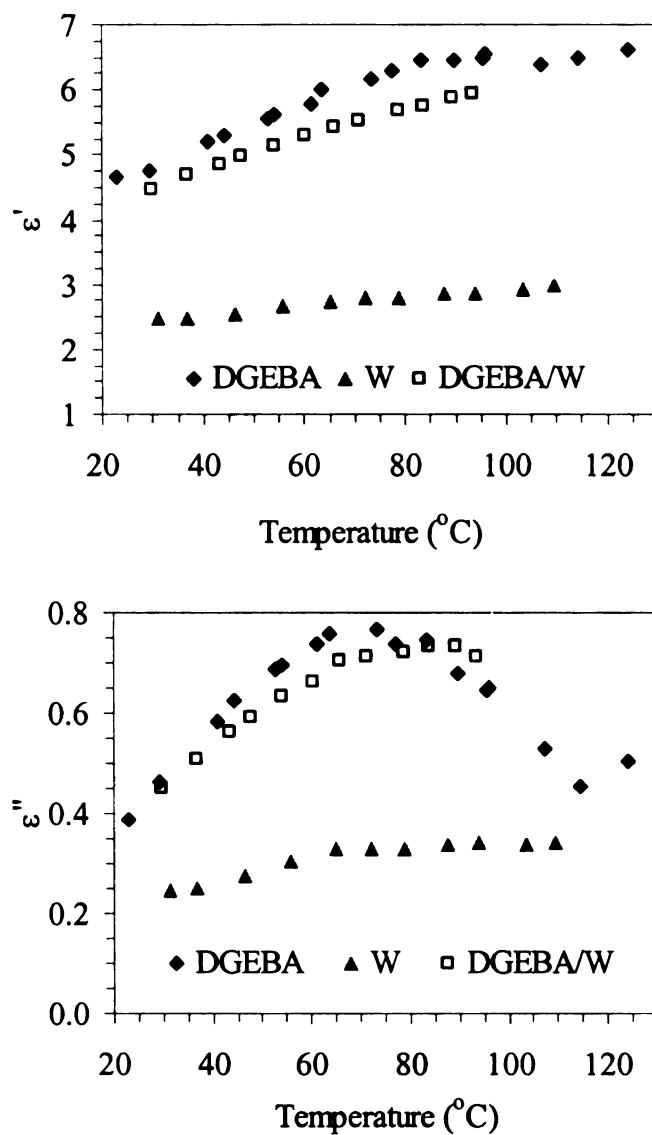


Figure 4.35 Dielectric properties vs. temperature for DGEBA, W, and uncured DGEBA/W mixture

The dielectric constant of DGEBA increases as the temperature increases from 20°C to 80°C, remains stable around 80°C to 100°C, and then decreases. The dielectric

loss factor increases first and then decreases with a peak value around 70°C. The dielectric constant and loss factor of W increases as the temperature increases. The dielectric properties of uncured DGEBA/W mixture are similar to those of DGEBA.

The dielectric constant and dielectric loss factor of reacting DGEBA/W epoxy resins over a temperature range of 20-130°C are shown in Figure 4.36. The extents of cure were calculated from DSC data, which are shown in Table 4.8.

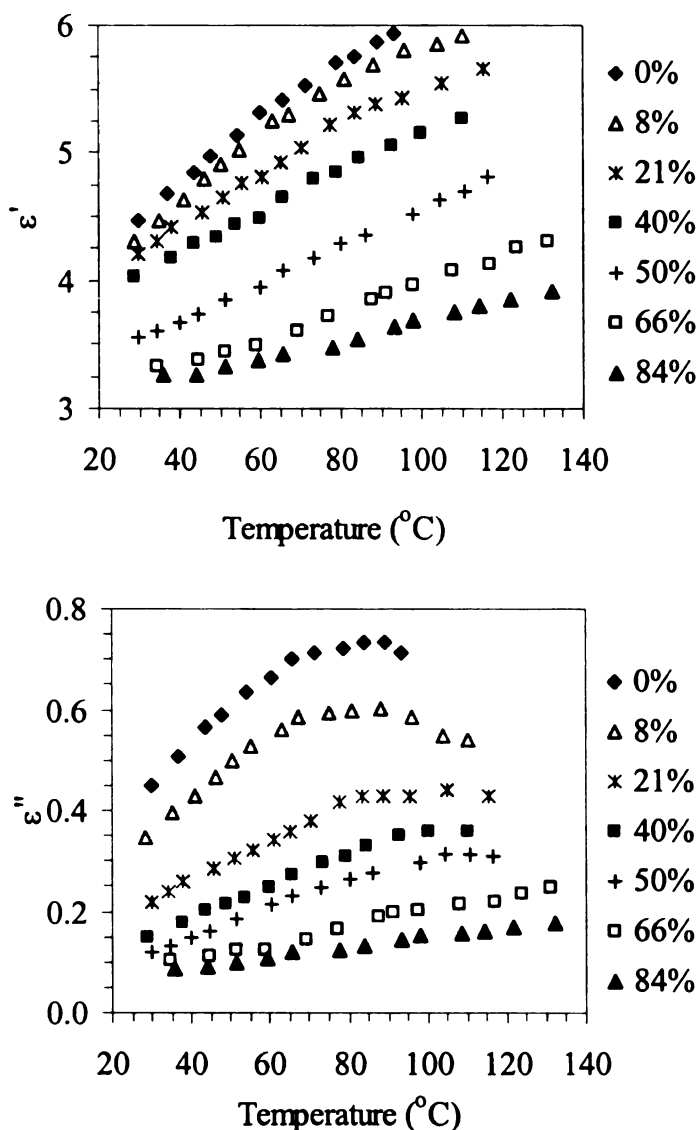


Figure 4.36 Temperature dependence of dielectric properties for the curing DGEBA/W system

Table 4.8 DSC results of the curing DGEBA/W system

Absorbed Heat (J/g)	309	257	245	157	167	75	35
	261	250	217	179	120	138	49
	282	276	213	175	142	80	52
Average	284	261	225	170	143	97	45
Extent of Cure	0%	8%	21%	40%	50%	66%	84%
Standard Error	5%	3%	4%	2%	5%	7%	2%
Physical state	Liquid	Liquid	Gel	Solid	Solid	Solid	Solid

The dielectric constant of the DGEBA/W epoxy resins increases as the temperature increases and decreases as the extent of cure increases. The dielectric loss factor of the DGEBA/W system first increases and then decreases as the temperature increases, except at 66% and 84% extents. The dielectric loss factor at 66% and 84% extents increases with temperature. Generally, the changes of the dielectric properties with  $(\omega\tau)$  are illustrated in Figure 4.1 and 4.2. An increase in temperature leads to a decrease in the relaxation time and  $(\omega\tau)$ . The changing pattern of the dielectric properties of DGEBA/W system is same as shown in Figure 4.1 and 4.2. It is known from Figure 4.36 that one relaxation exists in the DGEBA/W system. The reaction mechanism of the DGEBA epoxy resin system is shown in Figure 4.8. The predominant relaxation in the DGEBA epoxy resins at 2.45 GHz is the  $\gamma$  relaxation.

The Davidson-Cole model was used to describe the dielectric behavior of DGEBA/W epoxy resins while the simplified Davidson-Cole expression can be used to calculate the parameters. The Davidson-Cole model is given by Equation 4.13 while the simplified Davidson-Cole expression is shown in Equation 4.18. The calculation procedure is same as that for DGEBA/mPDA system in chapter 4.4.3.

Figure 4.37 shows the comparison of the experimental data with the calculated data from the Davidson-Cole model. The calculated values fitted the experimental data well for data at low temperatures and high extents of cure. The difference between the experimental data and the calculated data is, normally, caused by the calculation error based on the approximation functions and the experimental error due to fluctuation of measured data including temperature, resonant frequency, and half-power frequency bandwidth. The difference at low extents and high temperatures in Figure 4.37 is mainly caused by rapid reaction at low extents and high temperatures under microwave irradiation and the extent of cure changed during measuring the dielectric properties. Therefore, the dielectric properties deviated from the models, e.g. the Cole-Cole model, the Davidson-Cole model, the H-N model, and the simplified Davidson-Cole expression. The fitting results in Figure 4.37 are best from the models.

Table 4.9 shows the calculated parameters of the Davidson-Cole model and the Arrhenius expression. The gel point of DGEBA/mPDA epoxy resin is between 21% and 40% extents, shown in Table 4.8. Before the extent of cure reaches 21%, the reacting system is low in viscosity and the relaxation time is small.

Table 4.9 Values of the parameters for the curing DGEBA/W system

Extent of cure	n	$\epsilon_0$	$\epsilon_\infty$	$(\epsilon_0 - \epsilon_\infty)$	$E_a$ (kJ/mol)	A (s)
0%	0.161	7.10	2.70	4.40	1.57	64
8%	0.145	7.00	2.70	4.30	1.57	79
21%	0.123	6.40	3.04	3.36	1.57	94
40%	0.121	6.00	3.24	2.76	1.57	101
50%	0.123	5.30	2.92	2.38	1.57	110
66%	0.092	5.20	2.60	2.60	1.57	107
84%	0.084	4.90	2.56	2.34	1.57	94

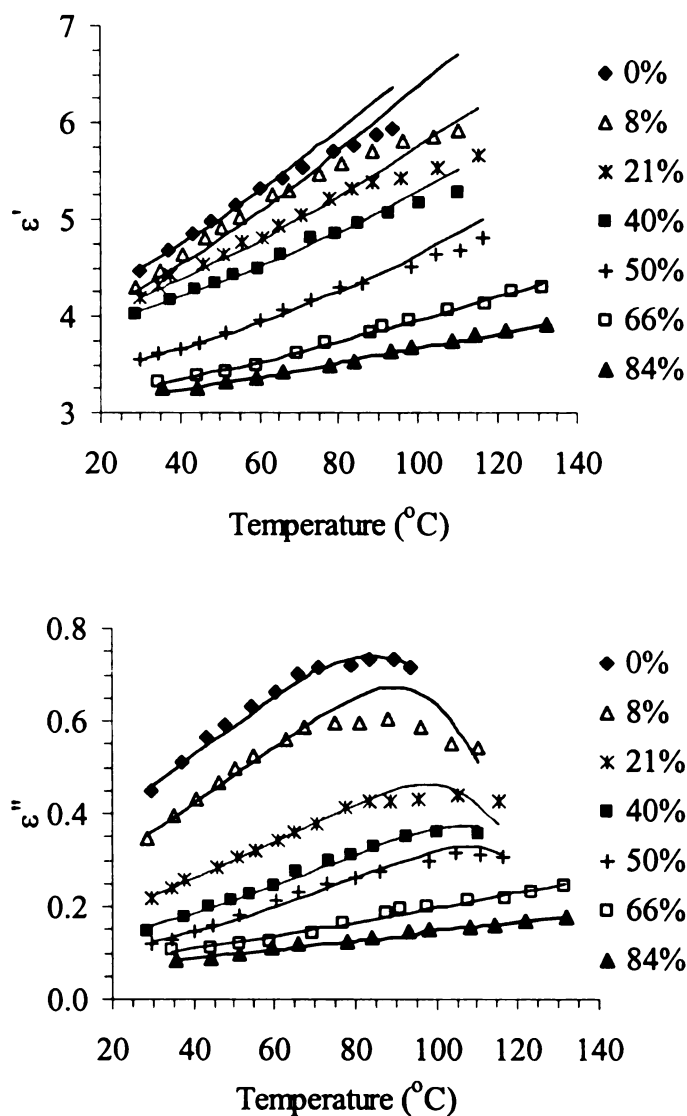


Figure 4.37 Comparison between the experimental and calculated data of the curing DGEBA/W system.

As the reaction goes on the parameter  $n$  decreases from 0.161 down to 0.084 (see Figure 4.38). The parameter  $n$  is mainly connected with the motion of dipolar groups for the secondary  $\gamma$  relaxation. During the reaction the motion of dipolar groups is hindered by curing epoxy resins. Therefore, the parameter  $n$  decreases. The parameter  $\epsilon_0$  represents the equilibrium behavior while  $\epsilon_\infty$  represents the instantaneous behavior. Therefore,  $(\epsilon_0 - \epsilon_\infty)$  is the effective moment of the orienting unit. The  $\gamma$  relaxation strength  $(\epsilon_0 - \epsilon_\infty)$  was

found to decrease during the polymerization, as shown in Figure 4.38. This is consistent with the decreasing number of the dipolar groups in the reactants.

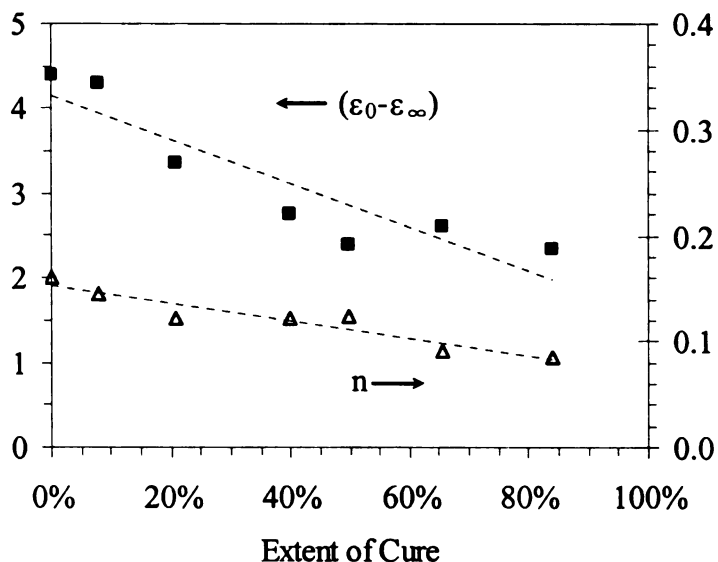


Figure 4.38  $n$  and  $(\epsilon_0 - \epsilon_\infty)$  vs. extent of cure for the curing DGEBA/W system

The activation energy of the  $\gamma$  relaxation of the DGEBA/W system first increases and then decreases during the reaction, shown in Figure 4.39. The increasing activation energy during cure is consistent with the fact that the viscosity of the reacting system increases as the polymerization progresses. However, after the extent of cure reaches around 40%, gel point shown in Table 4.9, the activation energy start to decrease. It may be explained by that the hindrance ability of the existing polymer chains may be weaker than that of dipoles in the reactants and thus less energy is needed for dipolar groups to relax after the peak point.

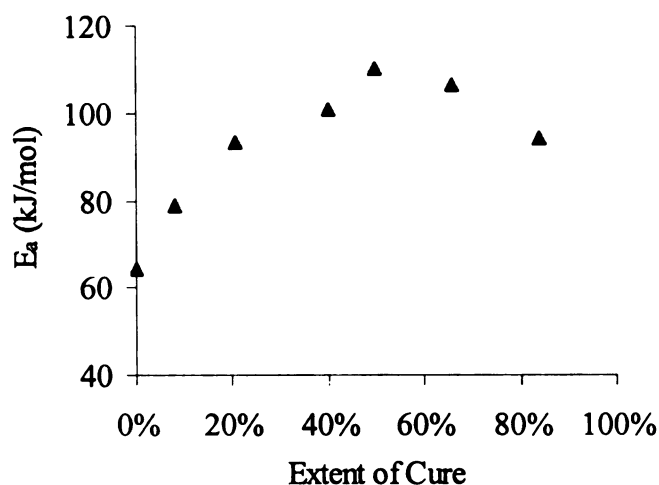


Figure 4.39  $E_a$  vs. extent of cure for the curing DGEBA/W system

Figure 4.40 shows the calculated  $\gamma$  relaxation time of the DGEBA/W epoxy resins at different temperatures. The relaxation time increases as the temperature decreases or the curing reaction goes on. The main reason for the remarkable increase of the relaxation time during the reaction is the rise of the medium viscosity.

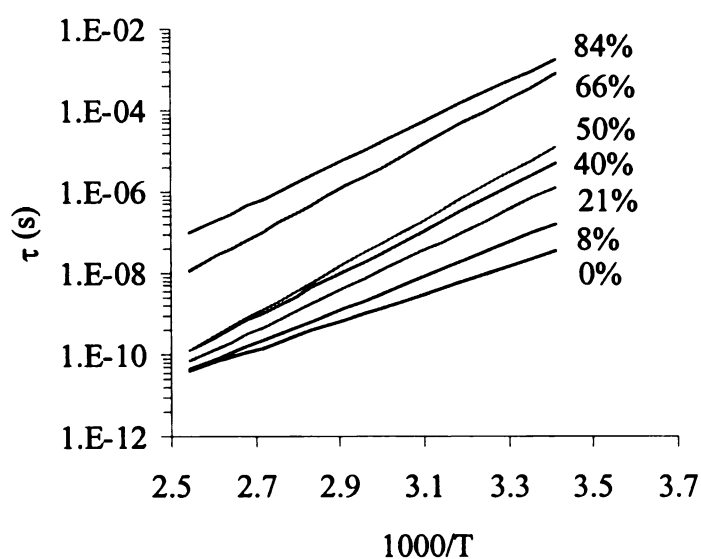


Figure 4.40  $\tau$  vs. 1000/T for the curing DGEBA/W system

**Conclusion:** The dielectric properties of a curing DGEBA/W epoxy resin system as a function of temperature in a range of 20-130°C at 2.45 GHz have been investigated. The dielectric constant and dielectric loss factor of the uncured DGEBA/W mixture are similar to those of DGEBA. The Davidson-Cole model can be used to describe the experimental data. The simplified Davidson-Cole expression was used to calculate the parameters and is also applicable to the experimental data at low temperatures or high extents of cure. The Arrhenius-like dependent  $\gamma$  relaxation has been identified. The evolution of the parameters in the models, e.g. the shape parameter  $n$ , the relaxation strength ( $\epsilon_0 - \epsilon_\infty$ ), the activation energy  $E_a$ , and the relaxation time  $\tau$ , can be related to facts that the dipolar groups in the reactants decrease in number and medium viscosity increases during the polymerization.

#### 4.4.5 Parameters in the Models for the Four Systems

The dielectric properties of the reacting systems of DGEBA epoxy resin and the four curing agents have been investigated at 2.45 GHz over a temperature range. The  $\gamma$  relaxation was identified in the four systems. The Davidson-Cole model in Equation 4.13 can describe the dielectric behaviors while the Arrhenius expression in Equation 4.11 was used to describe the  $\gamma$  relaxation time. Although the proposed simplified Davidson-Cole model in Equation 4.18 can only represent the dielectric properties of DGEBA/DDS system and part of those of the other three systems, it can be used to calculate the parameters in the Davidson-Cole model.

$$\tau = A \times e^{\left(\frac{E_a}{RT}\right)} \quad (4.11)$$

$$\begin{aligned}\varepsilon^* - \varepsilon_\infty &= \frac{(\varepsilon_0 - \varepsilon_\infty)}{(1 + j\omega\tau)^n} \\ \varepsilon' &= \varepsilon_\infty + \frac{(\varepsilon_0 - \varepsilon_\infty)\cos(n\theta)}{(1 + (\omega\tau)^2)^{\frac{n}{2}}} \\ \varepsilon'' &= \frac{(\varepsilon_0 - \varepsilon_\infty)\sin(n\theta)}{(1 + (\omega\tau)^2)^{\frac{n}{2}}}\end{aligned}\tag{4.13}$$

$$\theta = \arctan(\omega\tau)$$

$$\begin{aligned}\varepsilon^* &= \varepsilon_\infty + \frac{(\varepsilon_0 - \varepsilon_\infty)}{(j\omega\tau)^n} \\ \varepsilon' &= \varepsilon_\infty + \frac{(\varepsilon_0 - \varepsilon_\infty)\cos(n\frac{\pi}{2})}{(\omega\tau)^n} \\ \varepsilon'' &= \frac{(\varepsilon_0 - \varepsilon_\infty)\sin(n\frac{\pi}{2})}{(\omega\tau)^n}\end{aligned}\tag{4.18}$$

$(\varepsilon_0 - \varepsilon_\infty)$  is the effective moment of the orienting dipoles [249]. Figure 4.41 shows the  $\gamma$  relaxation strength as a function of extent of cure for the four reacting systems.  $(\varepsilon_0 - \varepsilon_\infty)$  was found to decrease during the polymerization of the four systems, which is consistent with the decreasing number of the epoxy and amine groups in the reactants. Researchers at University of Pisa reached same results for similar reacting systems [267, 269] while Sheppard and Senturia reported that the relaxed dielectric constant  $\varepsilon_\infty$  decreased as the reaction progressed and could be linearly related to the extent of cure for

DGEBA/DDS reacting system [273]. In addition, the relaxation strength was found to diminish with increasing molecular weight of DGEBA prepolymers [265].

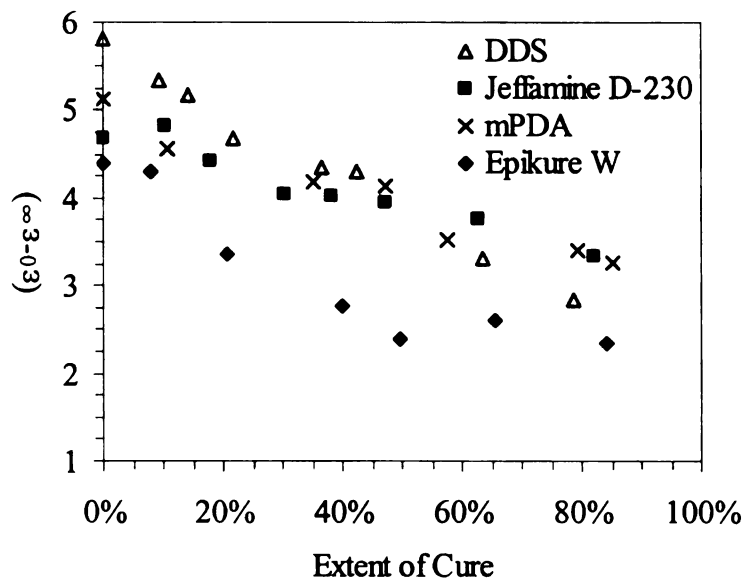


Figure 4.41 ( $\epsilon_0 - \epsilon_{\infty}$ ) vs. extent of cure for the four curing systems

Figure 4.42 shows the shape parameter  $n$  as a function of extent of cure for the four systems. As the reaction goes on,  $n$  decreases from 0.18 down to 0.06. The four systems have same trend. The parameter describes the skewness of the dispersion of the relaxation times, which increases as  $n$  ranges from unity to zero. The value of  $n$  for an ideal Debye material is unity while that for polymeric solutions is around 0.5 [285]. The relaxation time is mainly connected with the mobility of the dipolar groups. During the reaction, the motion of dipolar groups is hindered by the medium with increasing viscosity. Therefore, the parameter  $n$  decreases. The rationale is similar to the argument that  $n$  is connected with the local chain dynamics of a polymer and decreases in the range

0.5-0 with an increase of hindrance of orientational diffusion in the polymer [283]. Another similar result is that the parameter  $n$  for DGEBA prepolymers decreases as the molecule weight increases [265].

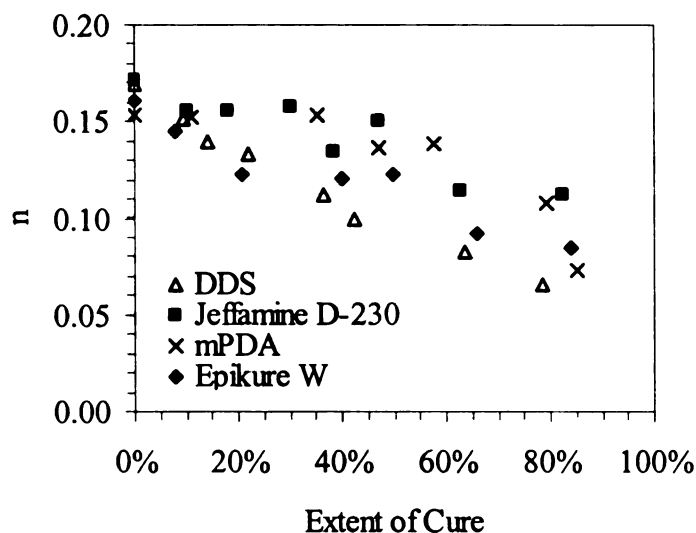


Figure 4.42  $n$  vs. extent of cure for the four curing systems

The activation energy of the  $\gamma$  relaxation for all four systems first increases, and then decreases during cure (see Figure 4.43). The activation energy is the mean value of a distribution of activation energies [251] and changes with the polymerization [259]. The phenomenon of increasing activation energy is consistent with the fact that the viscosity increases as the polymerization progresses. However, after the extent of cure reaches around 50%, the activation energy start to decrease. It may be explained by that the hindrance ability of the existing polymer chains may be weaker than that of dipoles in the reactants and thus less energy is needed for dipolar groups to relax after the peak point.

Inasmuch as the gel point for the DGEBA/DDS system is 58% [281] and, in this study, the changing temperatures of the other three systems from liquid to solid are around 40-50%, the peak around 50% extent may be related to the gel point of the curing system.

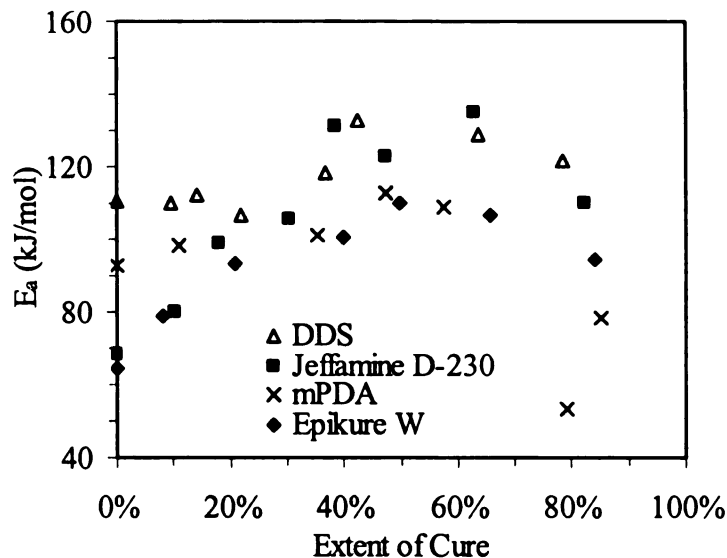


Figure 4.43  $E_a$  vs. extent of cure for the four curing systems

The relaxation time increases as the reaction proceeds. For instance, the calculated  $\gamma$  relaxation time at 80°C has been reported as a function of the extent of cure in Figure 4.44. This is consistent with Kauzman's study on relaxation on polymers [251]. The main reason for the remarkable increase of the relaxation time during the reaction is the rise of the medium viscosity. Furthermore, it is shown in Figure 4.44 that the relaxation time of DGEBA/DDS system is about two decades larger than that of DGEBA/Jeffamine, DGEBA/mPDA, and DGEBA/W systems.

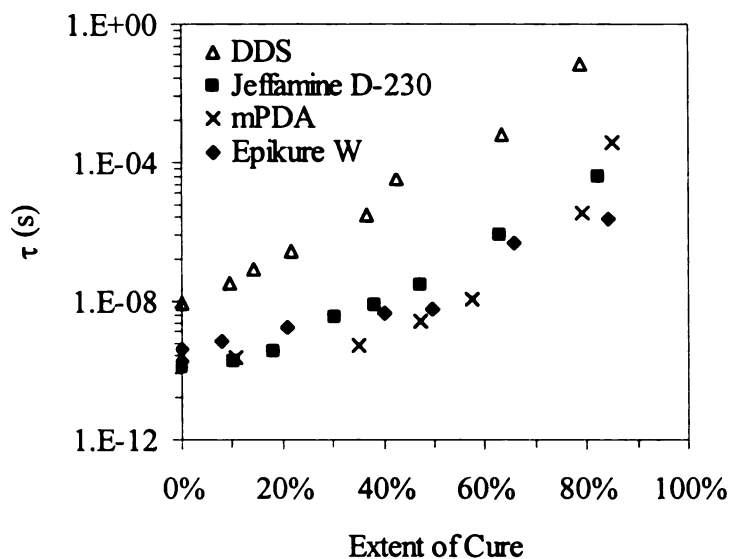


Figure 4.44  $\tau$  vs. extent of cure for the four curing systems at 80°C

Figure 4.45 shows the calculated dielectric constant as a function of extent of cure for the four isothermal curing systems. The dielectric constant exhibits a linear relation to the extent of cure and may be used to in-situ monitor the polymerization. Other researchers reached similar result [276].

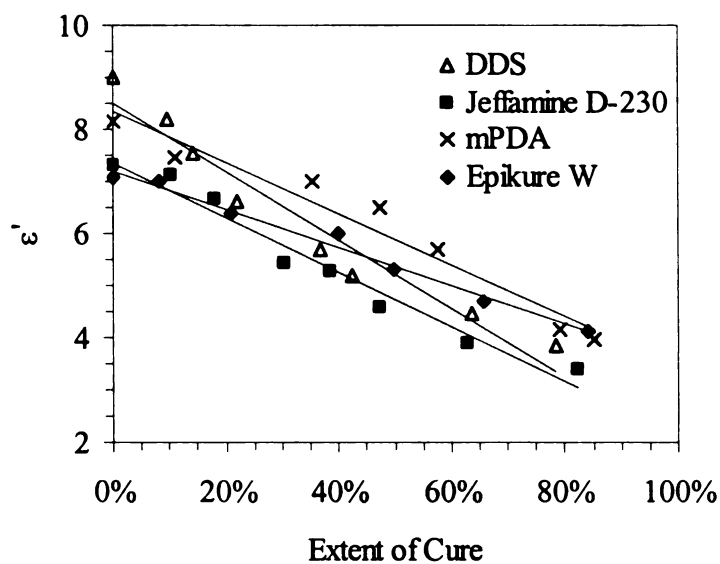


Figure 4.45 Calculated  $\epsilon'$  and  $\epsilon''$  vs. extent of cure for the four curing systems

## 4.5 Conclusions

A single-frequency microwave heating and diagnostic system, developed at Michigan State University, was used to heat and measure the dielectric constant and dielectric loss factor of curing epoxy resins. A cylindrical TM 012 mode cavity is used to process epoxy resins at 2.45 GHz. The epoxy resin was diglycidyl ether of bisphenol A (DGEBA). The four curing agents were 3, 3-diaminodiphenyl sulfone (DDS), a difunctional primary amine (Jeffamine D-230), m-phenylenediamine (mPDA), and diethyltoluenediamine (Epikure W). The mixtures of DGEBA and the four curing agents were stoichiometric. The four reacting systems were heated under microwave irradiation to certain cure temperatures, i.e. 145°C for DGEBA/DDS, 90°C for DGEBA/Jeffamine D-230, 110°C for DGEBA/mPDA, and 160°C for DGEBA/Epikure W. Measurements of temperature and dielectric properties using the swept frequency method were made during free convective cooling of the samples. The cooled samples were analyzed with a Differential Scanning Calorimeter to determine the extents of cure.

The major conclusions of this chapter are:

- The Davidson-Cole model can be used to describe the dielectric properties of the four curing systems.
- The simplified Davidson-Cole expression is proposed to describe the dielectric properties of polymeric materials. It works well for the DGEBA/DDS system and part of the data of the other three systems. The model is more specific than the Schonhals-Schlosser model. It can be used to calculate the parameters of the Davidson-Cole model as well. The simplified Davidson-Cole expression is as follows:

$$\varepsilon^* = \varepsilon_\infty + \frac{(\varepsilon_0 - \varepsilon_\infty)}{(j\omega\tau)^n}$$

$$\varepsilon' = \varepsilon_\infty + \frac{(\varepsilon_0 - \varepsilon_\infty)\cos(n\frac{\pi}{2})}{(\omega\tau)^n}$$

$$\varepsilon'' = \frac{(\varepsilon_0 - \varepsilon_\infty)\sin(n\frac{\pi}{2})}{(\omega\tau)^n}$$

where  $\varepsilon^*$  is the complex dielectric constant,  $\varepsilon'$  is the dielectric constant,  $\varepsilon''$  is the dielectric loss factor,  $j$  is the imaginary unit,  $\omega$  ( $=2\pi f$ ,  $f$  is the oscillator frequency in Hz) is the radial frequency of the electric field in  $s^{-1}$ ,  $\tau$  is the relaxation time in s,  $\varepsilon_0$  is the low frequency dielectric constant,  $\varepsilon_\infty$  is the high frequency dielectric constant, and  $n$  is the shape parameter with a range of  $0 \leq n \leq 1$ .

- The secondary  $\gamma$  relaxation has been identified in the four reacting systems.

The Arrhenius expression is applicable to the  $\gamma$  relaxation.

- The evolution of all parameters in the models, e.g. the shape parameter  $n$ , the relaxation strength ( $\varepsilon_0 - \varepsilon_\infty$ ), the activation energy  $E_a$ , and the relaxation time  $\tau$ , during cure was related to the facts that the number of the dipolar groups in the reactants decreases and medium viscosity increases during the polymerization.

- The relaxation strength ( $\varepsilon_0 - \varepsilon_\infty$ ) was found to decrease during the polymerization of the four systems, which is consistent with the decreasing number of the epoxy and amine groups in the reactants.

- The shape parameter  $n$  decreases as the reaction proceeds for four systems.  $n$  is related to the local chain dynamics. During the reaction the motion of dipolar groups

is hindered by the medium with increasing viscosity. Therefore, the parameter  $n$  decreases.

- The activation energy of the four systems increases first, and then decrease around 50% extent of cure. The increase of activation energy before the peak is consistent with increasing viscosity of the systems during cure. The decrease after the peak point may be explained by that the hindrance ability of the reacted polymer chains may be weaker than that of dipoles in the reactants and, thus, less energy is needed for dipolar groups to relax. The peak points are related to the gel points of the four systems.

- The relaxation time increases as the reaction proceeds due to increasing medium viscosity for the four systems.

- The dielectric constants of the four reacting systems exhibit a linear relation to the extent of cure and may be used to in-situ monitor the curing reaction.

## CHAPTER 5 SYNTHESIS OF CARBON NANOTUBES BY MPCVD

### 5.1 Introduction

Carbon is found in many different compounds in the world while carbon alone forms graphite, diamond, fullerene and nanotubes. The illustrations of four forms in which the element carbon exists are shown in Figure 5.1 [286].

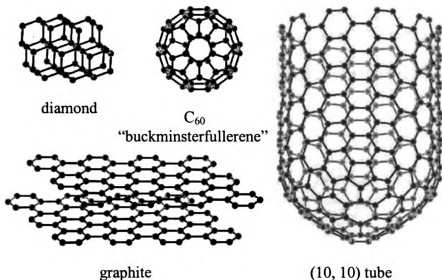


Figure 5.1 Schematic illustrations of four carbon forms

In diamond, the carbon atoms are connected to each other in all three dimensions, making it a very hard material. Graphite consists of layers of graphene sheets, layers of hexagonally patterned carbon atoms, which form a two-dimensional structure. The two-dimensionality of graphite makes it a softer material. Fullerenes consist of a caged structure similar to the shape of a soccer ball. Fullerenes were discovered in 1985 by Robert F. Curl Jr., Sir H. W. Kroto, and Richard E. Smalley, who were awarded the 1996

Nobel Prize in Chemistry. Fullerenes can be found in nature, whereas nanotubes are only man-made.

Carbon nanotubes (CNTs) were first discovered in 1991 by the Japanese electron microscopist Sumio Iijima of NEC Corporation, who was studying the material deposited on the cathode during the arc-evaporation synthesis of fullerenes [287]. A carbon nanotube is a tube-shaped material with a diameter measuring on the nanometer scale, which is made of carbon. CNTs are large macromolecules that are unique for their size, shape, and remarkable physical properties [288]. They are formed from hexagonal arrays of carbon atoms and can be thought of as a sheet of graphite rolled into a cylinder shown in Figure 5.2 [289].

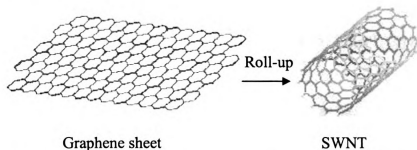


Figure 5.2 Schematic illustrations of relation between graphite and CNTs

There are two main types of CNTs that can have structural perfections, which are shown in Figure 5.3 [289]. Multi-wall nanotubes (MWNTs) comprise an array of such nanotubes that are concentrically nested like rings of a tree trunk. The CNTs that Sumio Iijima found in 1991 were MWNTs. Single-wall nanotubes (SWNTs), found in 1993 [290, 291] consist of a single graphite sheet seamlessly wrapped into a cylindrical tube. SWNTs can be defined by their diameter, length, and chirality. The SWNTs have a tubular form with a diameter as small as 0.4 nm [292] and a length of a few nanometers

to micrometers. The SWNTs with three different chiralities are shown in Figure 5.4 [289].

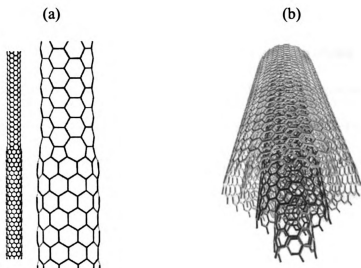


Figure 5.3 Schematic illustrations of CNTs: (a) SWNT, (b) MWNT.

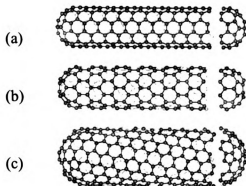


Figure 5.4 Schematic illustrations of three SWNTs of different chiralities: (a) armchair, (b) zigzag, (c) chiral.

CNTs possess many unique and remarkable chemical, physical, and electronic properties, which make them desirable for many applications.

SWNTs are incredibly stiff and tough mechanically. They may have a high Young's modulus (up to 1 TPa) [293] and high tensile strength (around 30 GPa) at an elongation of almost 6% [294, 295]. The density-normalized modulus and strength of SWNTs are around 20 and 50 times that of steel wire, respectively. Therefore, SWNTs are considered to be excellent reinforcement material for composites. The addition of a small weight percent of SWNT can result in significant improvement in mechanical properties of the composites. This demonstrates the potential of using SWNT for fibers at the microscale level.

Nanotubes conduct heat as well as diamond at room temperature. They are very sharp, and thus can be used as probe tips for scanning-probe microscopes, and field-emission electron sources for lamps and displays.

Although SWNTs are similar to a single sheet of graphite in structure, which is semiconductor with zero band gap, they may be either metallic or semiconducting, depending on the structures of SWNTs in Figure 5.4. The electronic properties of MWNTs are similar to those of SWNTs due to the weak coupling between the cylinders in MWNTs. Since both metals and semiconductors can be made from the same all-carbon system, CNTs are ideal candidates for molecular electronics technologies.

The first realized major commercial application of MWNTs is their use as electrically conducting components in polymer composites [296]. Other applications of CNTs include electrochemical devices, hydrogen storage, field emission devices, nanometer-sized electronic devices, sensors, probes [297].

The objective of this chapter is to synthesize carbon nanotubes on silicon substrates by microwave plasma chemical vapor deposition (MPCVD) of a mixture of methane and hydrogen. The catalyst was nickel, migrated from a small piece of catalyst supplier to the substrate surface during microwave plasma pretreatment. Scanning Electron Microscopy (SEM) and Transmission Electron Microscopy (TEM) were used to characterize the morphologies of the CNTs.

## 5.2 Literature review

CNTs are usually made by arc discharge, laser ablation, and chemical vapor deposition (CVD) methods. The arc discharge method produces high quality SWNTs with few structural defects and does not require a catalyst for synthesis of MWNT. But the purity of the nanotubes is usually low. For instance, Shi et al. synthesized SWNTs by d.c. arc discharge method [298]. A Y-Ni alloy composite graphite rod was used as anode for d.c. arc discharge. A cloth-like soot, containing about 40% SWNTs, was produced. The diameter of SWNTs is 1.3nm. Saito observed a bamboo-shaped carbon tube produced by the arc evaporation of nickel-loaded graphite [299]. The tube, shown in Figure 5.5, consists of a linear chain of hollow compartments that are spaced at nearly equal separation from 50-100  $\mu\text{m}$ . The outer diameter of the bamboo tubes is about 40 nm, and the length is typically several  $\mu\text{m}$ . A growth model of the bamboo tubes was proposed.



Figure 5.5 TEM picture of a bamboo-like carbon tube

The laser ablation method produces SWNTs with high quality and high purity, but the process is very costly. For example, the yield of SWNTs is about 80% in the literatures [300, 301]. The diameter of SWNTs is about 1.4 nm while the length is in the order of 1-10 micrometer.

The arc discharge and laser ablation methods involve high temperatures, e.g. 5,000-20,000°C for arc discharge, and 4,000-5,000°C for laser ablation. However, the CVD method is used for rapid synthesis of MWNTs with high purity at lower temperatures and is easy to scale up for commercial production. The nanotube alignment is easy to control with this method. However, the nanotubes synthesized with CVD usually have more structural defects compared with the other two methods. MWNTs with diameters of 10-100 nm were produced by the floating catalyst method [302]. Aligned nitrogenated amorphous carbon nano-rods, with a diameter of approximately 100-250 nm and a length of approximately 50-80  $\mu\text{m}$ , were synthesized on a porous alumina template, using an electron cyclotron resonance CVD system and a microwave-excited plasma of  $\text{C}_2\text{H}_2$  and  $\text{N}_2$  as precursors [303]. Mauron et al. synthesized oriented nanotube films (20-35  $\mu\text{m}$  thick) on flat silicon substrates by CVD of a gas mixture of acetylene and nitrogen. The diameter of the nanotubes is 20-25 nm. An iron nitrate ethanol solution was coated onto a silicon substrate before heating [304]. Long SWNTs, with lengths of 10 and 20 cm, were synthesized by an optimized catalytic CVD technique with a floating catalyst method [305].

Microwave plasma chemical vapor deposition (MPCVD) has gained increasing popularity as a controllable and deterministic method for growing vertically aligned CNTs while conventional thermal CVD has been successfully employed for self-oriented

growth of CNTs. A summary of literatures about synthesis of carbon nanotubes by MPCVD [306-330] is listed in Table 5.1. The well-aligned CNTs or carbon nanowires [306-308] synthesized by MPCVD are MWNTs. Silicon wafer are widely used as substrates while metals, e.g. Ni, Fe, are used as catalyst. Microwave plasma gas includes CH<sub>4</sub>, H<sub>2</sub>, C<sub>2</sub>H<sub>2</sub>, NH<sub>3</sub>, N<sub>2</sub>, and CO<sub>2</sub>. The key factors of synthesis of CNTs by MPCVD are gas composition, CNT growth temperature, pressure, growth time. The microwave power can affect the growth temperature. The growth pressure is usually far less than atmospheric pressure (736 Torr), approximately 1-80 Torr. However, one literature synthesized CNTs at atmospheric pressure [309]. Most CNT growth temperature ranges from around 600 - 800°C, except two references synthesizing CNTs at 300°C [310, 311]. The typical growth time is about 10-30 minutes. The CNTs synthesized by MPCVD are usually 1-100 μm long and 20-100 nm in diameter. The bamboo-like structure was found within MWNTs by many researchers.

Table 5.1 Literature summary on synthesis of CNTs by MPCVD

Ref.	Topic	Catalyst on substrate	Gas composition; Total flow rate (sccm)	MW Power; Temp. ; Pressure; Time	CNT Length; Diameter
306	Carbon nanowires having the sea urchin structure	Ni / Si			N/A; 46nm
307	Synthesis of interconnecting MWNT island	Ni / Si	CH <sub>4</sub> :H <sub>2</sub> =2.5:57.5 sccm	600 W; 80 Torr; 900°C; 5 min	N/A; 10-100 nm
308	Synthesis of high-density MWNT coils	Ni, Fe / Ti / Si	CH <sub>4</sub> :H <sub>2</sub> :N <sub>2</sub> =6:90:10 sccm	N/A; N/A; 650°C; 15 min	1-50 μm; 20-400 nm
309	Producing MWNTs at atmospheric pressure	Iron carbonyl gas / Al tube	Ar:CO:Fe(CO) <sub>5</sub> = 500-600:900:10-30 sccm	<1 kW; Atmospheric Pres.; >3000 K; 4 h	5 mm; 50 μm
310	Low temp. growth of vertically-aligned MWNTs	Fe / Si	CH <sub>4</sub> :CO <sub>2</sub> = 30:30 sccm	300 W; 15 Torr; <330 °C; 20 min	N/A; 15-20nm
311	A high yield of aligned MWNTs	Fe, Ti / Si	CH <sub>4</sub> :CO <sub>2</sub> =30:30 sccm	300 W; 15 Torr; <330 °C; 20 min	N/A; 15-300 nm

Table 5.1 Literature summary on synthesis of CNTs by MPCVD (cont'd)

Ref.	Topic	Catalyst on substrate	Gas composition; Total flow rate (sccm)	MW Power; Temp.; Pressure; Time	CNT Length; Diameter
312	Well-aligned CNTs perpendicular to Si substrate	Co (~2nm)/ Si	C <sub>2</sub> H <sub>2</sub> :NH <sub>3</sub> =10-30:100; Total 200 sccm	1 kW; 20 Torr; 825 °C; 2 min	12 μm; 30 nm
313	Simple and straightforward synthesis of MWNTs	Fe, Ni, Co / Si	CH <sub>4</sub> :H <sub>2</sub> :N <sub>2</sub> =20:80:80 sccm	1.5 kW; 6.6 kPa; 680 °C; 20 min	5 μm; 10-20 nm
314	Growth of MWNTs at low temp.	Ni / TiN / Si	CH <sub>4</sub> /(CH <sub>4</sub> +H <sub>2</sub> )=10-20%	400 W; 10 Torr; 520-700°C; 10-50 min	N/A; 10-15 nm
315	Synthesis of vertically aligned MWNTs	Ni / Si	CH <sub>4</sub> /(CH <sub>4</sub> +H <sub>2</sub> )=20%	400 W; 10 Torr; 700°C; 5 min	30 μm; 10-35 nm
316	Well aligned MWNTs with high aspect ratio	Ni / Si	CH <sub>4</sub> :NH <sub>3</sub> =150:150, 200:100; 240:60 sccm	2.2 kW; 21 Torr; 800°C; 40 min	100 μm; 20-50 nm
317	Plasma breaking of catalyst films for MWNT growth	Fe / Si	CH <sub>4</sub> :(CH <sub>4</sub> +N <sub>2</sub> )=2-30%; 100 sccm	700-900 W; 15 Torr; 850°C; 15 min	15 μm; 20-120 nm
318	Plasma breaking of catalyst films for MWNT growth	Fe / Si			200 μm; 5-30 nm
319	The effect of catalysis on MWNT growth	Ni/Cu alloy / Si	CH <sub>4</sub> :H <sub>2</sub> =0.5:100 sccm	1.1 kW; 30 Torr; 600°C;	N/A; 50-200 nm
320	Role of N <sub>2</sub> in CNT growth	Ni, Co / Si	CH <sub>4</sub> :H <sub>2</sub> or N <sub>2</sub> = 10:100 sccm	960 W; 16 Torr; 650°C; 10 min	10-20 μm; 50 nm
321	In-situ growth of Spiral shape CNTs	Ni / Al / Si	CH <sub>4</sub> :H <sub>2</sub> = 0.5:100 sccm	1.1 kW; 4 kPa; 600°C; 30 min	N/A; 100 nm
322	Bias-enhanced growth of aligned CNTs	Pd / Si	CH <sub>4</sub> :H <sub>2</sub> = 0.4:80 sccm	1.1 kW; 30 Torr; N/A; 2-20 min	2.3 μm; 40-90 nm
323	Synthesis of multi-branched CNTs	Pd / Si	CH <sub>4</sub> :H <sub>2</sub> = 0.5:100 sccm	1.1 kW; 4 kPa; N/A; 2-20 min	N/A; 60-300 nm
324	Synthesis of large area aligned CNTs	Fe / Si	C <sub>2</sub> H <sub>2</sub> :H <sub>2</sub> =15:60 sccm	100 W; 1200 mTorr; 700°C; 5-20 min	5-20 μm; 40-90 nm
325	Synthesis of MWNTs with narrow diameter	Ni / Si	CH <sub>4</sub> :H <sub>2</sub>	1 kW; 9.33 kPa; 850°C; N/A	10-20 μm; 2-30 nm
326	The influence of N <sub>2</sub> on CNT growth	Fe / Si	CH <sub>4</sub> :N <sub>2</sub> =20:80	700 W; N/A; 600°C; N/A	30 μm; 20-100 nm
327	In situ synthesis of branched Cu-filled CNTs	Cu electrodes / Si	CH <sub>4</sub> :H <sub>2</sub> =1:1	800 W; 2.3 kPa; 1150°C; 30 min	N/A; 40-80 nm
328	Analysis of diameter distribution of CNTs	Cu / Si	CH <sub>4</sub> :N <sub>2</sub> =20:80	N/A; 20 Torr; 700-800°C; 5-10 min	1 μm; 20-120 nm
329	Metal analysis of tip of MWNT by EDX	Ni, Fe-Ni-Cr substrates	CH <sub>4</sub> :H <sub>2</sub> =10-20:80-90 sccm	500 W; 250-300 Pa; 650°C; 30-60 min	1 μm; 60-80 nm
330	Large arrays of well-aligned CNTs	Ni / Glass	C <sub>2</sub> H <sub>2</sub> :NH <sub>3</sub> :N <sub>2</sub>	N/A; N/A <666°C; 3-25 min	20 μm; 180-350 nm

## 5.3 Experimental

### 5.3.1 Experimental System

The MPCVD system used in this study is illustrated in Figure 5.6. The system was built for diamond coating at first by the Fraunhofer Center for Coatings and Laser Applications at MSU. The synthesis process of CNTs by the system is filed to apply patent [331].

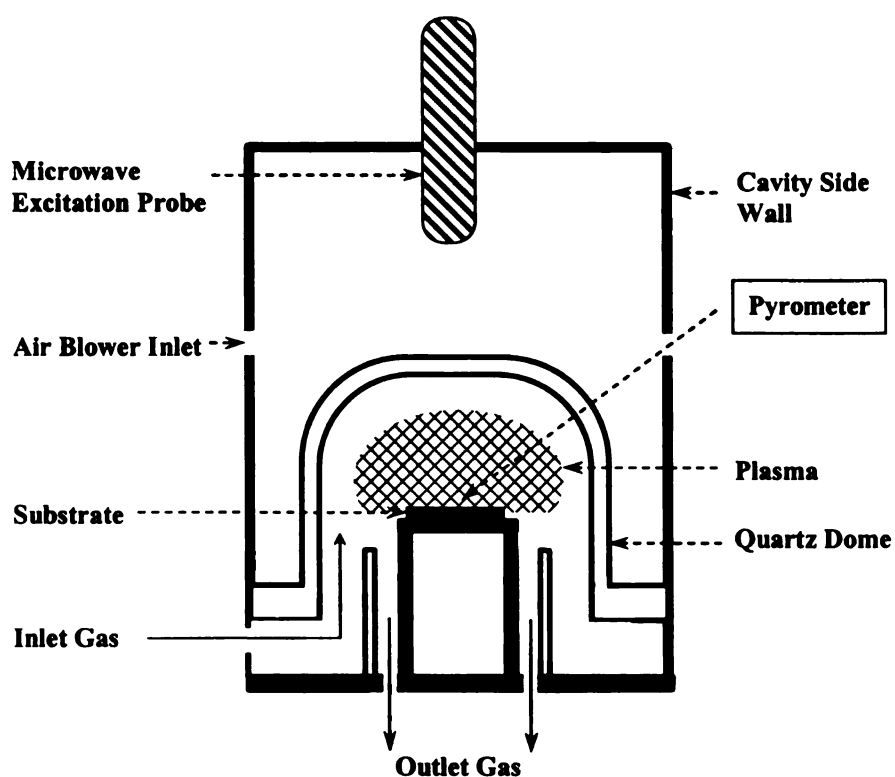


Figure 5.6 Schematic diagram of the MPCVD apparatus at MSU

The photos of the microwave plasma reactor and its control panel are shown in Figures 5.7 and 5.8, respectively. The microwave power was controlled by hand while the gas flows were controlled by the computer. The growth temperature of CNTs was measured by a pyrometer via the screen side window.

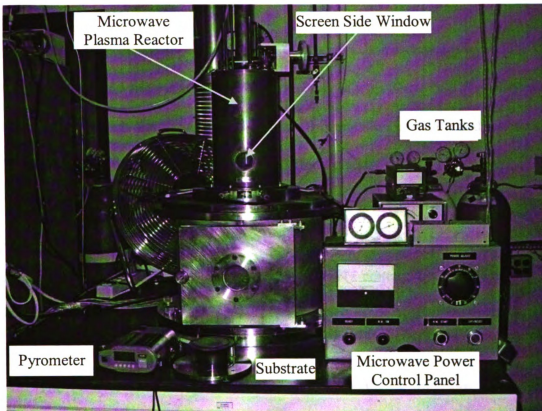


Figure 5.7 Photo of the microwave plasma reactor



Figure 5.8 Photo of the control panel of the microwave plasma reactor

### **5.3.2 Experimental Materials**

The silicon substrate used to grow CNTs is a boron-doped-p-type Si <100> substrate with an electric resistivity of 10  $\Omega$ cm from Silicon Sense Inc. The diameter of the Si wafer is 2 inch and the dopant is Boron. Its orientation is <100> and resistivity is 1-10 ohm-cm. Its thickness is 254-304  $\mu$ m and grade is test.

The unpurified SWNTs, which were coated on the Si wafers before CNT growth, are from the labs of Professor James M. Tour at Center of Nanoscale Science and Technology at Rice University. The unpurified SWNTs contain amorphous carbon, Fe, and SWNTs. The iron content of the SWNTs is on the order of 7%. The manufacturing method can be found in the literature [332].

The catalyst for CNT growth is Ni on a Si wafer. A thin film of Ni with a thickness of 30 nm is deposited using dc magnetron sputtering on a Si wafer. A 3 inch pure Ni (99.999%) target from K. J. Lesker Company was used. The deposition of Ni films was carried out under an Ar pressure of 4.0 mTorr at a substrate temperature of 400°C. The working distance from the Ni target to the Si wafer was 2.5 inch while deposition power was 200W.

### **5.3.3 Experimental Procedure**

1 mg unpurified SWNT was mixed with 40mL HPLC grade acetone in a beaker. The mixture was stirred two hours under ultrasonic agitation. The beaker was covered with aluminum foil to prevent evaporation loss and spill. Then, the Si wafer was coated with 0.15-0.2 ml SWNT mixture. The Si wafer was dried in atmosphere.

Three small pieces (around  $5 \times 5 \text{ mm}^2$ ) of Ni catalyst supplier were placed on one quarter of one SWNT-coated Si wafer. The Si wafer was placed on a graphite plate (see Figure 5.9) and the plate was put into the microwave plasma reactor of the MPCVD system in Figure 5.7.

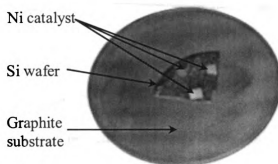


Figure 5.9 Photo of Si wafer on a graphite substrate

The system was vacuum pumped to a base pressure of less than 5 mTorr and purged with Argon at 365 sccm (Standard Cubic Centimeters per Minute) for 20 minutes. After turning off Ar gas, the system was pumped to around 0 torr for 5 minutes.

Hydrogen with a set flow rate started and microwave plasma was ignited at 2kW when the pressure of the reactor reached 5 Torr. The Ni catalysts were heated by  $\text{H}_2$  plasma to about  $700^\circ\text{C}$  with a microwave power of 1.7 kW (total power 2 kW). Then, methane with a set flow rate was introduced into the plasma chamber to start CNT growth. Microwave power was increased to 2.2 kW with a total power of 3 kW to keep the CNT growth temperature is about  $750\text{-}800^\circ\text{C}$ . If the temperature was higher than  $800^\circ\text{C}$ , the microwave power should be lowered. The growth time was 20 minutes.

After synthesis of CNTs, a SEM (JEOL 6300F) was used to examine the morphology of the CNTs. A small piece of CNTs on Si wafer was cut and mounted on a SEM holder (45° tilted). The sample was coated gold before SEM study. A TEM (JEM-2200FS) was used to investigate the microstructure of CNTs.

## 5.4 Results and discussion

### 5.4.1 CNT Growth Conditions

The growth conditions of CNTs for five samples are shown in Table 5.2. CH<sub>4</sub> was the source of carbon and the percentage of CH<sub>4</sub> in the gas mixture of CH<sub>4</sub> and H<sub>2</sub> changed from 10% to 100%. The MW power in five experiments was 2.2 kW except experiment 2, the power in which was 1.7 kW. The CNT growth pressure in experiment 1-4 were around 34 Torr while that in experiment 5 was lower than 30 Torr, shown in Table 5.3. Experiment 5 stopped at 12 minute due to disappearance of MW plasma.

Table 5.2 Experimental conditions of the CNT growth

No	Grown CNTs	CH <sub>4</sub> : H <sub>2</sub>	Total flow rate (sccm)	Power (kW)
1	Some	10:90	100	2.2
2	Many	20:80	100	1.7
3	Some	30:70	100	2.2
4	None	50:50	60	2.2
5	None	100:0	36.8	2.2

Table 5.3 CNT growth pressure (Torr)

Time (min)	Sample 1	Sample 2	Sample 3	Sample 4	Sample 5
0	37.5	27.0	28.2	28.7	13.5
2	32.0	30.6	32.4	32.2	16.2
4	36.7	34.6	33.4	36.2	18.8
6	33.9	34.1	34.3	34.3	21.4
8	34.3	34.4	34.2	34.0	23.9
10	34.2	34.2	34.2	34.1	26.6
12	34.2	34.2	34.2	34.1	29.1
14	34.2	34.1	34.2	34.1	
16	34.2	34.2	34.1	34.2	
18	34.1	34.2	34.1	34.2	
20	34.2	34.2	34.1	34.1	

The temperature data in five experiments are listed in Table 5.4 while the temperature profiles in experiments 1-4 are shown in Figure 5.10. The temperatures of Si and Ni are the highest temperatures on Si wafer and Ni catalyst suppliers, respectively.

Table 5.4 CNT growth and catalyst temperatures (°C)

Time (min)	No.1		No. 2		No. 3		No. 4		No. 5	
	Si	Ni	Si	Ni	Si	Ni	Si	Ni	Si	Ni
0	679	737	676	706	640	680	660	696	662	692
2	722	737	706	748	732	748	703	731	666	714
4	761	750	800	N/A	739	747	709	714	650	686
6	770	765	810	727	760	780	720	743	679	699
8	770	790	810	741	769	760	717	789	639	671
10	765	798	810	752	799	761	721	756	619	624
12	762	790	810	768	797	780	726	737	590	737
14	769	764	804	778	740	779	728	764		
16	760	787	793	756	753	776	734	802		
18	760	792	787	737	753	776	N/A	N/A		
20	759	793	808	740	799	767	745	819		

The CNT growth temperature in experiment 1 was about 760-770°C and the catalyst temperature was around 790°C. The CNT growth temperature in experiment 2

was stable around 800-810°C, which was higher than the catalyst temperature ranging from 740 to 770°C. The CNT growth temperature in experiment 3 changed from 740 to 800°C and the catalyst temperature was about 760-780°C. The Si wafer temperature in experiment 4 was lower than 730°C while that in experiment 5 was lower than 700°C. The catalyst temperature in experiment 4 was higher than the Si wafer temperature, ranging from 730 to 800°C but that in experiment 5 was lower than 700°C.

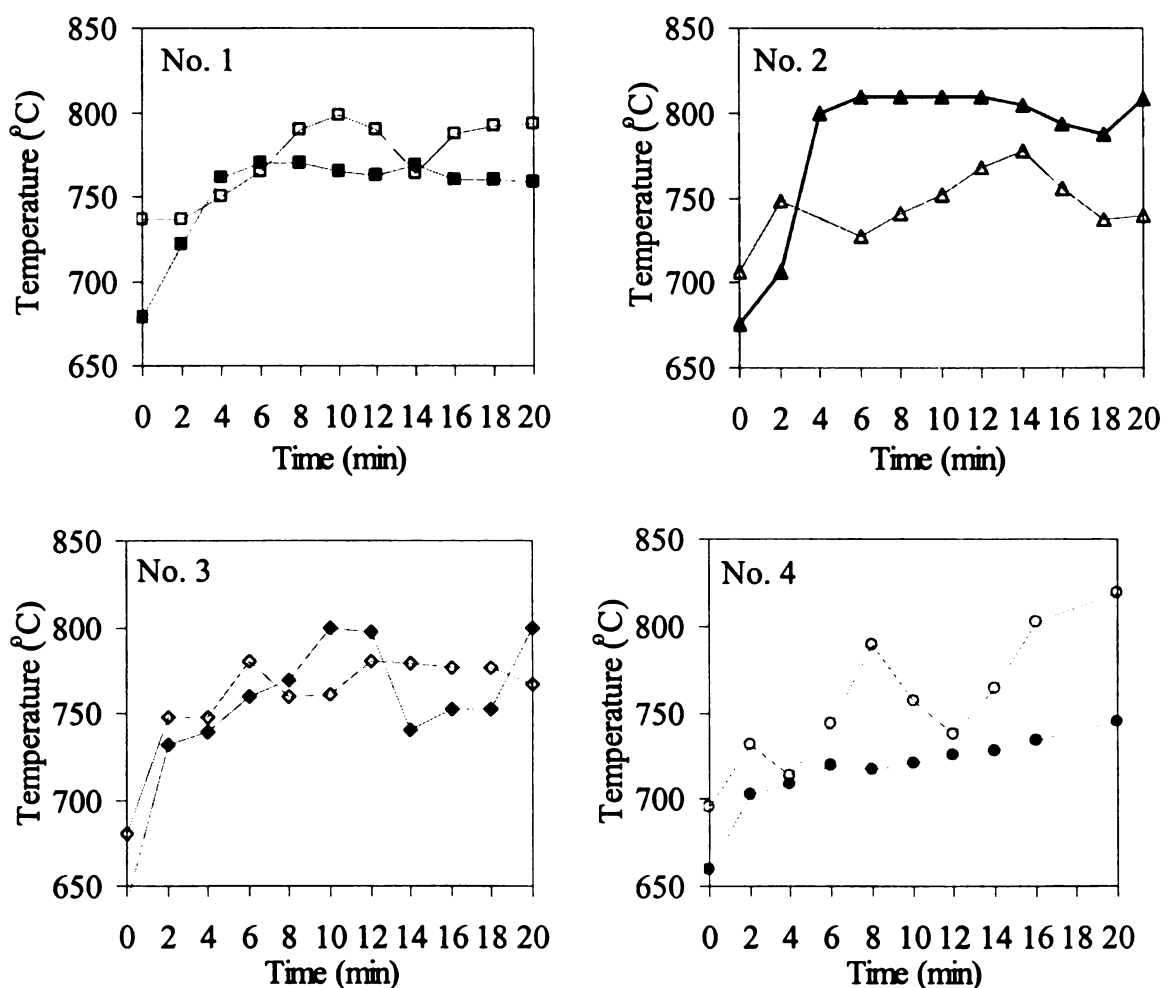


Figure 5.10 Temperature profile during CNT growth in experiment No. 1-4: solid points represent Si wafer; hollow points represent Ni catalysts.

### 5.4.2 CNT Growth Results

Figure 5.11 shows photos of SWNT-coated Si wafer before CNT growth and after synthesis in experiment 1-5. Unpurified SWNTs on a Si wafer were visible in Figure 5.11 (a). After CNT synthesis, a layer of dark film of CNTs was visible to the eyes. Visual observation of the Si wafers suggests that CNTs grew on Si wafers in experiment 1-3 while the thickest CNTs happened in experiment 2. No CNT grew in experiments 4 and 5. Further, unpurified SWNTs were blown off by microwave plasma gas.

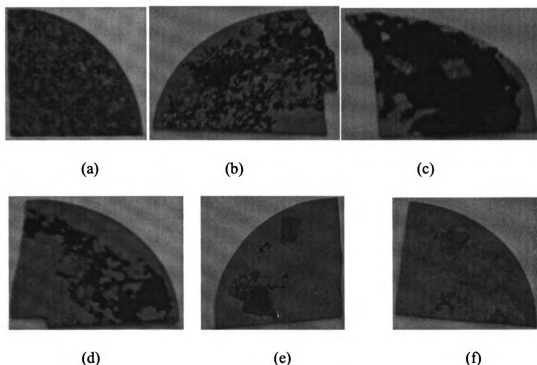


Figure 5.11 Optical images of the Si wafers: (a) before CNT growth, after CNT growth in (b) experiment 1, (c) experiment 2, (d) experiment 3, (e) experiment 4, (f) experiment 5.

Pictures of a graphite substrate with Si wafer and Ni catalyst before and after CNT growth in experiment 3 are shown in Figure 5.12. CNTs grew not only on the Si wafer, but on the graphite substrate and Ni catalyst as well.

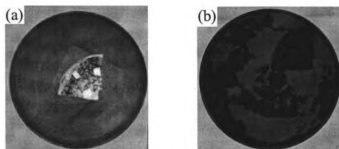


Figure 5.12 Optical images of the graphite substrate with Si wafer and Ni catalyst in experiment 3: (a) before CNT growth, (b) after CNT growth.

### 5.4.3 Morphology of CNTs by SEM

The morphology of grown CNTs of samples 1-3 was investigated by SEM. Figures 5.13-5.15 show SEM images (45° tilted) of CNTs of samples 1-3 while the summary of information about morphology, length, and diameter of samples is shown in Table 5.5. Vertically aligned CNTs can be found in three samples while the diameters of three samples are similar, around 30-60 nm. Nevertheless, the lengths of CNTs and morphologies of samples are different.

Table 5.5 Summary of morphology, length, and diameter of CNTs

Sample No.	Morphology	CNT length ( $\mu\text{m}$ )	CNT diameter(nm)
1	Not well aligned CNTs	40-60	30-60
2	Well aligned CNTs	350-500	30-50
3	Two parts: curled CNTs and aligned CNTs	0.9-1.1	20-50 (curled CNTs) 40-60 (aligned CNTs)

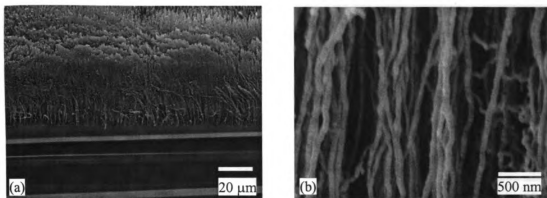


Figure 5.13 SEM images (45° tilted) at different magnifications of CNTs in sample 1

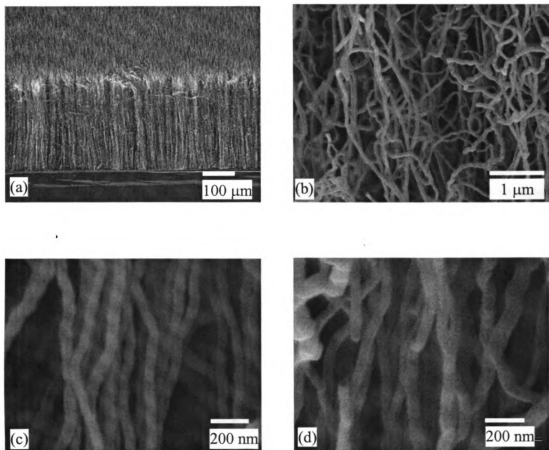


Figure 5.14 SEM images (45° tilted) at different magnifications of CNTs in sample 2

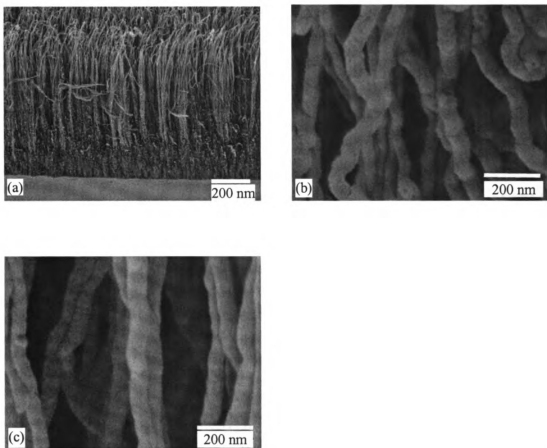


Figure 5.15 SEM images ( $45^\circ$  tilted) at different magnifications of CNTs in (a) sample 3, (b) curled CNT part and (c) aligned CNT part.

Sample 2 has longest vertically well-aligned CNTs with a length of approximately 350-500  $\mu\text{m}$ , which may be the longest CNTs synthesized by MPCVD, compared with a CNT length range of 1-100  $\mu\text{m}$  according to the available literatures [306-330]. The aspect ratio (Length/Diameter) of sample 2 is around 10,000, which is comparable to calculated L/D ratio in the literature [318] and larger than that in other surveyed literatures by MPCVD. The CNTs of sample 2 connected to each other when taken at larger magnifications, showing in Figure 5.14 (b)-(d). Figures 5.14 (c) and (d) shows different parts of CNTs of sample 2.

According to Figures 5.11 and 5.13-5.15, the inlet gas composition in sample 2 was 20% methane. This is same as synthesis condition in the literatures [313-315, 329]. The CNT growth pressure of samples 1-3 was around 34 Torr (see Table 5.3). The growth temperature of sample 2 is about 800-810°C while the growth temperature of samples 1 and 3 was changing from 740-800 °C (see Table 5.4 and Figure 5.10). Other researchers reached similar results about growth temperature with a range of 800-850°C [312, 316, 317, 325]. Since the graphite substrate was heated directly by plasma without other heating sources, the temperature difference among samples 1-5 was caused by the CNT growth. Taking into account of lower microwave power in experiment 2 than in other experiments (see Figure 5.2), 1.7 kW vs. 2.2 kW, it is proposed that more growing CNTs, higher growth temperature.

The CNTs in sample 1, shown in Figure 5.13 (a) and (b), have a shorter length but maybe a wider distribution than those of sample 2. The length of CNTs in sample 3 (<1  $\mu\text{m}$ ) is far less than that in sample 1 (20-40  $\mu\text{m}$ ) and 2 (250-350  $\mu\text{m}$ ). Furthermore, the CNTs in sample 3 have different structure. The cross-sectional structure of sample 3 in Figure 5.15 (a) consists of two parts, one aligned upper section and one curly or random lower section. The length of the curled part is about 150 nm while that of the aligned part is around 600 nm. The aligned CNT density, shown in Figure 5.15 (c), is higher than the curly CNT density in Figure 5.15 (b).

#### **5.4.4 TEM Results**

The TEM images of CNTs in samples 1-3 are shown in Figures 5.16-5.18. Bamboo-like CNTs exist in three samples. Other researchers had similar observation

[299, 308, 313, 316, 317, 320]. The width of a hollow region is around 20-30 nm, with a wall thickness in the range of 10-15 nm. The heights of the hollow compartments are not equal. The inside diameters of the CNTs are around 20-30 nm and the external diameters are about 40-60 nm. The tip of the arrowhead is in the range of 20-30 nm and no catalyst particles found inside the tip. The root of CNTs is open-ended while one catalyst particle is found with the root in sample 3. These phenomena suggest a root-growth mechanism.

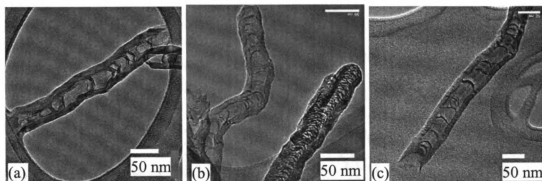


Figure 5.16 TEM images of CNTs in sample 1: (a) body, (b) tip, (c) root.

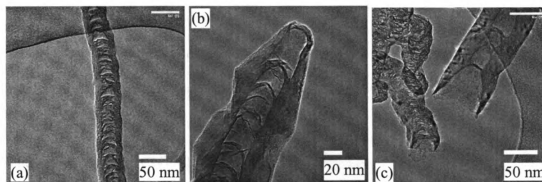


Figure 5.17 TEM images of CNTs in sample 2: (a) body, (b) tip, (c) root.

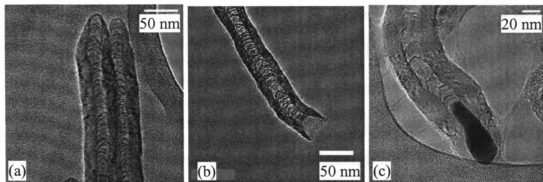


Figure 5.18 TEM images of CNTs in sample 3: (a) body, (b) root, (c) root with a catalyst particle.

#### 5.4.5 CNT Growth Mechanism

The  $\text{CH}_4$  source gas was an atomic carbon source for CNTs while Ni was catalyst. The question is why unpurified SWNTs were coated on Si wafers before experiments. This study was based on previous research results by Shuangjie Zhou within the research group. The unpurified SWNTs, coated on Si wafer before experiments, contain amorphous carbon, Fe, and SWNTs. In order to investigate if the unpurified SWNTs were essential for CNT growth, the comparable experiments were carried out. The result that no CNT grew without the unpurified SWNTs showed that the unpurified SWNTs were not catalyst for CNT growth. The comparable experiments to investigate if Fe was catalyst for CNT growth were carried out with and without Ni catalyst supplier on the Si wafer. The result that no CNT grew without Ni catalyst supplier suggested that Fe in the unpurified SWNTs was not catalyst for CNT growth. The comparable experiments to investigate if amorphous carbon in the unpurified SWNTs was important for CNT growth were carried out using purified SWNTs without amorphous carbon. The result that nothing grew suggested that the amorphous carbon coated on Si wafer is essential for CNT growth.

Growth mechanisms of bamboo-shape MWNTs have been discussed [299, 311, 316, 333]. The root-growth mechanism of bamboo-shaped MWNTs in this study is illustrated in Figure 5.19. The Ni catalyst supplier was etched by H<sub>2</sub> microwave plasma before the temperature of catalyst reached 700°C, shown in Figure 5.19 (a). The nano-sized Ni grains formed under the hydrogen plasma heating migrated from the catalyst supplier to the Si wafer, attaching to the amorphous carbons from unpurified SWNTs coated on the Si wafer (see Figure 5.19 (b)). The role of amorphous carbons was to hold Ni nanoclusters on the Si wafer. The Ni particles in this process remained solid because the temperatures of growing CNTs and catalysts were lower than 810°C, which is far below the melting temperature of nickel (1455°C). After CH<sub>4</sub> was introduced into the microwave plasma reactor, the hydrocarbon species decomposed on the surfaces of the Ni particle, shown in Figure 5.19 (c). Carbon atoms, disassociated from methane, deposited on the Ni surfaces to form a saturated carbon film, shown in Figure 5.19 (d). After the Ni and Si substrate surfaces were saturated with carbon layers, the graphitic sheath was pushed upward while carbon atoms were depositing into graphite layers, illustrated in Figure 5.19 (e). The graphitic sheath left the Ni particle and another graphitic sheath deposited on the Ni particle. Therefore, compartments were formed while carbon atoms were continuous supplied and diffused onto the vertically growing MWNTs, shown in Figure 5.19 (f). DC bias imposed on the substrate surface was used to align MWNTs in some literatures [310, 311, 319, 322, 323], but it is not required in this process.

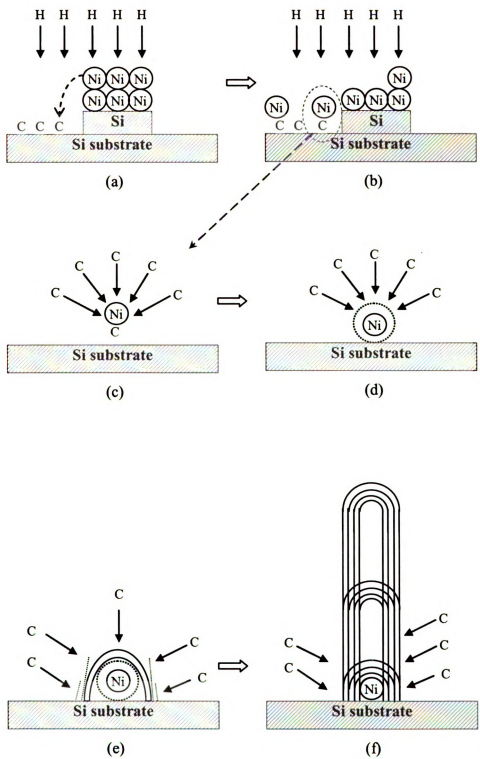


Figure 5.19 Schematic illustrations of root-growth mechanism of a bamboo-like CNT

## 5.5 Conclusions

Carbon Nanotubes were synthesized on silicon substrate by microwave plasma chemical vapor deposition (MPCVD) of a gas mixture of methane and hydrogen. The catalyst was nickel, which was not deposited on the substrates directly but migrated from a small piece of catalyst supplier to the substrate surface during microwave plasma pretreatment. The Si wafer was coated with amorphous carbon before synthesis. Additional heating sources and DC bias on graphite substrate are not required. SEM and TEM were used to characterize the morphologies and microstructures of the CNTs. The lengths and diameters of CNTs changed with gas composition and growth temperature. Long vertically-aligned CNTs with a length range of 350-500  $\mu\text{m}$  were synthesized. The plasma gases included 20 sccm methane and 80 sccm hydrogen. The CNT growth temperature was 800-810 $^{\circ}\text{C}$ . The growth time was 20 minutes. The diameter of CNTs is around 30-60 nm. The CNTs exhibit bamboo-like structure and may grow via a root-growth mechanism.

## CHAPTER 6 CONCLUSIONS

In this study, experimental research was conducted in three sections. The first section was investigation of the curing kinetics of epoxy resins. The second section was study on dielectric properties of several epoxy resin reacting systems over a temperature range at 2.45 GHz. The last section was synthesis of carbon nanotubes by microwave plasma chemical vapor deposition.

The curing of diglycidyl ether of bisphenol A (DGEBA) and 3, 3'-diaminodiphenyl sulfone (DDS) system under microwave radiation at 145 °C was governed by an autocatalyzed reaction mechanism. A kinetic model was used to describe the curing progress.

$$\frac{d\alpha}{dt} = (k_1 + k_2\alpha^m)(1 - \alpha)^n$$

where  $k_1$  is the non-catalytic polymerization reaction rate constant,  $k_2$  is the autocatalytic polymerization reaction rate constant,  $m$  is the autocatalyzed polymerization reaction order, and  $n$  is the non-catalyzed polymerization reaction order.

A single frequency microwave heating and diagnostic system, developed at Michigan State University, was used to heat and measure the dielectric constant and dielectric loss factor of curing epoxy resins. A cylindrical TM 012 mode cavity is used to process epoxy resins at 2.45 GHz. The epoxy resin was DGEBA. The four curing agents were DDS, a difunctional primary amine (Jeffamine D-230), m-phenylenediamine (mPDA), and diethyltoluenediamine (Epikure W). The mixtures of DGEBA and the four curing agents were stoichiometric. The four reacting systems were heated under

microwave irradiation to certain cure temperatures, i.e. 145°C for DGEBA/DDS, 90°C for DGEBA/Jeffamine D-230, 110°C for DGEBA/mPDA, and 160°C for DGEBA/Epikure W. Measurements of temperature and dielectric properties using the swept frequency method were made during free convective cooling of the samples. The cooled samples were analyzed with a Differential Scanning Calorimeter to determine the extents of cure. The major conclusions of this section are:

- The Davidson-Cole model can be used to describe the dielectric properties of the four curing systems.
- A simplified Davidson-Cole model is proposed to describe the dielectric properties of polymeric materials. It works well for the DGEBA/DDS system and low-temperature or high-extent-of-cure data of the other three systems. It can be used to calculate the parameters of the Davidson-Cole model as well. The simplified Davidson-Cole expression is as follows:

$$\begin{aligned}\epsilon^* &= \epsilon_\infty + \frac{(\epsilon_0 - \epsilon_\infty)}{(j\omega\tau)^n} \\ \epsilon' &= \epsilon_\infty + \frac{(\epsilon_0 - \epsilon_\infty)\cos(n\frac{\pi}{2})}{(\omega\tau)^n} \\ \epsilon'' &= \frac{(\epsilon_0 - \epsilon_\infty)\sin(n\frac{\pi}{2})}{(\omega\tau)^n}\end{aligned}$$

where  $\epsilon^*$  is the complex dielectric constant,  $\epsilon'$  is the dielectric constant,  $\epsilon''$  is the dielectric loss factor,  $j$  is the imaginary unit,  $\omega$  ( $=2\pi f$ ,  $f$  is the oscillator frequency in Hz) is the radial frequency of the electric field in  $s^{-1}$ ,  $\tau$  is the relaxation time in s,  $\epsilon_0$  is the low

frequency dielectric constant,  $\epsilon_\infty$  is the high frequency dielectric constant, and  $n$  is the shape parameter with a range of  $0 \leq n \leq 1$ .

- The secondary  $\gamma$  relaxation has been identified in the four reacting systems.

The Arrhenius expression is applicable to the  $\gamma$  relaxation.

- The evolution of all parameters in the models, e.g. the shape parameter  $n$ , the relaxation strength ( $\epsilon_0 - \epsilon_\infty$ ), the activation energy  $E_a$ , and the relaxation time  $\tau$ , during cure was related to the facts that the number of the dipolar groups in the reactants decreases and medium viscosity increases during the polymerization.

- The relaxation strength ( $\epsilon_0 - \epsilon_\infty$ ) was found to decrease during the polymerization of the four systems, which is consistent with the decreasing number of the epoxy and amine groups in the reactants.

- The shape parameter  $n$  decreases as the reaction proceeds for four systems.  $n$  is related to the local chain dynamics. During the reaction the motion of dipolar groups is hindered by the medium with increasing viscosity. Therefore, the parameter  $n$  decreases.

- The activation energy of the four systems increases first, and then decrease around 50% extent of cure. The increase of activation energy before the peak is consistent with increasing viscosity of the systems during cure. The decrease after the peak point may be explained by that the hindrance ability of the reacted polymer chains may be weaker than that of dipoles in the reactants and, thus, less energy is needed for dipolar groups to relax. The peak temperatures of the four systems may be related to the gel points.

- The relaxation time increases as the reaction proceeds due to increasing medium viscosity for the four systems.

- The dielectric constants of the four reacting systems exhibit a linear relation to the extent of cure and may be used to in-situ monitor the curing reaction.

Carbon Nanotubes (CNTs) were synthesized on silicon substrate by microwave plasma chemical vapor deposition of a gas mixture of methane and hydrogen. The catalyst was nickel, which was not directly deposited on the substrates but migrated from a small piece of catalyst supplier to the substrate surface during microwave plasma pretreatment. The Si wafer was coated with amorphous carbon before synthesis. Additional heating sources and DC bias on graphite substrate were not employed. Scanning Electron Microscopy and Transmission Electron Microscopy were used to characterize the morphologies and microstructures of the CNTs. The lengths and diameters of CNTs changed with gas composition and growth temperature. Long vertically-aligned CNTs with a length range of 350-500  $\mu\text{m}$  were synthesized. The plasma gases included 20 sccm methane and 80 sccm hydrogen. The CNT growth temperature was 800-810°C. The growth time was 20 minutes. The diameter of CNTs is around 30-60 nm. The CNTs exhibit bamboo-like structure and may grow via a root-growth mechanism.

## CHAPTER 7 FUTURE WORK

Development of mathematical models for microwave heating is beneficial for the process in a number of ways. In addition to setting criteria for material selection and realizing smooth and precise control, the occurrence of hot spots and thermal runaway can be predicted with the model and procedures can be taken to avoid these undesired phenomena. Therefore, modeling of electromagnetic fields and curing reaction is an essential to scale-up and apply microwave processing of polymer and composites.

Regarding synthesis of carbon nanotubes, many interesting topics should be investigated: effect of growth time on CNT growth, effect of catalysts other than Ni, effect of adding other gas (e.g. N<sub>2</sub>), the growth mechanism (root-growth or tip-growth), the possible applications of CNTs.

## REFERENCES

1. Maxwell JC. A Treatise on Electricity and Magnetism. Dover, New York, 1954.
2. Harrington RF. Time Harmonic Electromagnetic Fields. McGraw-Hill, New York 1961.
3. Ku CC, Liepins R. Electrical Properties of Polymers: Chemical Principles. Hanser, Munich, 1987.
4. Saliel C, Datta AK. Advances in Heat Transfer 1999, 33, 1.
5. Zong L, Zhou S, Sun L, Kempel LC, Hawley MC. J Polym Sci Part B: Polym Phys 2004, 42, 2871.
6. Zong L, Zhou S, Sgriccia N, Hawley MC, Kempel LC. J Microwave Power E E 2003, 38, 49.
7. Besecker KD, Rhoades CB Jr., Jones BT, Barnes KW. Atom Spectrosc 1998, 19, 55.
8. Jankowski K, etc. Analytica Chimica Acta 2001, 440, 215.
9. LeBlanc GN. Am Lab 2000, 32, 32.
10. Matusiewicz H. Anal Chem 1994, 66, 751.
11. Wang Q, Wood PJ, Cui W. Carbohydr Polym 2002, 47, 35.
12. Bakass M, Mokhlisse A, Lallemand M. Thermochim Acta 2000, 356, 159.
13. Contat-Rodrigo L, Haider N, Ribes-Greus A et al. J Appl Polym Sci 2001, 76, 1101.
14. Costley CT, Dean JR, Newton I et al. Anal Commun 1997, 34, 89.
15. Latham RJ, Linford RG, Pynenburg RAJ. Solid State Ionics 1993, 60, 105.
16. Nielson RC. J Liq Chromatogr 1993, 16, 1625.
17. Richter RC, Shah S. Am Lab 2000, 32, 14.
18. Vandenburg HJ, Clifford AA, Bartle KD, et al. Analyst 1997, 122, 101R.
19. Chen M, Siochi EJ, Ward TC, Mcgrath JE. Polym Eng Sci 1993, 33, 1092.

20. Chen M, Siochi EJ, Ward TC, Mcgrath JE. *Polym Eng Sci* 1993, 33, 1110.
21. Zhou S, Yang H, Zong L, Hawley MC. *Proc 2001 SPE Auto Compos Conf* 2001.
22. Meghal P, Ubale S, Adgaonkar CS. *Indian J Eng Mater S* 2001, 8, 55.
23. Achour ME, Malhi ME, Miane JL, et al. *J Appl Polym Sci* 1996, 61, 2009.
24. Achour ME, Malhi ME, Miane IL, et al. *J Appl Polym Sci* 1999, 73, 969.
25. Chang JT, Fanning MW, Meaney PM, etc. *IEEE T Electromagn C* 2000 42, 76.
26. Lucchese L, Liauw CM, Allen NS, et al. *Polym Bull* 2000, 44, 187.
27. Kanynak A, Polat A, Yilmazer U. *Mater Res Bull* 1996, 31, 1195.
28. Barnes A, Despotakis A, Wright PV, et al. *Electrochimica Acta* 1998, 43, 1629.
29. Biernholtz H, Kenig S, Dodiuk H. *Polym Advan Technol* 1992, 3, 125.
30. Gan YX, Chen CQ, Li CG. *Sci Eng Compos Mater* 1994, 3, 23..
31. Golosovsky M, Tsindlekht M, Davidov D. *Phys Rev* 1992, 46, 439.
32. Schultz JW, Colton JS, Berkowitz CK. *Intl SAMPE Symp* 2000, 45, 1863.
33. Yoshida S, Sato M, Sugawara E, et al. *J Appl Phys* 1999, 85, 4636.
34. Khan SM, Negi S, Khan IM. *Polym News* 1997, 22, 414.
35. Negi S, Gordon K, Khan SM, Khan IM. *ACS Sym Ser* 1999, 726, 145.
36. Negi S, Gordon K, Khan SM, Khan IM. *Polym Prepr* 1998, 39, 721.
37. Osaki S. *J Polym Sci Part B: Polym Phys* 1995, 33, 685.
38. Faez R, Martin IM, DePaoli M, Rezende MC. *J Appl Polym Sci* 2002, 83, 1568.
39. Jousse F, Delnaud L, Olmedo O. *SAMPE Quart* 1995, 360.
40. Wan M, Li J, Li S. *Polym Advan Technol* 2001, 12, 651.
41. Sengwa RJ. *Polym Int* 1998, 45, 202.
42. Sengwa RJ. *Polym Int* 1998, 45, 43.

43. Sengwa RJ, Chaudhary R. *Polm Int* 2001, 50, 432.
44. Zoughi R, Lai J, Munoz K. *Mater Eval* 2002, 60, 171.
45. Osaki S, Tashiro K. *Macromolecules* 1998, 31, 1661.
46. Gray S, Ganchev S, Qaddoumi N, et al. *Mater Eval* 1995, 53, 404.
47. Kim YJ, De Flaviis F, Jofre L, Feng MQ. *Proc 46<sup>th</sup> Intl SAMPE Symp* 2001, 439.
48. Qaddoumi N, Carriveau G, Ganchev S, Zoughi R. *Mater Eval* 1995, 53, 926.
49. Parneix JP, Miane JL. *European Association for Composite Materials* 1992, 821.
50. Prevors L, Pabiot J. *Materiaux et Techniques* 1994, 82, 17.
51. Mijovic J, Wijaya J. *Polym Composite* 1990, 11, 184.
52. Wang TB, Liu J. *J Electron Manuf* 2000, 10, 181.
53. Mijovic J, Corso WV, Nicolais L, et al. *Polym Advan Technol* 1998, 9, 231.
54. Chen M, Hellgeth JW, Ward TC, Mcgrath JE. *Polym Eng Sci* 1995, 35, 144.
55. Day RJ, Yau SHC, Hewson KD. *Plast Rub Compos Pro* 1998, 27, 213.
56. Fu B, Hawley MC. *Polym Eng Sci* 2000, 40, 2133.
57. Gourdenne, A. *Polym Mater Sci Eng* 1992, 66, 430.
58. Hawley MC, Wei J, Adegbite V. *Mater Res Soc Symp Proc* 1994, 347, 669.
59. Hedreul C, Galy J, Dupuy J. *J Appl Polym Sci* 1998, 68, 543.
60. Hedreul C, Galy J, Dupuy J, Delmotte M, More C. *J Appl Polym Sci* 2001, 82, 1118.
61. Jullien H, Petit A. *Polym Mater Sci Eng* 1992, 66, 378.
62. Jullien H, Petit A, Merienne C. *Polymer*, 1996, 37, 3319.
63. King RJ, Werner MJ, Mayorga GD. *J Reinf Plast Comp* 1993, 12, 173..
64. King RJ, Werner M, Mayorga G. *SAMPE J* 1993, 28, 35.
65. Liu F, Turner I, Siores E, Groombridge P. *J Microwave Power E E* 1996, 31, 71.

66. Lefeuvre S, Azzouz F, Salmoria GV, et al. *Ceramic Transactions* 2001, 111, 153.
67. Liptak SC, Wilkinson SP, Hedrick JC, et al. *Polym Prepr* 1990, 31, 320.
68. Mallon FK, Ray WH. *J Appl Polm Sci* 1998, 69, 1203.
69. McMillan, A; Lauf, RJ; Paulauskas, FL. *Proc. Am Chem Soc* 1995, 72..
70. Methven J. *Mater Technol* 1999, 14, 183.
71. Methven JM, Ghaffariyan SR, Abidin AZ. *Polym Composite* 2000, 21, 586.
72. Muhtarogullari IY, Dogan A, et al. *J Appl Polym Sci* 1999, 74, 2971.
73. Outifa L, Jullien H, More C, Delmotte M. *Ind Eng Chem Res* 1995, 34, 688.
74. Prime B. *Thermal Characterization of Polymeric Materials*. Academic Press, 1981.
75. Qiu Y, Adegbite V, Hawley MC. *Proc 27<sup>th</sup> Int SAMPE Technol Conf* 1995, 173.
76. Tanikella RV, Allen SAB, Kohl PA. *J Appl Polym Sci* 2001, 83, 3055.
77. Thostenson ET, Chou TW. *Polym Composite* 2001, 22, 197.
78. Wei J, Hawley MC, Delong JD. *Polym Eng Sci* 1993, 33, 1132.
79. Wei J, Hawley MC, Demeuse MT. *Polym Eng Sci* 1995, 35, 461.
80. Youngs I, Power T, Robinson D, et al. *Ceramic Transactions* 2001, 111, 93.
81. Yousefi A, Lafleur PG, Gauvin R. *Polym Composite* 1997, 18, 157.
82. Chia LHL, Jacob J, Boey FYC. *J Mater Process Tech* 1995, 48, 445.
83. Ng LT, Chia LHL. *Polym Int* 1999, 48, 952.
84. Fang X, Hutcheon R, Scola DA. *J Polym Sci Part A: Polym Chem* 2000, 38, 2526.
85. Mallakpour SE, Hajipour AR, Khoee S. *J Appl Polym Sci* 2000, 77, 3003.
86. Liu Y, Sun XD, Xie XQ. *J Polym Sci Part A: Polym Chem* 1998, 36, 2653.
87. Liu Y, Xiao Y, Sun X. *J Appl Polym Sci* 1999, 73, 2391.
88. Memon, MS; Yunus, N; Razak, AAA. *Int J Prosthodont* 2001, 14, 214.

89. Boey FYC, Lee WL. J Mater Sci Lett 1990, 9, 1172.
90. Rodrigues DE, Wilkes GL. Polym Mater Sci Eng 1992, 384.
91. Ward TC, Chen M. Polym Mater Sci Eng 1992, 335.
92. Fang X, Scola DA. J Polym Sci Part A: Polym Chem 1999 37, 4616.
93. Fang X, Hutcheon R, Scola DA. J Polym Sci Part A: Polym Chem 2000, 38, 1379.
94. Madras G, Karmore V. Polym Int 2001, 50, 1324.
95. Zhou S, Hawley MC. Proc 46th Int SAMPE Symp 2001, 2243.
96. Hager N, Domszy R. Time-Domain-Reflectometry Cure Monitoring. A Materials and Processes Odyssey; Book 2 of 2 Books (USA), 2001, 2252.
97. Shull PJ, Hurley DH, Spicer JWM, Spicer JB. Polym Eng Sci 2000, 40, 1157.
98. Lye SW, Boey FYC. Mater Manuf Process 1994, 9, 851.
99. Pichon L, Meyer O. IEEE T Magn 2002, 38, 977.
100. Joly A, Joly JP, Karmazsin E, Veau JL. J Therm Anal 1993, 39, 1285.
101. Joly A, Joly JP, Veau JL, Karmazsin, E. J Therm Anal 1995, 45, 375.
102. Boey FYC, Rath SK. Adv Polym Tech 2000, 19, 194.
103. Karmazsin E, Bechu S. J Therm Anal 1994, 41, 1639.
104. Wei J, Hawley MC. Am Chem Soc 1995, 10.
105. O'Brien KT, Kasturi S, Mekkaoui AM. Polym Composite 1994, 15, 231.
106. Pham TA, Lancaster GM. Auszuge aus den Europaischen Patentanmeldungen, Teil I 1991, 7, 4189.
107. Kathirgamanathan, P. Polymer 1993, 34, 3105.
108. Margolis JM. Rev Plast Mod 1990, 59, 377.
109. Reitz WE, Oman RM. Adv Mater Process 2000, 158, 49.
110. Staicovici S, Wu CY, Benatar A. J Reinf Plast Comp 1999, 18, 35.

111. Wu CY, Benatar A. Technomic 1992, 1771.
112. Wu CY, Benatar A. Polym Eng Sci 1997, 37, 738.
113. Zhou S, Hawley MC. Compos Struct 2003, 61, 303.
114. Wei JB, Ngo K, Tucker D, et al. J Microwave Power E E 1998, 33, 10.
115. Ku HS, Ball JAR, MacRobert M, Siores E. Plast Rubber Compos 2000, 29, 278.
116. Shanker B, Lakhtakia A. J Compos Mater 1993, 27, 1203.
117. Lu J, Jiang Q, Zhu X, Wang F. J Appl Polym Sci 2001, 79, 312.
118. Mallakpour SE, et al. J Polym Sci Part A: Polym Chem 2000, 38, 1154.
119. Mallakpour SE, Hajipour AR, Faghihi K. Polym Int 2000, 49, 1383.
120. Mallakpour SE, Hajipour AR, Zadhoush A, et al. J Appl Polym Sci 2001, 79, 1317.
121. Mallakpour SE, Hajipour AR, Habibi S. Eur Polym J 2001, 37, 2435.
122. Mallakpour SE, Hajipour AR, Mahdavian AR, et al. Eur Polym J 2001, 37, 1199.
123. Mallakpour SE, Hajipour AR, Faghihi K, et al. J Appl Polym Sci 2001, 80, 2416.
124. Mallakpour SE, et al. J Appl Polym Sci Part A: Polym Chem 2001, 39, 177.
125. Srinivasan SA, Joardar SS, Kranbeuhl D, et al. J Appl Polym Sci 1997, 64, 179.
126. Hurduc N, Abdelylah D, Buisine JM, et al. Eur Polym J 1997, 33, 187.
127. Chen J, Chen Q, Yu X. J Appl Polym Sci 1996, 62, 2135.8 (1996).
128. Kishanprasad VS, Gedam PH. J Appl Polym Sci 1993, 50, 419.
129. Imai Y, Nemoto H, Watanabe S, Kakimoto MA. Polym J 1996, 28, 256.
130. Imai Y, Nemoto H, Kakimoto MA. J Polym Sci Part A: Polym Chem 1996, 34, 701.
131. Park KH, Watanabe S, Kakimoto M, Imai Y. Polym J 1993, 25, 209.
132. Liao LO, et al. J Polym Sci Part A: Polym Chem 2002, 40, 1749.
133. Jacob J, Chia LHL, Boey FYC. J Appl Polym Sci 1997, 63, 787.

134. Stoffer JO, Zhang D, Crivello JV. *Polym Mater Sci Eng* 1999, 81, 118.
135. Stoffer JO, Zhang D, Crivello JV. *Am Chem Soc Div Polym Chem* 1999, 40, 669.
136. Dhanalakshmi K, Sundararajan G. *Polym Bull* 1997, 39, 333.
137. Bogdal D, et al. *Polimery* 2000, 45, 363.
138. Jung KS, et al. *Polym-Korea* 2001, 21, 609.
139. Correa R, Gonzalez G, Dougar V. *Polymer* 1998, 39, 1471.
140. Lu J, Zhu X, Zhu J, Yu J. *J Appl Polym Sci* 1997, 66, 129.
141. Lu J, Zhu X, Ji S, Zhu J, Chen Z. *J Appl Polym Sci* 1998, 68, 1563.
142. Lu J, Chen N, Ji S, Sun S, Ding M, Zhu X. *J Appl Polym Sci* 2001, 82, 1356.
143. Xu W, Bao J, Zhang J, Shi M. *J Appl Polym Sci* 1998, 70, 2343.
144. Palacios J, Sierra J, Rodriguez MP. *New Polym Mat* 1992, 3, 273.
145. Reis RL, Ribeiro AS, Malafaya PB. *31<sup>st</sup> Int Biomater Symp* 1999, 555.
146. Chan CM, Ko TM, Hiraoka H. *Surf Sci Rep* 1996, 24, 3.
147. Coen MC, Groening P, Schlapbach L. *Le Vide: Science Technique et Applications* 1999, 54, 162.
148. Li RZ, Ye L, Mai YW. *Compos Part A-Appl* 1997, 28, 73.
149. Konig U, et al. *Colloid Surface B* 2002, 24, 63.
150. Shenton MJ, et al. *J Polym Sci Part A: Polym Chem* 2002, 40, 95.
151. Hillborg H, et al. *Polymer* 2000, 41, 6851.
152. Hollander A, et al. *J Polym Sci Part A: Polym Chem* 1995, 33, 2013.
153. Lianos L, Parrat D, Hoc TQ, Duc TM. *J Vac Sci Technol A* 1994, 12, 2491.
154. Walther M, Spallels M. *Surf Coat Tech* 1996, 80, 200.
155. Etemadi R, et al. *J Vac Sci Technol A* 1994, 12, 320.
156. Hofrichter A, Bulkin P, Drevillon B. *J Vac Sci Technol A* 2002, 20, 245.

157. Rats D, Hajek V, Martinu L. *Thin Solid Films* 1999, 340, 33.
158. Bergeron A, et al. *J Vac Sci Technol A* 1998, 16, 3227.
159. Inagaki N. *Macromol Symp* 2000, 159, 151.
160. Lennon P, et al. *Int J Adhes Adhes* 1999, 19, 273.
161. Shi MK, et al. *J Adhes Sci Technol* 2000, 14, 1485.
162. Klemberg-Sapieha JE, Shi MK, et al. *Society Plastics Engineers* 1995, 2862.
163. Keil M, et al. *Appl Surf Sci* 1998, 125, 273.
164. Felix J, Gatenholm P, Schreiber HP. *J Appl Polym Sci* 1994, 51, 285.
165. Schreiber HP, St Germain F. *J Adhes Sci Eng* 1990, 4, 319.
166. Aumann T, Theirich D, Engemann J. *Surf Coat Tech* 2001, 142, 169.
167. Tomcik B, Popovic DR, Jovanovic IV, Prtrovic ZL. *J Polym Res* 2001, 8, 259.
168. Peng J, Jian XG, Li Q, Deng XL, Gu B. *ACTA Polymerica SINICA* 2000, 3, 354.
169. Zhou XT, et al. *Surf Coat Tech* 2000, 123, 273.
170. Korzec D, Traub K, Werner F, Engemann J. *Thin solid films* 1996, 281-282, 143.
171. Graff W, Matson M, Kellner T, et al. *Solid State Technol* 2001, 44, 37.
172. Nitschke M, Schmack G, Janke A, et al. *J Biomed Mater Res* 2002, 59, 632.
173. Nitschke M, Menning A, Werner C. *J Biomed Mater Res* 2000, 50, 340.
174. Sodhi RNS, Sahi VP, Mittelman MW. *J Electron Spectrosc* 2001, 121, 249.
175. Schroder K, Meyer-Plath A, Keller D, et al. *Contrib Plasm Phys* 2001, 41, 562.
176. Wickson BM, Brash JL. *31<sup>st</sup> Int Biomater Symp* 1999, 57.
177. Chou NJ, Marwick AD, Goldblatt RD, et al. *J Vac Sci Technol* 1992, 10, 248.
178. Kobayashi T, Sasama T, Wada H, Fujii N. *J Vac Sci Technol* 2001, 19, 2155.
179. Castro RM, Verdonck P, Pisani MB, et al. *IEEE T Plasms Sci* 2000, 28, 1043.

180. Schmitt BR, Kim H, Urban MW. *J Appl Polym Sci* 1999, 71, 1.
181. Bichler CH, Langowski HC, Moosheimer U, et al. *J Adhes Sci Eng* 1997, 11, 233.
182. Normand F, Granier A, Leprince P, et al. *Plasma Chem Plasma P* 1995, 15, 173.
183. Ringengbach A, Jugnet Y, Duc TM. *J Adhes Sci Technol* 1995, 9, 1209.
184. Kaiser M, Walker M, Baumgartner KM, et al. *Surf Coat Tech* 1998, 105, 165.
185. Schwarz J, Schmidt M, Ohl A. *Surf Coat Tech* 1998, 98, 859.
186. Behnisch J, Mehdorn F, Hollander A, et al. *Surf Coat Tech* 1998, 98, 875.
187. Groning P, Schneuwly A, Schlapbach L, et al. *J Vac Sci Technol A* 1996, 14, 3043.
188. Hlavac M, Ohlidal M, Slavinska D, *Int J Electron* 1992, 73, 1067.
189. Biederman H, Osada Y. *Plasma Polymerization Processes*. Elsevier, 1992.
190. Ludlow-Palafox C, Chase HA. *Ind Eng Chem Res* 2001, 40, 4749.
191. Kleps T, Piaskiewicz M, Parasiewicz W. *J Therm Anal Calorim* 2000, 60, 271.
192. Klun U, Krzan A. *Polymer* 2000, 41, 4361.
193. Krzan A. *J Appl Polym Sci* 1998, 69, 1115.
194. Danko GA, Silberglitt R. *J Am Ceram Soc* 2000, 83, 1617.
195. Hernandez MT, Gonzalez M. *Euro Ceramics VII (1-3)* 2002, 206-2, 71.
196. Yang ST, Zhang YF, Lu QZ, et al. *J Inorg Mater* 2000, 15, 309.
197. Wu C, Gao J, Li M, Zhang WM, Jiang M. *Macromol Symp* 2000, 150, 219.
198. Spatz J, Mossmer S, Moller M, et al. *Adv Mater* 1998, 10, 473.
199. Srikanth H, Hajndl R, Chirinos C, *Appl Phys Lett* 2001, 79, 3503.
200. Tu WX, Lin HF. *Chem Mater* 2000, 12, 564.
201. Szabo DV, Vollath D, Arnold W. *Ceramics Transactions* 2001, 111, 217.
202. Szabo DV, Vollath D. *Adv Mater* 1999, 11, 1313.

203. Vollath D. Mater Technol 1997, 12, 89.
204. Willert-Porada MA. MRS Bull 1993, 18, 51.
205. White WC. Proc Inst Radio Electron Eng 1962, 50, 1129.
206. Chabinsky IJ. Mater Res Soc Symp Proc 1988, 17, 124.
207. Krieger B. Proc Am Chem Soc Div Polym Mater Sci Eng 1992, 66, 339.
208. Smith RD. EPRI Report EM-3645 (1984).
209. Nelson SO. J Microwave Power E E 1985, 30, 65.
210. Vetsuypens JP, Looock WV. J Microwave Power E E 1986, 31, 110.
211. Lightsey G, et al. J Microwave Power E E 1988, 33, 11.
212. Thiebaut JM, Akye C, Roussy G. IEEE T Instrum Meas 1988, 37, 114.
213. Lightsey G, George C, Russell LD. J Microwave Power E E, 1986, 31, 86.
214. Lee, SM. International Encyclopedia of composites. VCH publishers, New York, 1990, 6, 339.
215. Finzel M. PhD Dissertation. Michigan State University, 1991.
216. Wei J. PhD Dissertation. Michigan State University 1992.
217. Adegbite V. PhD Dissertation, Michigan State University 1995.
218. Jow J. PhD Dissertation. Michigan State University, 1988.
219. Qiu Y. PhD Dissertation. Michigan State University 2000.
220. Zhou S. PhD Dissertation, Michigan State University, 2002.
221. Lewis DA, Summers JD, et al. J Polym Sci Part A: Polym Chem 1992, 30, 1647.
222. Marand E, Baker KR, Graybeal JD. Macromolecules 1992, 25, 2243.
223. Hedrick JC, Lewis DA, et al. Proc ACS Div Polym Mater Sci Eng 1989, 60, 438.
224. Lee H, Neville K. Epoxy Resins: Their Applications and Technology. McGraw-Hill, New York, 1957, 41.

225. Schechter L, Wynstra J, Kurkjy RP. *Ind Eng Chem* 1956, 48, 94.
226. Sourour S, Kamal MR. *Thermochim Acta* 1976, 14, 41.
227. Lee WI, Loos AC, Springer GS. *J Compos Mater* 1982, 16, 510.
228. Dannenberg H. *SPE Trans* 1963, 3, 78.
229. Horie K, Hiura H, Sawada M, Mita I, Kambe H. *J Polym Sci A1* 1970, 8, 1337.
230. Dusek K, Ilavsky M, Lunak S. *J Polym Sci Pol Sym* 1976, 53, 29.
231. Riccardi CC, Adabbo HE, Williams RJ. *J Appl Polym Sci* 1984, 29, 2481.
232. Acitally MA, Prime RB, Sacher E. *Polymer* 1971, 12, 335.
233. Kamal MR. *Polym Eng Sci* 1974, 14, 231.
234. Kamal MR, Sourour S. *Polym Eng Sci* 1973, 13, 59.
235. Dutta A, Ryan ME. *J Appl Polym Sci* 1979, 24 635.
236. Mijovic J. *J Appl Polym Sci* 1986, 31, 1177.
237. Moroni A, Mijovic J, Pearce EM, Foun CC. *J Appl Polym Sci* 1986, 32, 3761.
238. Progelhof RC, Throne JL. *Polym Eng Sci* 1975, 15, 690.
239. Chan AW, Hwang ST. *Polym Eng Sci* 1991, 31, 1149.
240. Lin R, Lee LJ, Liou M. *Intern Polym Process* 1991, VI, 356.
241. Gebart BR. *J Appl Polym Sci* 1994, 51, 153.
242. The LUXTRON model 750 Fluoroptic Thermometry TM System Service and Technical Reference Manual. LUXTRON Fluoroptic TM Temperature Sensing, California, 1986.
243. The NoEMI-TSTM Family Fiberoptic Thermometer Systems User's Guide. Nortech Fibronic Inc., Quebec Canada. 1996.
244. Levine WS. *The control handbook*. Boca Raton Fla CRC Press, 1996.
245. Daniel VV. *Dielectric Relaxation*. London Academic Press, 1967.
246. Debye P. *Polar Molecules*. Dover, New York, 1945.

247. Cole KS, Cole RHJ. Chem Phys 1941, 9, 341.
248. Davidson DW, Cole RHJ. Chem Phys 1951, 19, 1484.
249. Havriliak S, Negami S. J Polym Sci Part C 1966, 14, 99.
250. Havriliak S, Negami S. Polymer 1967, 8, 161.
251. Kauzmann W. Rev Mod Phys 1942, 14, 12.
252. Eyring H. J Chem Phys 1936, 4, 283.
253. Williams ML, Landel RF, Ferry JD. J Am Chem Soc 1955, 77, 3701.
254. Delmonte J. J Appl Polym Sci 1959, 2, 108.
255. Haran EN, Gringras H, Katz D. J Appl Polym Sci 1965, 9, 3505.
256. Kranbuehl D, Delos S, Yi E, et al. Polym Eng Sci 1986, 26, 338.
257. Day DR. Polym Eng Sci 1986, 26, 362.
258. Lane JW, Seferis JC, Bachmann MA. J Appl Polym Sci 1986, 31, 1155.
259. Lane JW, Seferis JC, Bachmann MA. Polym Eng Sci 1986, 26, 354.
260. Sanjana ZN. Polym Eng Sci 1986, 26, 373.
261. Senturia SD, Seppard NF. Adv Polym Sci 1986, 80, 1.
262. Zukas WX, Wentworth SE. Polym Compos 1987, 8, 232.
263. Pochan JM, Gruber RJ, Pochan DF. J Polym Sci Polym Phys 1981, 19, 143.
264. Koike T. Adv Polym Sci 1999, 148, 139.
265. Koike T, Tanaka R. J Appl Polym Sci 1991, 42, 1333.
266. Casalini R, Fioretto D, Livi A, et al. Phys Rev B 1997, 56, 3016.
267. Butta E, Livi A, Levita G, et al. J Polym Sci Part B: Polym Phys 1995, 33, 2253.
268. Casalini R, Livi A, Rolla PA, Levita G, Fioretto D. Phys Rev B 1996, 53, 564.
269. Gallone G, Capaccioli S, Levita G, et al. Polym Int 2001, 50, 545.

270. Domenici C, Levita G, Marchetti A, Frosini V. *J Appl Polym Sci* 1987, 34, 2285.
271. Simpson JO, Bidstrup SA. *J Polym Sci Part B: Polym Phys* 1993, 31, 609.
272. Sheppard NF, Senturia SD. *J Polym Sci Part B: Polym Phys* 1989, 27, 753.
273. Sheppard NF, Senturia SD. *Polym Eng Sci* 1986, 26, 354.
274. Corezzi S, Capaccioli S, Gollone G, et al. *J Phys-Condens Mat* 1997, 9, 6199.
275. Capaccioli S, Corezzi S, Gallone G, et al. *J Non-Cryst Solids* 1998, 235-237, 576.
276. Livi A, Levita G, Rolla PA. *J Appl Polym Sci* 1993, 50, 1583.
277. Carrozzino S, Levita G, Rolla P, Tombari E. *Polym Eng Sci* 1990, 30, 366.
278. Eloundou JP, Gerard JF, Pascault JP, et al. *Macromol Chem Phys* 2002, 203, 1974.
279. Kortaberria G, Arruti P, Mondragon I. *Polym Int* 2001, 50, 957.
280. Lairez D, Emery JR, Durand D, Pethrick RA. *Macromolecules* 1992, 25, 7208.
281. Simpson JO, Bidstrup SA. *J Polym Sci, Part B: Polym Phys* 1995, 33, 55.
282. Zong L, Charvat GL, Kempel LC, Hawley MC. 26th AMTA Meeting & Symp, Stone Mountain, GA, 2004.
283. Schonhals A, Schlosser E. *Colloid Polym Sci* 1989, 267, 125.
284. Schlosser E, Schonhals A. *Colloid Polym Sci* 1989, 267, 133.
285. Viovy JL, Monnerie L, Brochon JC. *Macromolecules* 1983, 16, 1845.
286. <http://cohesion.rice.edu/naturalsciences/smalley/emplibrary/allotropes.jpg>
287. Iijima, S. *Nature* 1991, 354, 56.
288. <http://www.labs.nec.co.jp/Eng/innovative/E1/top.html>
289. <http://www.nanotech-now.com/nanotube-buckyball-sites.htm>
290. Iijima S, Ichihashi T. *Nature* 1993, 363, 603.
291. Bethune DS, Kiang CH, DeVries MS, et al. *Nature* 1993, 363, 605.
292. Qin L, Zhao X, Hirahara K, Miyamoto Y, Ando Y, Iijima S. *Nature* 2000, 408, 50.

293. Gao G, Cagin T, Goddard WA. *Nanotechnology* 1998, 9, 184.
294. Yu M, Files BS, Arepalli S, Ruoff RS. *Phys Rev Lett* 2000, 84, 5552.
295. Wong EW, Sheehan PE, Lieber CM. *Science* 1997, 277, 1971.
296. <http://www.fibrils.com>
297. Baughman RH, Zakhidov AA, DeHeer WA. *Science* 2002, 297, 787.
298. Shi Z, Lian Y, Zhou X, et al. *Carbon* 1999, 37, 1449.
299. Saito Y. *Carbon* 1995, 33, 979.
300. Maser WK, Munoz E, Benito AM, et al. *Chem Phys Lett* 1998, 292, 587.
301. Puretzky AA, Geohegan DB, Fan X, Pennycook SJ. *Appl Phys Lett* 2000, 76, 182.
302. Ci L, Li Y, Wei B, Liang J, Xu C, Wu D. *Carbon* 2000, 38, 1933.
303. Liu XW, Lin JH, Hsieh WJ, Shih HC. *Diam Relat Mater* 2002, 11, 1193.
304. Mauron Ph, Emmenegger Ch, Zuttel A, et al. *Carbon* 2002, 40, 1339.
305. Zhu HW, Xu CL, Wu DH, Wei BQ, Vajtai R, Ajayan PM. *Science* 2002, 296, 884.
306. Ting J, Liu R. *Carbon* 2003, 41, 579.
307. Kim S, Park J, Kim B, et al. *Mater Sci Eng C* 2004, 24, 297.
308. Kim U, Pcionek R, Aslam DM, Tomanek D. *Diam Relat Mater* 2001, 10, 1947.
309. Chen C, Perry WL, Xu H, Jiang Y, Phillips J. *Carbon* 2003, 41, 2555.
310. Chen M, Chen C, Chen C. *J Mater Sci* 2002, 37, 3561.
311. Chen M, Chen C, Koo H, Chen C. *Diam Relat Mater* 2002, 37, 3561
312. Bower C, Zhu W, Jin S, Zhou, O. *Appl Phys Lett* 2000, 77, 830.
313. Chen L, Wen C, Liang C, et al. *Adv Funct Mater* 2002, 12, 687.
314. Choi YC, Bae DJ, Lee YH, et al. *J Vac Sci Technol A* 2000, 18, 1864.
315. Choi YC, Shin YM, Lee YH, et al. *Appl Phys Lett* 2000, 76, 2367.

316. Cui H, Zhou O, Stoner BR. *J Appl Phys* 2000, 88, 6072.
317. Gao, JS, Umeda K, Uchino K, et al. *Mater Sci Eng A* 2003, 352, 308.
318. Gao, JS, Umeda K, Uchino K, et al. *Mater Sci Eng B* 2004, 107, 113.
319. Jong WJ, Lai SH, Hong KH, Lin HN, Shih HC. *Diam Relat Mater* 2002, 11, 1019.
320. Lin CH, Chang HL, Hsu CM, Lo AY, Kuo CT. *Diam Relat Mater* 2003, 12, 1851.
321. Tsai SH, Shiu CT, Lai SH, et al. *J Mater Sci Lett* 2002, 21, 1709.
322. Tsai SH, Chao CW, Lee CL, Shih HC. *Appl Phys Lett* 1999, 74, 3462.
323. Tsai SH, Shiu CT, Lai SH, Shih HC. *Carbon* 2002, 40, 1597.
324. Wang YH, Lin J, Huan CHA, Chen GS. *Appl Phys Lett* 2001, 79, 680.
325. Wang SG, Zhang Q, Yoon SF, Ahn J. *Scripta Mater* 2003, 48, 409.
326. Wang EG, Guo ZG, Ma J, et al. *Carbon* 2003, 41, 1827.
327. Zhang GY, Wang EG. *Appl Phys Lett* 2003, 82, 1926.
328. Zhu YB, Wang WL, Liao KJ, Ma Y. *Diam Relat Mater* 2003, 12, 1862.
329. Okai M, Muneyoshi T, Yaguchi T, Sasaki S. *Appl Phys Lett* 2000, 77, 3468.
330. Ren ZF, Huang ZP, Xu JW, et al. *Science* 1998, 282, 1105.
331. Hawley MC, Asmussen J, Zhou S, Zuo S. An integrated catalyst deposition and nanotube growth process with microwave plasma chemical vapor deposition. Patent application in process.
332. Nikolaev P, Bronikowski MJ, Bradley RK, et al. *Chem Phys Lett* 1999, 313, 91.
333. Harris PJF. *Carbon Nanotubes and Related Structures*. Cambridge University Press. 1999, 30-33.